Tampere University

TUOMAS JOKIAHO

Residual Stress, Microstructure and Cracking Characteristics of Flame Cut Thick Steel Plates

Towards Optimized Flame Cutting Practices

Tampere University Dissertations 159

Tampere University Dissertations 159

TUOMAS JOKIAHO

Residual Stress, Microstructure and Cracking Characteristics of Flame Cut Thick Steel Plates

Towards Optimized Flame Cutting Practices

ACADEMIC DISSERTATION
To be presented, with the permission of
the Faculty of Engineering and Natural Sciences
of Tampere University,
for public discussion in the auditorium K1702
of the Konetalo, Korkeakoulunkatu 6, Tampere,
on 15 November, at 12 o'clock.

ACADEMIC DISSERTATION
Tampere University, Faculty of Engineering and Natural Sciences
Finland

Responsible supervisor and Custos	Professor Minnamari Vippola Tampere University Finland	
Supervisor	Professor Pasi Peura Tampere University Finland	
Pre-examiners	D.Sc.(Tech.) Taina Vuoristo Swerim AB Sweden	Professor Jari Larkiola University of Oulu Finland
Opponents	Emeritus professor David Porter University of Oulu Finland	D.Sc.(Tech.) Taina Vuoristo Swerim AB Sweden

The originality of this thesis has been checked using the Turnitin OriginalityCheck service.

Cover design: Roihu Inc.

ISBN 978-952-03-1318-0 (print)
ISBN 978-952-03-1319-7 (pdf)
ISSN 2489-9860 (print)
ISSN 2490-0028 (pdf)
http://urn.fi/URN:ISBN:978-952-03-1319-7

PunaMusta Oy – Yliopistopaino
Tampere 2019

PREFACE

This study was mostly carried out in the Materials Science department of the Faculty of Engineering and Natural Sciences at Tampere University (formerly Tampere University of Technology) during 2015-2019. The research was funded by the University's Graduate School and SSAB Europe Oy. The work was wisely guided and supervised by Professor Minnamari Vippola. In addition, my co-supervisor Professor Pasi Peura and Dr. Suvi Santa-aho instructed and helped me during the research process. I want to thank them for the support and guidance that they have given me during these years.

I would also like to thank Tuomo Saarinen, M.Sc., formerly of SSAB, who introduced me to the research topic and provided the materials in the early stages of this research. In addition, I am grateful to Dr. Mari Honkanen, Henri Järvinen, M.Sc., and Dr. Matti Isakov for the help that they have provided me with whenever I have needed it. Also special thanks go to Turo Salomaa, M.Sc., who carried out the mechanical tests at the SSAB Europe Oy Raahe Steelworks. In addition, I want to thank SSAB's Dr. Pasi Suikkanen and Pertti Mikkonen, M.Sc., for their interest and support towards this project. I also wish to thank every colleague and person who has assisted me and been involved in this project.

I am very grateful to my family and friends, who have always supported me and pushed me forward. They gave me the extra motivation and push that I needed during both the good and hard times over these years.

Tampere, October 2019

Tuomas Jokiaho

ABSTRACT

High hardness, strength, and toughness are the properties required of thick wear-resistant steel plate. To meet these requirements, special care must be taken in the manufacture of the plate. The manufacturing steps for thick plate involve thermal cutting, such as flame cutting, which is the most generally applied cutting method for thick plate in the steel industry. Flame cutting is performed with a heating flame and oxygen jet, which creates a cut edge on the steel plate. It is a suitable method for thick steel plates and high production rates due to the exothermal reaction during the cutting process. However, flame cutting also causes problems. Due to the steep thermal gradient, a heat affected zone (HAZ) is formed at the cut edge. The HAZ includes microstructural changes and hardness variations. In addition, high residual stresses are generated in the cut edge. In the worst case, the flame cutting causes cracking of the plates.

The main purpose of this work is to identify the main contributors behind the cracking phenomenon of thick plates in flame cutting. In addition, the goal is to give guidelines for a more effective flame cut process and to determine the most suitable microstructural characteristics for thick wear-resistant steel plates and flame cutting. To achieve these goals, a trial batch of thick wear-resistant steel plates was manufactured. The plates were flame cut with different cutting parameters and the residual stress state of the flame cut samples was measured by X-ray diffraction. In addition, both original and flame cut samples were characterized by electron microscopy and mechanical tests.

The results of this study showed that residual stress formation during flame cutting can be controlled by choosing the right cutting parameters. Preheating and a slow cutting speed produced the most beneficial residual stress state: higher compressive stresses and lower tensile stresses. In addition, it was shown that cracking increased with increasing segregations in the plate structure. Furthermore, long horizontal prior austenite grain boundaries were found to create beneficial sites for crack formation and propagation. Therefore, in plate manufacturing it is recommended to aim for a small and equiaxed prior austenite grain structure. In addition, it is advantageous to reduce the amount and severity of the segregations in the structure when possible.

TIIVISTELMÄ

Paksuilta kulutuskestäviltä teräksiltä vaaditaan korkeaa kovuutta, lujuutta ja sitkeyttä. Näiden ominaisuuksien saavuttaminen vaatii erityistä huomiota levyjen valmistuksessa. Valmistusvaiheisiin kuuluu levyjen leikkaaminen, jossa usein käytetään polttoleikkausta. Se on yleisimmin teollisuudessa käytetty menetelmä paksujen teräslevyjen leikkaukseen. Polttoleikkauksessa levy leikataan käyttäen kontrolloitua lämmitysliekkiä sekä happisuihkua. Leikkauksessa tapahtuvan eksotermisen reaktion vuoksi menetelmä soveltuu hyvin paksuille levyille sekä suuriin valmistusmääriin. Polttoleikkaus aiheuttaa kuitenkin myös ongelmia. Suuren lämmöntuonnin vuoksi leikkausreunaan syntyy lämpövaikutusalue, jossa tapahtuu mikrorakennemuutoksia sekä kovuusvaihtelua. Lisäksi leikkausreunaan muodostuu korkeita jäännösjännityksiä ja pahimmassa tapauksessa säröjä.

Tutkimuksen päätavoite on tunnistaa paksujen levyjen polttoleikkauksen yhteydessä tapahtuvan säröilyn päätekijät. Tavoitteena on myös antaa ohjeet entistä tehokkaampaan polttoleikkausprosessiin ja määrittää polttoleikkauksen kannalta suotuisimmat mikrorakenteelliset ominaisuudet paksuille levyille. Tutkimusta varten valmistettiin koesarja paksuja kulutuskestäviä teräslevyjä. Levyt leikattiin eri leikkausparametreja käyttäen ja leikkausreunan jäännösjännitystila määritettiin röntgendiffraktiolla. Lisäksi sekä polttoleikatut että leikkaamattomat perusmateriaalinäytteet karakterisoitiin elektronimikroskoopeilla ja mekaanisilla testeillä.

Tutkimuksen tulokset osoittivat, että jäännösjännitysten muodostumista leikkausreunaan voidaan kontrolloida polttoleikkausparametrien avulla. Esilämmitys ennen leikkausta ja hidas leikkausnopeus tuottivat parhaan jännitystilan: enemmän puristusjännitystä ja alhaisemman vetojännityksen. Lisäksi havaittiin, että levyjen halkeilu lisääntyi, kun levyissä olevien suotaumien määrä kasvoi. Rakenteessa olevat pitkät horisontaaliset alkuperäisen austeniitin raerajat muodostavat suotuisia paikkoja särön muodostumiselle sekä etenemiselle. Näistä syistä on suositeltavaa, että levyjen valmistamisessa tähdätään pienikokoiseen ja tasa-aksiaaliseen primääriausteniittiin. Lisäksi valmistuksen tulisi minimoida rakenteessa olevien suotaumien määrää sekä pyrkiä heikentämään niiden pitoisuutta.

CONTENTS

LIST OF SYMBOLS AND ABBREVIATIONS

a_0	Notch length
A_{c1}	Temperature at which austenite begins to form during heating
A_{c3}	Temperature at which austenite formation is completed during heating
d0	Original diameter
Fe2.4C	ε-iron carbide
Fe_3C	Cementite
Lc	Parallel length
E	Young's modulus
d	Interplanar lattice spacing
m	Slope from the lattice spacing d vs. $\sin^2\psi$ curve
n	1, 2, 3…
θ	Diffraction angle
λ	Wavelength of the X-rays
σ	Residual stress in measurement direction
ψ	Angle between specimen normal and the normal with the diffracting plane
ϑ	Poisson's ratio
ϕ	Rotations (measurement directions)

bcc	Body-centered cubic crystal structure
bct	Body-centered tetragonal crystal structure
EBSD	Electron backscatter diffraction
EDS	Energy dispersive X-ray spectrometer
fcc	Face-centered cubic crystal structure
HAZ	Heat affected zone
NDT	Non-destructive testing
OES	Optical emission spectroscopy
PAGB	Prior austenite grain boundary
SEM	Scanning electron microscope

TE	Temper embrittlement
TEM	Transmission electron microscope
TME	Tempered martensite embrittlement
XRD	X-ray diffraction

ORIGINAL PUBLICATIONS

Publication I T. Jokiaho, T. Saarinen, S. Santa-aho, P. Peura, M. Vippola, The Characterization of Flame Cut Heavy Steel – The Residual Stress Profiling of Heat Affected Surface Layer, Key Engineering Materials, Vol. 674 pp. 103-108, 2016.

Publication II T. Jokiaho, A. Laitinen, S. Santa-aho, M. Isakov, P. Peura, T. Saarinen, A. Lehtovaara, M. Vippola, Characterization of Flame Cut Heavy Steel – Modeling of Temperature History and Residual Stress Formation, Metallurgical and Materials Transactions B, Vol. 48, pp. 2891-2901, 2017.

Publication III T. Jokiaho, S. Santa-aho, H. Järvinen, M. Honkanen, P. Peura, M. Vippola, Effect of Microstructural Characteristics of Thick Steel Plates on Residual Stress Formation and Cracking During Flame Cutting, Materials Performance and Characterization, Vol. 7, 2018.

Publication IV T. Jokiaho, S. Santa-aho, P. Peura, M. Vippola, Role of Steel Plate Thickness on the Residual Stress Formation and Cracking Behavior During Flame Cutting, Metallurgical and Materials Transactions A, 2019.

Unpublished manuscript

Publication V T. Jokiaho, S. Santa-aho, P. Peura, M. Vippola, Cracking and Failure Characteristics of Flame Cut Thick Steel Plates, pp. 1-16.

AUTHOR'S CONTRIBUTION

In Publications I-V, Tuomas Jokiaho was the main author and researcher. He planned the experiments along with his supervisors and conducted most of the research work. He carried out all the residual stress measurements, most of the electron microscopy and wrote the manuscripts. The experimental parts and manuscripts were guided and commented on by the supervisor Prof. Minnamari Vippola, co-supervisor Prof. Pasi Peura, and Dr. Suvi Santa-aho. In addition, in the early stages of the thesis work, Tuomo Saarinen, M.Sc., gave advice and organized the production and testing of the samples at SSAB Europe Oy Raahe Steelworks (formerly Ruukki until 2014). Publication II was based on the model that was designed by Arttu Laitinen, M.Sc. In Publication III, the electron backscatter diffraction measurements were made by Henri Järvinen, M.Sc. and the transmission electron microscopy studies by Dr. Mari Honkanen. The mechanical testing made in SSAB Europe Oy Raahe Steelworks was organized by Turo Salomaa, M.Sc. In addition, Dr. Matti Isakov gave advice and comments on Publications II and IV. All the co-authors commented on the publications presented in this thesis.

1 INTRODUCTION

Thick wear-resistant steel plates are utilized in demanding applications where high hardness and strength are needed, for example in the mining industry and mining-related wear components. One important step in the production of such components is the cutting of the plates with a thermal cutting method such as flame cutting. Flame cutting is the most commonly applied method as it is suitable for thick plates and high production rates. Cutting is performed with a controlled flame and oxygen jet, which burns the steel and forms the cut edge. However, the flame cutting of thick wear-resistant steel plates also causes problems. Flame cutting forms a heat affected zone (HAZ) and high residual stresses at the cut edge of the steel plate. In the worst case, the wrong cutting practices can cause the cut edge to crack, which leads to rejection of the plates.

Residual stresses are internal stresses inside the material or component and are caused by practically every manufacturing or processing method. In general, tensile stresses are harmful and compressive stresses are beneficial, for example in fatigue resistance or preventing crack formation. Residual stresses in flame cutting can be divided into thermal stresses and transformation stresses, depending on their origin. Thermal stresses are caused by temperature differences, which induces local thermal expansion and contraction. In contrast, transformation stresses arise from local microstructural transformations, which are accompanied by changes in volume.

To achieve high hardness and toughness, thick wear-resistant steel plates have a certain type of microstructure and alloying elements. Generally, these steels have a mainly hard martensitic microstructure, which is formed due to quenching (heating and fast cooling) and alloying elements are used to increase the hardenability (i.e., ability to form martensite). However, the thickness of the plates makes production and cooling complicated, which often leads to segregations and microstructural banding. For this reason, both the mechanical properties and microstructure of the plates can differ depending on the location of the thickness direction. The layered structure combined with the high residual stresses formed during flame cutting can create an adverse environment, which increases the risk of crack formation.

1.1 Aim of the work

The aim of this study is to identify the main contributors behind the cracking phenomenon of thick wear-resistant steel plate in flame cutting. In addition, the objective is to present suitable cutting practices that reduce the cracking of steel plate and therefore increase the effectiveness of the flame cutting process. Another goal is to identify the most beneficial microstructural characteristics and mechanical properties of thick wear-resistant steel plate to improve cracking resistance in cutting. The results of the work will eliminate or reduce plate cracking in flame cutting and therefore increase the quality and efficiency of the process. A further aim is to provide guidelines and improve the processing of thick plate in both the steel industry and among end users. In addition, this study will contribute to knowledge of residual stress formation and the cracking phenomenon, which can also be utilized for example in welding applications.

In order to achieve these goals, a trial batch of thick wear-resistant steel plates were industrially manufactured for this study. Both original and flame cut plate samples were comprehensively studied by electron microscopy and mechanical testing. In addition, the residual stresses formed at the cut edge were measured extensively by X-ray diffraction to evaluate their effect on cracking and to determine the optimal cutting practices.

The research was done in collaboration with the SSAB Europe Oy Raahe Steelworks (formerly Ruukki until 2014) and includes five publications. The structure of the research work and the publications are presented in Figure 1.

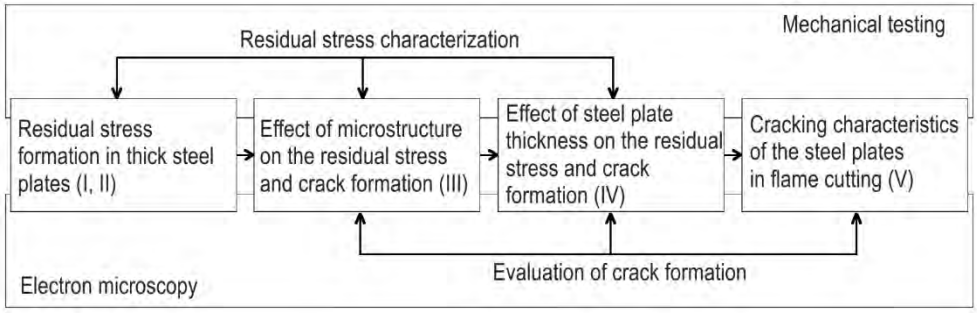

Figure 1. The structure of the research work including Publications I-V.

1.2 Research questions

The two main research questions of this thesis are as follows:

1. What are the main factors contributing to the cracking phenomenon of thick wear-resistant steel plates in the flame cutting process?

2. How can flame cutting practices and steel plate characteristics be optimized in order to avoid cracking and have an effective cutting process?

The factors include steel characteristics such as alloying, segregation, impurities, microstructure, heat treatment history, and manufacturing history. These research questions are answered and the main scientific contribution of this work is presented in Chapter 5.

2 THEORY

This chapter explains the basic theory behind this work and gives the reader a general overview of the topic. The theory is explained to make the results and conclusions more understandable.

2.1 Thick wear-resistant steel plate

Wear-resistant steels are well known for their excellent hardness, toughness, and strength. Due to these abilities, steel plate can withstand demanding conditions, like those faced for example in the mining industry (Figure 2). Typically, wear-resistant steels are exposed to the abrasive wear of soil, rocks, concrete, and other materials as they are used in crushers, materials and waste handling machinery, wear parts, and cutting plates. The qualities demanded of steel plate are durability, safety, long service life, and high performance in all typical wear applications. [1; 2] The wear resistance ability of steel plate depends mostly on its manufacturing process and chemical composition. The manufacturing of plate includes processes such as hot rolling and quenching. Hot rolling is executed for steel slabs at a specified temperature and force to ensure a certain prior austenite grain morphology and thickness for the manufactured plate. The prior austenite morphology can vary from elongated to equiaxed grains, which affects the mechanical properties of the steel. [3] The aim of quenching is to produce high hardness by means of martensitic transformation. The quenching is mainly carried out either conventionally (reheating and cooling) or by direct quenching (cooling directly on the production line). [4]

Figure 2. The mining industry is a typical application area for thick wear-resistant steel plate. [5]

As previously mentioned, the manufacture of thick wear-resistant steel plate generally aims at a martensitic microstructure, which has high hardness and strength. A martensitic microstructure can be produced by quenching, which means the fast cooling of steel having an austenitic microstructure (above ~800 °C, depending on the alloying of the steel). Martensitic transformation depends mostly on the cooling conditions, the carbon content, and the other alloying elements of the steel. Fast cooling prevents phase transformations from occurring by the diffusion mechanism (ferrite and pearlite transformations). Therefore, in fast cooling, carbon atoms do not have enough time to diffuse and they are trapped inside the solid solution of ferrite (bcc). Martensitic transformation occurs via a displacive mechanism, which includes a change in volume and high strain energy due to the trapped carbon atoms. During the transformation, the face-centered cubic (fcc) crystal structure of austenite changes to the highly strained body-centered tetragonal (bct) structure of martensite. [3; 6-8] Figure 3 presents the crystal structures of a) austenite (fcc), b) ferrite (bcc), and c) martensite (bct).

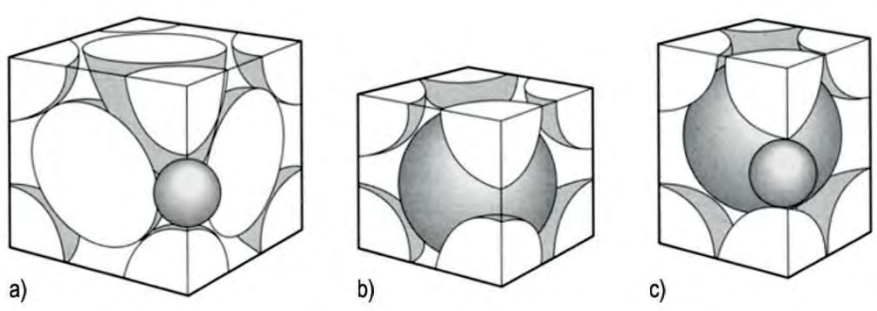

Figure 3. Crystal structures of (a) austenite (fcc), (b) ferrite (bcc), and (c) martensite (bct) (modified from [8]).

However, obtaining a martensitic structure in thick sections can be difficult, as the cooling rates may be slower in the interior. This can lead to bainite transformation, which takes place at slightly slower cooling rates compared to martensite transformation. Bainite transformation also includes a displacive mechanism. In spite of this, carbon atoms do have time to move and therefore they are not trapped as they are in martensite. [4; 9] The bainite structure consists of ferrite plates and cementite (iron carbide, Fe_3C) particles. The cementite particles are formed either between the ferrite plates (upper bainite) or mostly inside the ferrite plates and also between the ferrite plates (lower bainite), depending on the cooling rate and carbon content [7]. The bainitic structure is less strained and therefore has lower hardness compared to the martensitic structure [7; 10].

However, microstructural uniformity over the whole section of the plate and the martensite transformation can be enhanced by increasing the hardenability (i.e., ability to form martensite) of the steel. This is conventionally achieved by means of alloying elements, which suppress the diffusional transformations [3; 7]. Carbon is the main factor in increasing both the hardness and hardenability of the steel. On the other hand, large amounts of carbon also decrease the toughness and weldability of the steel. Besides carbon, other typical alloying elements that increase the hardenability are manganese, chromium, molybdenum, silicon, vanadium, and boron. In addition, the hardenability increases with increasing prior austenite grain size, as the nucleation sites of ferrite decrease. [9] However, a large prior austenite grain size is not desirable as it also leads to lower toughness [7; 11].

Moreover, the solidification process of thick plate is complex. Solidification in continuous casting can occur unevenly and can be at different stages in different depths in the thickness direction. This can lead to uneven distribution of solutes

between solid and liquid, as the solubility in the solid phase is relatively small compared to that of the liquid phase [12; 13]. Therefore, the excess solutes of the solidifying phase are rejected in the coexisting liquid phase at the solid-liquid interface, which leads to solute build-up in the liquid phase. Consequently, the final solidifying liquid phases have a significantly higher solute content compared to the nominal composition of the steel. [13] These solute-enriched regions are called segregations and they can create a layered structure in the plate. [3; 13-15] The layered structure has an effect on both the microstructure [3; 16] and the mechanical properties of the plate [14-17]. Segregations can be classified as macrosegregations or microsegregations depending on their size [18; 19]. Microsegregations are confined in microscopic areas and are often considered less harmful, as they generally contain a smaller amount of segregated atoms [18]. However, macrosegregations extend beyond microscopic and their size can vary from a few hundred to several thousand microns. They can extend throughout the length of the casting and therefore are considered to be more harmful in relation to the steel properties. [20; 21] The formation of macrosegregations is mainly caused by a build-up of microsegregations [19]. Segregations are typically located in the center of the plate and they have been shown to contain significantly larger amounts of carbon, phosphorus, and manganese compared to the nominal composition of the steel [13]. In addition, Pikkarainen et al. [22] showed that segregations have elevated concentrations of carbon, silicon, manganese, chromium, nickel, and molybdenum. Both of the latter studies showed that the amount and severity of the segregation depend on the manufacturing process of the plate [13; 22].

2.2 Flame cutting

Manufacturing and processing of thick wear-resistant steel plate involves cutting. However, the high hardness, strength, and toughness of the plate and high production rates of the steel industry set certain limitations on cutting. As the thickness, hardness, and strength of the plate increase, more energy is required for cutting. Therefore, mechanical cutting for example is not practically suitable for this kind of application as it is both difficult and slow. The most commonly applied methods for thick plate in the steel industry are thermal cutting methods such as flame cutting. Figure 4 shows some industrial flame cutting equipment.

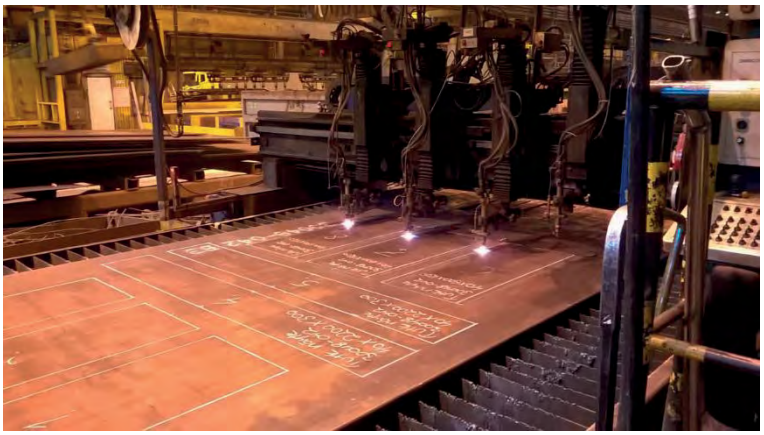

Figure 4. Industrial flame cutting equipment.

Flame cutting is performed with a heating flame and oxygen jet, which provides a continuous chemical reaction between oxygen and iron [23]. The ignition temperature of pure iron is above 870 °C and the rapid oxidation of iron occurs via three reactions [24]:

1. $Fe + O \rightarrow FeO + heat\ (267\ kJ)$

2. $3Fe + 2O_2 \rightarrow Fe_3O_4 + heat\ (1120\ kJ)$

3. $2Fe + 1.5O_2 \rightarrow Fe_2O_3 + heat\ (825\ kJ)$

The second reaction releases the most heat from the oxidation reactions. The first reaction releases the least heat and is a supplementary reaction in most cutting applications. In addition, the third reaction mostly occurs in heavy cutting applications. [24] As the reactions between oxygen and iron release heat (energy), the flame cutting process is exothermal. This generated heat maintains the cutting process and enables cutting of thick sections, which is one of the biggest advantages compared to other thermal cutting methods such as plasma and laser cutting. [25; 26]

In practice, the flame cutting process consists of three steps [23; 25; 27; 28]:

1. Steel is locally heated to its ignition temperature with an oxyfuel gas flame.

2. The heated location is then exposed to an oxygen jet, which reacts with iron forming iron oxide and creates a cut edge on the steel.

3. The oxygen jet removes the iron oxide from the cut edge and exposes the new clean surfaces for further cutting.

Flame cutting also sets certain conditions on the cut material [28]:

- The cut material must burn with pure oxygen and form fluid oxides, which can be removed from the cut edge by the oxygen jet.

- The melting temperature of the material must be higher than the ignition temperature; otherwise, the cut location melts before the ignition temperature is reached.

- The heat generated should be as high as possible. If the burning reaction does not produce enough heat, the ignition temperature cannot be maintained during cutting.

- The cut material should have low thermal conductivity. High thermal conductivity prevents reaching of the ignition temperature and thus flame cutting (for example copper).

- The melting point of the formed oxide should be lower than the melting point of the cut material.

Pure iron and most steels fulfil these conditions. The flame cuttability of steels depends on the alloying. A higher carbon content elevates the ignition temperature and therefore deteriorates flame cuttability. In addition, nickel, chromium, and wolfram worsen the flame cuttability as their oxides have high melting points. [28]

During flame cutting, the temperature gradient near the cut edge is very steep over a short distance. For this reason, a heat affected zone (HAZ) is formed at the cut edge of the plate, similarly for example to the zone formed in welding [29; 30]. HAZ contains hardness variations and microstructural changes [26; 29; 31; 32]. Higher hardness values are observed closer to the cut edge and the values decrease while going deeper the cut edge [26; 29]. During flame cutting, the structure closest to the cut edge partially exceeds the A_{c3} temperature and therefore is transformed

into austenite. During cooling, these austenitic regions are transformed into martensite or bainite, depending on the cooling rate [33]. Behind this region, the rest of the HAZ structure undergoes elevated temperatures, causing the tempering of the structure.

Tempering is generally divided into four stages [7; 34]:

- < 250 °C: martensite partially loses its tetragonality as trapped carbon atoms diffuse from the lattice. Formation of ε-iron carbide ($Fe_{2.4}C$).

- 200 – 300 °C: decomposition of retained austenite.

- 200 – 350 °C: formation of cementite (Fe_3C), which most likely nucleates in ε-iron carbide interfaces and in both interlath boundaries of martensite or prior austenite boundaries. Martensite loses its tetragonality.

- >350 °C: coarsening and spheroidizing of cementite and recrystallization of ferrite.

However, the above-described reactions are also affected by both the tempering time and the composition of the steel. In addition, there has not been any evidence of ε-iron carbide formation in the first stage of tempering in low carbon steel [35]. The aim of tempering is generally to reduce the brittleness of martensite while it also lowers the hardness and strength of the structure [3; 7].

In addition, flame cutting parameters affect the properties and width of the HAZ. A slow cutting speed produces a wider HAZ and the width decreases by increasing the cutting speed [32]. The HAZ is also wider on the top surface and the bottom side of the plate, as the cutting torch heats the upper side of the plate and the molten iron oxide heats the bottom side of the plate. [26] There have also been results [36] showing that the chemical composition of the cut edge changes during flame cutting. The content of silicon, chromium, and manganese decreased while the carbon content increased near the cut edge. This was explained by the fact that elements have different affinities to oxygen than iron has. Nevertheless, the carbon content increased due to the carburizing of the cut edge as the steel interacted with gases containing carbon compounds. [36] Other studies have also indicated increased carbon content close to the cut edge [33; 37].

2.3 Residual stresses

Residual stresses are an unavoidable by-product of almost all manufacturing processes and can also arise during service [38]. Many unexpected failures have been initiated by the presence of residual stresses combined with service stresses. Residual stresses exist in the material without external load. They arise as an elastic response to incompatible local strains in the material, for example, due to non-uniform plastic deformations. The surrounding material must deform elastically to maintain the dimensional continuity thus creating residual stresses. [39] They have a significant effect on component performance and service life [40; 41]. Generally, residual compressive stress state is favorable, as it increases fatigue resistance and prevents cracking. In contrast, residual tensile stress state is typically unfavorable and has the reverse effect. [42; 43] For example, in cracking point of view, residual compressive stresses press the structure together and therefore prevent the crack initiation and propagation. In contrast, residual tensile stresses pull the structure apart and therefore promote the crack initiation and propagation. Sometimes residual compressive stresses are introduced deliberately, for example shot peening is applied to produce compressive residual stresses in the surface layer of the components to improve their fatigue life. [41; 44; 45]

Residual stresses can be divided into three types (I, II, III) depending on their range and magnitude. Type I stresses are macrostresses, which have long-range effect and are often referred to as the most important because they equilibrate over macroscopic distances, such as components and structures. In contrast, types II and III are microstresses, which are short-range and therefore predicting their effect can be difficult. Type II stresses act on the grain scale and normally exist in a polycrystalline structure where the elastic and thermal properties between neighboring grains can vary. Type III stresses are atomic scale and are balanced within the grain. Typical sources can be dislocations or point defects in the structure. [39; 40] The residual stress types are schematically presented in Figure 5. These three residual stress types have to be considered when choosing the residual stress measuring method. Most of the material removal methods, such as hole drilling, only measure type I stresses as the shorter range stresses (type II and III) are averaged to zero in the sampling area. However, in diffraction-based measuring methods, type II stresses can be recorded superimposed on type I as the sampled area can have a particular phase or grain orientation and the stress value is derived from a specific wavelength and diffraction condition [40].

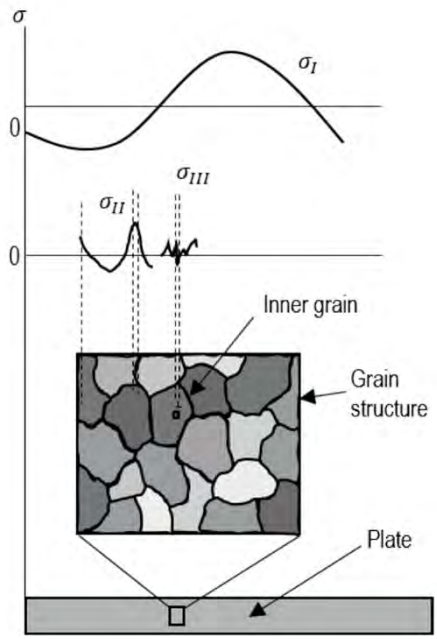

Figure 5. Residual stress types: macrostresses (σ_I) and microstresses ($\sigma_{II}, \sigma_{III}$) (modified from [40]).

2.3.1 Residual stresses in flame cutting

Flame cutting causes an uneven temperature distribution in the plate, which introduces residual stresses. In the case of flame cutting, residual stresses can be divided into two types: thermal and transformation stresses. Thermal stresses originate from the different heating and cooling rates experienced by the surface and interior of the steel plate. [7] These temperature changes cause volume expansions at the cut edge, which are constrained by cold surroundings. As the temperature rises, the yield strength of the heated region decreases and eventually the stress exceeds the reduced yield strength, leading to a plastically deformed (compressed) region near the cut surface. During cooling, the contraction of the plastically deformed surface region is restricted by undeformed regions, thus causing residual tensile stress state close to the cut edge. In contrast, transformation stresses arise from different microstructural transformations, which are accompanied by volume changes. For example, martensite transformation is known to induce volume expansion. This volume expansion can be incompatible with the surroundings,

which leads to the formation of residual compressive stress state in the martensite region and tensile stresses in the surrounding regions. [7] In both cases, residual stresses originate from volume misfits of different regions of the material [40; 41]. Residual stresses have a significant effect on the mechanical behavior of the materials or components. The magnitude of residual stresses depends on the material properties, component geometry and utilized manufacturing methods such as heat treatments and cutting processes. [46; 47]

Lindgren et al. [48] studied the residual stress state of the flame cut edges of 50 mm thick steel plates by hole-drilling strain gauge method and simulations. Close to the flame cut edge there was a narrow area of residual compressive stresses (or low tensile stresses). This compressive stress region was around 1 mm wide and after this region, the residual stress state changed rapidly to high tensile stress. The peak tensile stress values were around 2-3 mm from the flame cut edge. There were more compressive stresses and the tensile stress values were considerably lower in the preheated samples. After the tensile stress peak, the residual stresses leveled back to zero. In addition, Thomas et al. [33] studied residual stresses of flame cut steel plates with strain gauges and notch sawing. Investigations showed a narrow compressive stress area near the cut edge after which there was tensile stresses. Thiébaud et al. [49] studied residual stresses produced by flame cutting with sectioning of the plates. In their investigations, there was a high tensile stress peak near the flame cut edge, which was balanced by compressive stresses deeper in the material. Based on their results, Thiébaud et al. [49] concluded that the three main factors affecting residual stress formation are heat input, plate geometry, and previous residual stress state. Zhiyuan et al. [50] studied the factors affecting residual stress distribution, i.e., cutting speed, cutting dimensions, and constraint conditions by simulations and impact-indentation stress measurement method. The residual tensile stresses were distributed over quite a narrow zone and the width of the tensile stress zone decreased with increasing cutting speed. The maximum values of the tensile stress were not changed much by different cutting speeds. [50]

2.4 Residual stress measurement methods

The measurement of residual stresses is challenging, as they exist inside the material. In addition, residual stresses can be rather local which further complicates the measurements. The measurements are indirect as strain or the displacement is measured, from which the stresses are subsequently interpreted. Figure 6 shows the

variety of different residual stress measuring methods, their depth penetrations, and spatial resolutions. Residual stress measurement methods can be divided into destructive testing and non-destructive testing (NDT). [39]

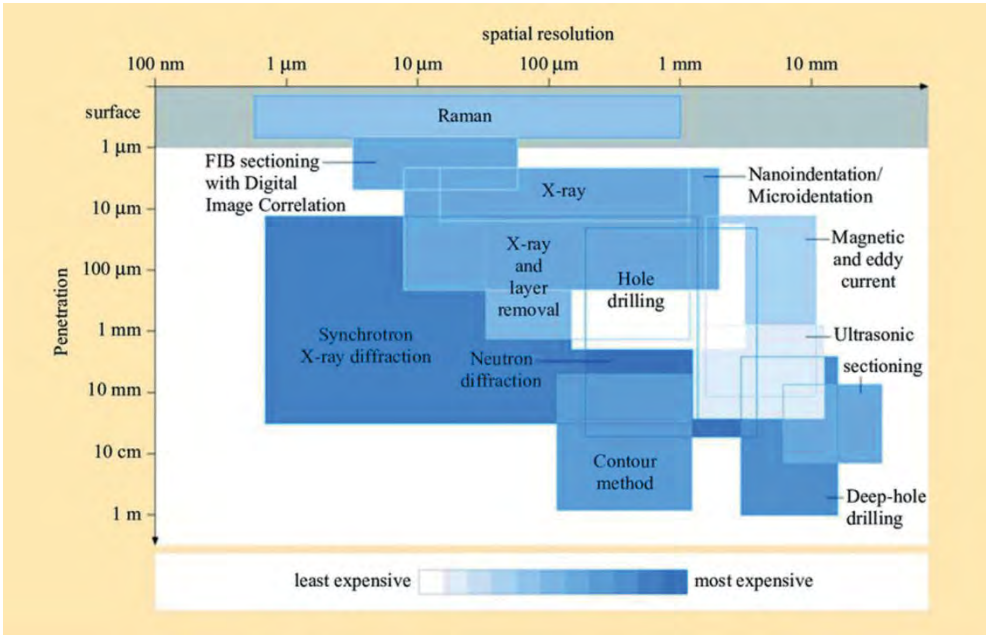

Figure 6. Different residual stress measurement methods and their depth penetration vs. spatial resolution [39].

Destructive methods are based on the relaxation of the residual stresses by cutting or material removal. This relaxation or elastic deformation exhibits a relationship between material deformation and released residual stresses. This is the basic concept of destructive methods and there are many different technologies for cutting and measuring the deformations. [39] Typical examples of destructive methods are hole drilling and sectioning. These mechanical measuring methods are necessarily destructive and therefore cannot be directly checked by repeat measurement. In addition, their spatial and depth resolution are less than those of X-ray diffraction. [51]

Hole-drilling method

The hole-drilling method [52] is probably the most commonly applied destructive technique for measuring residual stresses. It includes drilling a small hole into the surface of the sample and measuring the deformations of the surrounding surface. The deformations are traditionally measured by strain gages or using optical techniques. Hole-drilling method is widely used as it is quite fast and gives reliable results from different types of samples. [39] Several studies [53-55] have used the hole-drilling method effectively for residual stress determination.

Sectioning method

The sectioning method involves sequential cutting of the sample. The deformations of the sample are typically measured by strain gages, which are placed on the sample before cutting. The deformations measured from the various parts provide information which can be used to determine both the amount and the location of the original residual stresses. [39; 56; 57]

Non-destructive techniques (NDT) such as diffraction methods measure residual stresses without any cutting or sectioning of the sample. Therefore, the sample can remain in service after the residual stress measurement. Diffraction methods are based on the ability of electromagnetic radiation to measure the distance between atomic planes in crystalline or polycrystalline. The methods can effectively measure inter-planar crystal dimensions, which can be related to the magnitude and directions of the residual stresses existing in the material. Examples of diffraction methods are X-ray diffraction, synchrotron X-ray, and neutron diffraction. [39]

X-ray diffraction

X-ray diffraction (XRD) methods are some of the most commonly used techniques to determine residual stresses. These methods enable the measurement of the inter-atomic lattice spacing, which contains information on the strains from the irradiated location. The strains can be used to determine the residual stress state of the material. XRD is considered to be a surface stress measurement method as the applied wavelengths are capable of penetrating only a few microns into most materials. [39; 51] XRD techniques have been used, for example, to measure residual stresses from the surface of thick plate welds as they provide rapid, accurate, and high-resolution results [58]. The X-ray diffraction method used in this research is described more precisely in section 3.2.1.

Synchrotron diffraction

Synchrotron diffraction applies X-rays in a similar fashion to the traditional XRD method. However, the X-rays are much more intense and possess higher energy and therefore penetrate deeper into the material (tens or even hundreds of mm). This enables measuring of the bulk stresses of the samples. The source of these X-rays are at synchrotron facilities and the commonly used X-rays have energy greater than 50 kV. This method is not considered to be as accurate as for example XRD. [39] However, the development of detector technology has made the synchrotron method more possible by increasing precision in energy measurements [59].

Neutron diffraction

As with the previous method, neutron diffraction utilizes penetrating radiation to measure residual stresses. However, the neutrons interact directly with the nucleus of the atom as the X-rays interact with the electrons and therefore the contribution to the diffraction intensity is different. In addition, neutrons penetrate low Z (atomic number) and high Z materials equally well. The penetration depth of the neutrons is several centimeters and therefore the method can be used to measure the residual stresses inside the material without any sectioning. However, deeply penetrating methods, such as synchrotron X-ray and neutron diffraction, require precisely known unstressed lattice spacing of the measured crystallographic planes, as measured stress state is tri-axial. [39; 60] Neutron diffraction method has been used, for example, to investigate residual stress state in thick welded steel plates [61; 62].

As shown above, there are many possible methods to measure residual stresses and many factors have to be considered when choosing a suitable method: Why are residual stresses measured? Can the specimen be destroyed during the measurement? What is the specimen material, dimensions, and shape? Are measurements taken in the laboratory or in the field? What equipment and experience are available? Moreover, what is the location of the residual stresses (surface or interior)? [39]

There are not many studies related to the residual stress formation in the flame cutting. Previously, hole-drilling and sectioning methods were utilized to study residual stresses formed in flame cutting [48; 49]. However, residual stress measurements are mostly used as verification for modeling the residual stress state [48; 50]. Lindgren et al. [48] applied hole drilling with the strain gage method to determine the residual stresses from a flame cut edge. The measurements were performed in nine locations around the flame cut surface and the results were used

to verify the results of the model. Thiébaud et al. [49] utilized a sectioning method to study the residual stress formation of thick steel plates during flame cutting. 60 mm thick plates were sectioned into 10 and 20 mm wide strips to determine the residual stress state of the plate. However, the residual stress measurement methods utilized in above described studies have challenges for measuring residual stresses in flame cutting. Hole-drilling and sectioning methods are destructive methods and therefore measurements cannot be repeated. In addition, the accuracy and resolution of these methods do not necessarily match the residual stress state of flame cut steel plate.

2.5 Crack formation in thick steel plates due to flame cutting

In the worst case scenario, flame cutting causes cracks at the cut edge of steel plates. Typically, cracks are formed in the center region of the plates at the cut edge. In most cases, the cracks are small (~0.5-2 mm) and just beneath the cut edge. They are not open to the surface and therefore can only be detected with non-destructive ultrasonic inspections. However, sometimes the cracks could also be propagated catastrophically throughout the whole plate. Cracking is presented schematically in Figure 7. The cracking tendency increases as the plate hardness and thickness increases. However, it has been noticed that preheating lowers the residual tensile stresses and prevents cracking. Cutting without preheating creates large tensile stresses at the cut edge and results in cracking. [48] The cracking in flame cutting is sometimes called cut edge cracking and it has been suggested that it might also be related to hydrogen cracking [63]. In addition, the cracking of martensitic steels is often related to tempered martensite embrittlement (TME) [3; 64; 65] or temper embrittlement (TE) [3; 7; 64; 66]. Attempts have been made to overcome cracking in flame cutting in several ways: by changing the process gas [32; 67], reducing the cutting speed [63], and applying preheating [48; 63].

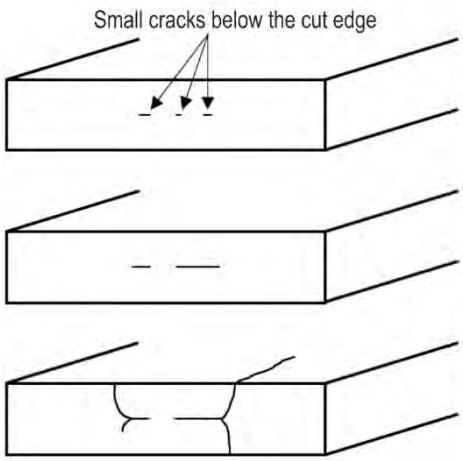

Figure 7. Crack formation in thick steel plates in flame cutting (modified from [68]).

Hydrogen can be very harmful to steel and can lead to steel part failures. This phenomenon is known as hydrogen embrittlement and has been widely studied [69-72]. Hydrogen may lead to damage whenever it is involved with metal during manufacturing. Hydrogen is highly mobile and soluble in molten steel and can be trapped inside the metal at high cooling rates [38]. Diffusible hydrogen is especially harmful and can lead to cracking or dramatic loss of toughness in steels. The stronger and harder the steel, the more susceptible it is to hydrogen embrittlement. Hydrogen atoms are attracted to stress concentrations such as crack tips. [7] In addition, the detrimental effects of the hydrogen are often enhanced with combination of residual tensile stresses. Hydrogen embrittlement can cause delayed cracking, which can occur even after a long period of time. [73] It can be avoided by controlling the hydrogen levels, the magnitude of the residual stresses, or the hardness of the local microstructure at the potential crack initiation sites [38].

Martensitic steels exposed to elevated temperatures are susceptible to TME or TE. The danger of TME comes from tempering at around 300 °C and it is associated mostly with the formation of hard and brittle cementite in the interlath sites of martensite or in the prior austenite grain boundaries. Therefore, it lowers the toughness of the steel. In TME, the fracture surface is mostly transgranular (through the grain). In contrast, TE occurs at around 500 °C and is mostly related to the accumulation of impurity elements, such as antimony, phosphorus, tin, or arsenic, at the prior austenite grain boundaries, thus reducing the toughness of the steel. TE is usually more severe with steel containing a greater amount of alloying elements than

plain carbon steels. The fracture caused by TE is intergranular and depends on the co-segregation of substitutional alloying elements, which generally requires high temperatures and long times for diffusion, and impurity atoms at the prior austenite grain boundaries. The danger of TME and TE lies not only in these harmful temperature ranges but also slow cooling through these ranges can cause embrittlement of the steel. [3; 7; 64]

3 MATERIALS AND METHODS

This chapter introduces the materials studied in this work. In addition, the experimental procedures are described so that the origins of the results of the work will be more understandable.

3.1 Materials

A trial batch of thick wear-resistant steel plates was manufactured at SSAB Europe Oy Raahe Steelworks (formerly Ruukki) for this study. The plates were hot-rolled using two different parameters (A, B), where steel plate A was hot-rolled above 900 °C and steel plate B was hot-rolled below 900 °C. The hardness of the steels was 400 HV and the plates were manufactured in three different thicknesses: 20, 40, and 60 mm. The plates were sectioned into smaller pieces as shown in Figure 8. These pieces were then flame cut utilizing an oxyfuel propane gas flame and different flame cutting parameters such as different cutting speeds and preheating (performed in an industrial furnace under normal atmosphere). The length and width of the flame cut samples were 150 mm. Examples of a flame cut sample and the original plate are shown in Figure 8.

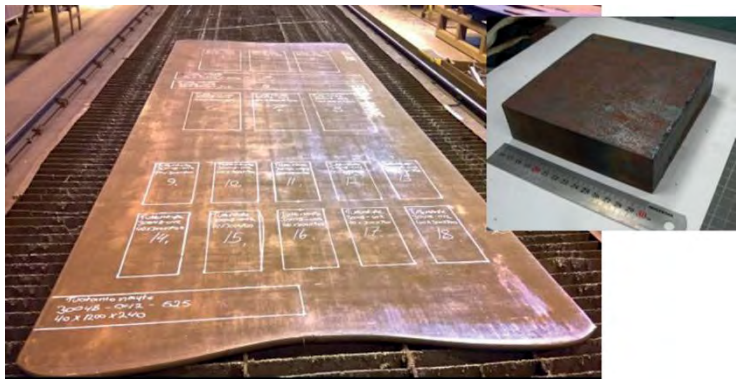

Figure 8. Wear-resistant steel plate with sectioning plan and an example of studied flame cut sample.

The compositions (analyzed by optical emission spectrometry (OES)) of the studied samples are listed in Table 1. In addition, glow discharge optical emission spectroscopy (GDOES) profiles were measured from some of the flame cut surfaces. The measurements were carried out using a GDA 750/GDA 550 spectrometer.

Table 1. Compositions of studied steels.

Thickness	C%	Si%	Mn%	Cr%	Mo%	Al%	Ni%	V%	Ti%	P%
20 mm A	0.14	0.60	1.08	0.61	0.41	0.043	0.20	0.041	0.017	0,01
40 mm A	0.15	0.62	1.10	0.62	0.42	0.048	0.20	0.042	0.017	0.01
40 mm B	0.14	0.55	1.05	0.57	0.36	0.044	0.19	0.039	0.015	0.01
60 mm A	0.16	0.61	1.09	0.61	0.40	0.047	0.20	0.040	0.016	0.01
60 mm B	0.14	0.60	1.07	0.60	0.40	0.043	0.20	0.040	0.015	0.01

Ultrasonic inspection

After flame cutting, the samples were inspected by ultrasound using Phasor XS 16/16 Olympus ultrasonic equipment (Figure 9) and a MSEB 4 dual probe (4 MHz). The ultrasonic inspection results were verified by two separate researchers and by sectioning some of the samples after inspection. Figure 10 shows an example of an inspection view of an intact and a cracked sample. The inspection view of the intact sample shows only the back wall echo peak. However, the view of the cracked sample shows another peak besides the back wall echo peak. This smaller peak is from the crack and the peak location indicates that the location of the crack is in the central region of the plate.

Figure 9. Ultrasonic inspection equipment (Phasor XS 16/16 Olympus).

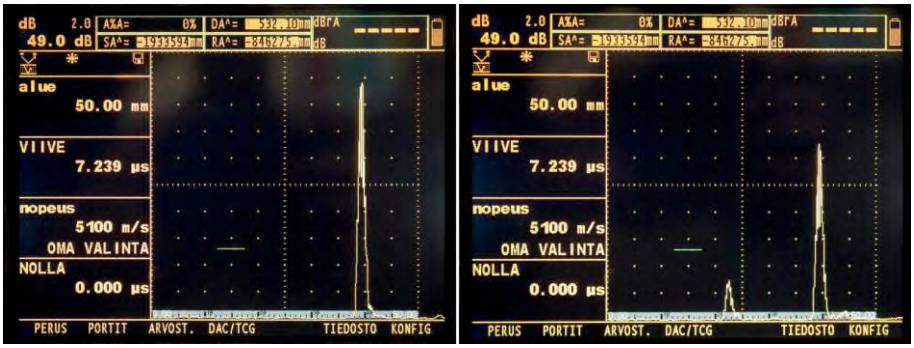

Figure 10. Inspection view of intact sample (left) and sample with defect (right).

3.2 Material characterization

3.2.1 Residual stress measurements

Residual stress measurements of the flame cut samples were performed by the X-ray diffraction method (XRD). The equipment used was XStress 3000 (Stresstech Oy), shown in Figure 11.

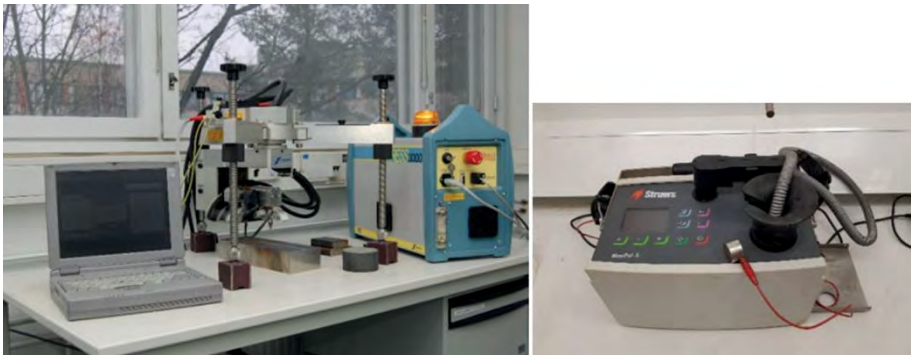

Figure 11. On the left, the residual stress measurement equipment (XStress 3000) and on the right, the electropolishing machine (Movipol 5).

The measurement method is known as the modified Chi method [74], which is based on Bragg's law:

$$2dsin\theta = n\lambda \quad (1)$$

where d is the interplanar lattice spacing, θ is the diffraction angle, n is the integer constant (1, 2, 3…), and λ is the wavelength of the X-rays. The measuring of residual stresses is established on the calculation of the interplanar lattice spacing of the ferrite [211] plane from Bragg's diffraction angle of 156°. The lattice plane spacing changes from a stress-free value to some other value, depending on the residual stress affecting the measurement location. For example, the lattice spacing is stretched by residual tensile stress and shortened by compressive stress. The lattice spacing d is measured using different ψ tilts, where the ψ is the angle between the normal of the specimen and the normal with the diffracting plane. The measured d values form a slope as a function of $\sin^2\psi$, which can be used with elastic constants to calculate the residual stresses from the measured location. Residual stresses are calculated using the following equation [75]:

$$\sigma = \left(\frac{E}{(1+\vartheta)}\right) m \quad (2)$$

where σ is the residual stress in the measurement direction, E is Young's modulus of the measured steel, ϑ is Poisson's ratio, and m is the slope from the lattice spacing d vs. $\sin^2\psi$ curve. The steeper the gradient m, the higher the residual stress level in the measurement location. The measurement parameters are shown in Table 2.

Table 2. Residual stress measurement parameters.

Parameters:			
ϕ rotations (measurement directions)	0° and 90°	Modulus of elasticity	211 GPa
Collimator	3 mm	Poisson's ratio	0.3
ψ tilt angles in one direction (side / side)	6 / 6	Voltage	30 kV
Maximum tilt angle	40°	Current	6.7 mA
ψ oscillation	5°	Radiation	CrKα

The residual stress measurements were performed in the centerline of the samples in two perpendicular directions (ϕ): the flame cut direction (0°) and the thickness direction (90°). These directions were chosen because they are the most critical

orientations for crack formation. In particular, residual stresses in the thickness direction are critical for cracking and for that reason they are the focus of this work. Measurement directions and locations are presented in Figure 12.

To provide residual stress-depth profiles from the samples, the residual stress measurements were combined with electrochemical polishing (Movipol 5, Figure 11) to remove material from the measurement locations. Electrochemical polishing is one of the gentlest ways to remove material layers without disturbing the existing residual stress state in the sample [76]. The polishing was carried out using Struers A2 electrolyte (a mixture of 60 % perchloric acid, 65-85 % ethanol, 10-15 % 2-butoxyethanol, and 5-15 % water) and the depth of the material removal was verified with a dial indicator. The bottom of the polished location was monitored during the making of the profiles for any irregularities that may affect to the results. The residual stress measurement results were analyzed with XTronic software and the analyzed results were used to plot the residual stress-depth profiles.

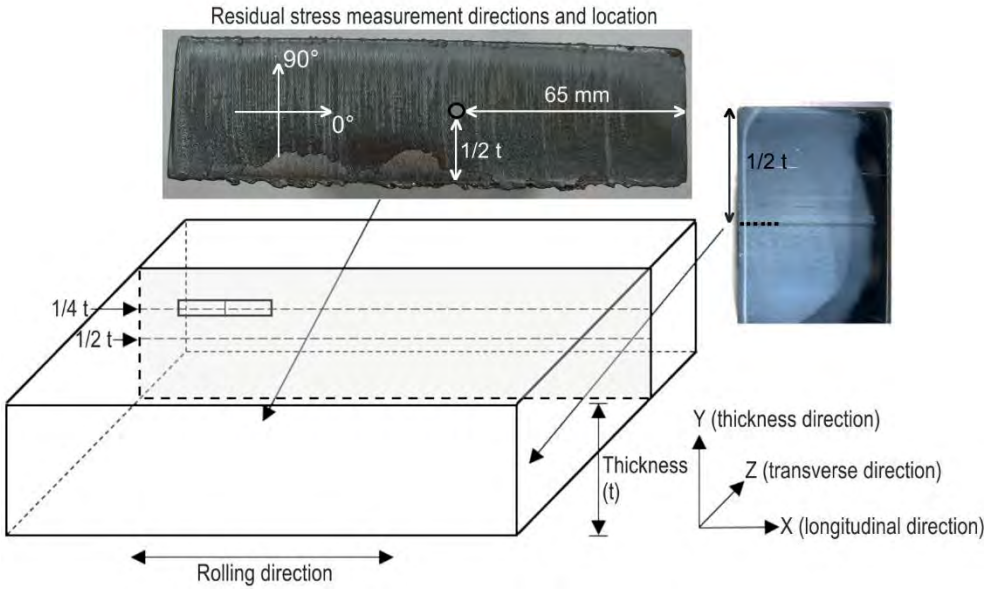

Figure 12. Test locations and directions on the steel plate.

3.2.2 Electron microscopy

The flame cut samples were sectioned for microstructural analysis performed with scanning electron microscopes (SEMs). The sectioned samples were ground using abrasive silicon carbide papers and polished with 3 and 1 μm diamond suspensions. After grinding and polishing, the samples were etched with 4 % Nital solution. The microstructural characterization was performed with a Philips XL-30 SEM and an ULTRAplus field emission SEM (ZEISS) equipped with an X-MaxN 80 (Oxford Instruments) Energy Dispersive X-ray Spectrometer (EDS). In addition, the samples were analyzed using a SEM with an HKL Premium-F Channel Electron Backscatter Diffraction (EBSD) system equipped with a Nordlys F400 detector. These EBSD samples were sectioned and ground with abrasive silicon carbide paper and then polished with a colloidal silica suspension (0.004 μm). The acceleration voltage used was 20 kV and the step size 0.1 μm in the cross-sectional EBSD analysis areas of 209 by 144 μm. The EBSD data from the microstructure was a starting point for the reconstruction of the prior austenite grain boundaries, which is described in more detail in publication III. The reconstruction was made with a Matlab-based iterative algorithm, originally developed by Nyyssönen et al. [77].

In addition, precipitates in the microstructure were analyzed with a JEM-2010 transmission electron microscope (TEM) equipped with a Noran Vantage Si(Li) detector EDS. The TEM samples were prepared using the extraction replica technique: the sectioned sample was polished in a traditional metallographic manner and then etched (Nital 4 % solution) to remove the matrix so that the precipitates stood proud of the sample surface. After etching, a carbon film was evaporated on the surface of the sample and then scored into ~1 mm^2. Then the etching was continued to dissolve the matrix, and the carbon film squares carrying the precipitates were floated in distilled water and collected on copper TEM grids.

3.2.3 Mechanical tests

This section introduces the mechanical tests carried out during this study. The tests were used to evaluate the mechanical properties of both the original structure and the flame cut edge of the steel plates. The test locations and directions are presented in Figure 12 and the sample geometries in Figure 13. Tests were performed at Tampere University (formerly Tampere University of Technology) and the SSAB Europe Oy Raahe Steelworks (formerly Ruukki).

Hardness tests

Hardness profiles were carried out for both the original steel structures and flame cut samples. For the original steel structure, the hardness profiles (HV 5 kg) were performed in the thickness direction of the steel plate and measurements were carried out using a Struers DuraScan 80. For the flame cut samples, the measurements were hardness depth profiles (HV 0.2 kg) starting from the flame cut surface (Figure 12). The hardness depth profiles were performed using a Matsuzawa MMT-X7 digital microhardness tester.

Tensile tests

Tensile tests were performed in the thickness direction of the plates. The tests were carried out with an MTS 250 kN, according to the EN-ISO 6892-1 standard [78]. The test samples were round bars with the original diameter (d0) of 6, 10, and 10 mm and the parallel length (Lc) of 11, 22, and 42 mm for the plate thicknesses of 20, 40, and 60 mm, respectively. The sample geometry is presented in Figure 13a.

Charpy-V impact tests

The Charpy impact tests were carried out according to the EN-ISO 148-1 standard [79] and the samples were square bars with dimensions of 10 mm x 10 mm x 55 mm. The sample geometry is presented in Figure 13b. The studied samples were in longitudinal and transverse directions in relation to the rolling direction, and the test temperatures were -40 °C, -20 °C, -10 °C, 0 °C, and 20 °C. In addition, the 40 and 60 mm thick plates were tested at ½ and ¼ thickness in both longitudinal and transverse directions. The 60 mm plates were also tested with samples made in the thickness direction at temperatures of -10 °C, 0 °C, 22 °C, and 60 C°. These tests were made for both the original and the heat-treated structures of the plate. The heat treatments were designed to resemble the structure of the tempered region of the flame cut edge as much as possible and were done in a furnace under normal atmosphere. Samples were retained for 70 minutes at a temperature of 300 °C. Each of the Charpy-V impact test results shown in this study is an average of at least three repetitions.

Fracture toughness tests

Fracture toughness tests were performed to the samples made in the thickness direction for the 60 mm plates according to the ASTM E1820 standard [80]. The tests were carried out at temperatures of -40 °C, -20 °C, 0 °C, and 22 °C and the presented results are an average of three tests. The sample dimensions were 10 mm x 10 mm x 60 mm, the notch length (a_0) was 3 mm, and the crack length extended approximately to a depth of 5 mm in the sample. The sample geometry is presented in Figure 13c. Tests were carried out on both original and heat-treated samples. The heat treatment was performed under normal atmosphere in a furnace and the samples were kept for 70 minutes at temperatures of 300 °C and 600 °C to resemble the temperatures of the tempered region of the cut edge. These temperatures were chosen as they are often critical and cause tempered martensite embrittlement (300 °C) and temper embrittlement (600 °C).

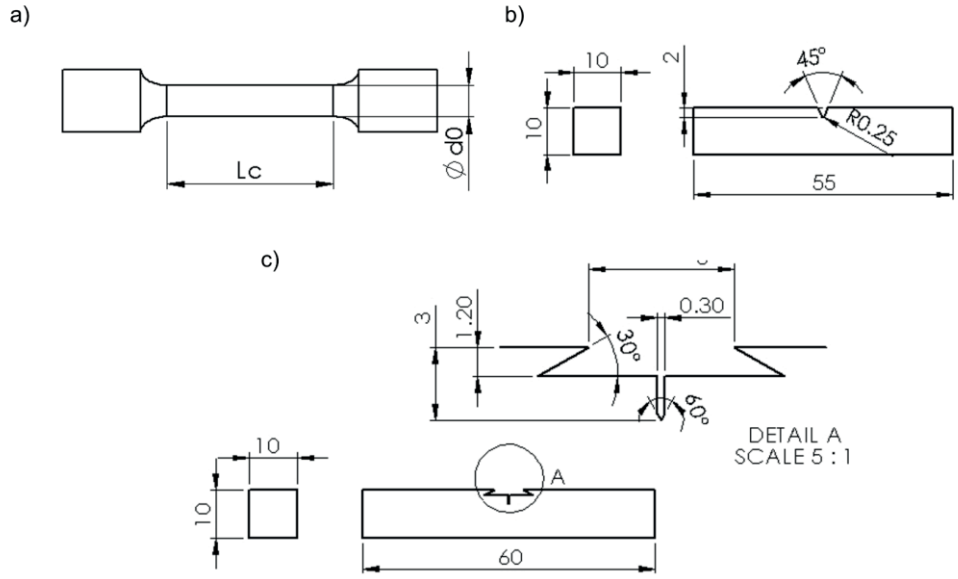

Figure 13. Sample dimensions (mm) of a) tensile tests, b) Charpy-V impact tests, and c) fracture toughness tests.

4 RESULTS AND DISCUSSION

This chapter summarizes and discusses the main results of the whole study and the five articles related to this work. Some unpublished findings are also presented.

4.1 Residual stress formation in thick steel plates

Flame cutting of thick wear-resistant steel plates causes a steep thermal gradient, which creates a heat affected zone (HAZ) at the cut edge. Therefore, both volume and microstructural changes occur in the HAZ, which causes residual stresses at the cut edge. Residual stresses formed in flame cutting can be divided into thermal stresses and transformation stresses depending on their origin. The residual stress profile measured from the flame cut sample is the sum of these two residual stresses.

Thermal stresses

Flame cutting causes an uneven temperature distribution at the cut edge of the steel plate. Figure 14 presents the simulated temperature curves formed during flame cutting at speeds of 150 and 300 mm/min (40 mm thick plate). The faster cutting speed creates a steeper temperature profile compared to the lower cutting speed.

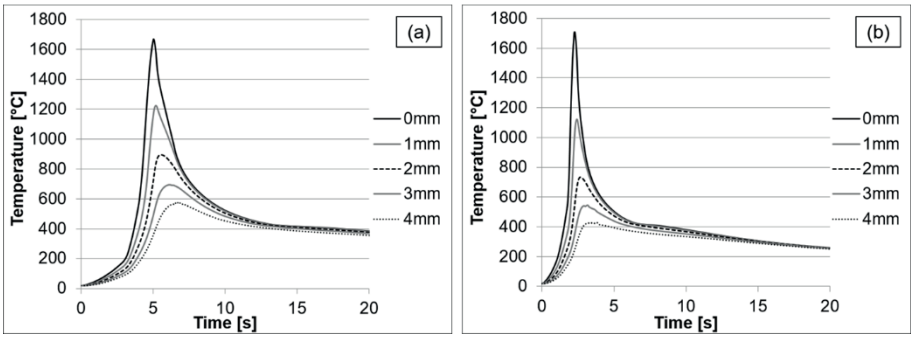

Figure 14. Simulated temperature curves from different distances from the flame cut edge at (a) 150 mm/min and (b) 300 mm/min cutting speeds (Publication II).

Rapid temperature changes create differing degrees of thermal expansion and contraction at the cut edge and consequently residual thermal stresses. The temperature rise causes volume expansion at the cut edge, which is constrained by the cold interior and therefore creates compressive stress state near the cut edge. However, with increasing temperature, the yield limit of the material lowers. Eventually the compressive stresses exceeds the yield limit and produces a plastically deformed (compressed) region near the cut edge. During cooling, the contraction of this plastically compressed region is restrained by the undeformed interior. Therefore, the deformed region near the cut edge contains high residual tensile stresses (thermal), which are balanced by compressive stresses deeper in the subsurface. Figure 15 presents the simulated thermal stress distribution (without any phase transformations) formed during flame cutting at speeds of 150 and 300 mm/min (40 mm thick plate).

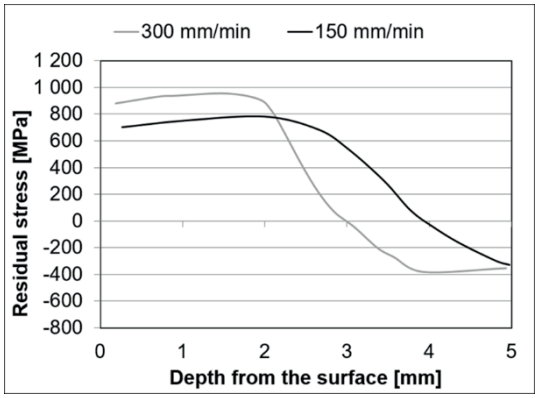

Figure 15. Simulated thermal stresses (without phase transformation) generated during 150 and 300 mm/min flame cutting speeds (modified from Publication II).

Figure 15 shows that the faster cutting speed produces higher thermal stress state at the cut edge compared to the lower cutting speed. The reason for this is that the faster cutting speed creates higher temperature differences between the cut edge and the cold interior and consequently higher thermal stresses.

Transformation stresses

The high temperatures and fast cooling during flame cutting cause microstructural changes in the HAZ. These microstructural changes are accompanied by local volume changes and therefore generate transformation stresses at the cut edge. To understand the generation of transformation stresses, it is important to identify the different microstructural regions formed at the cut edge.

Three distinct microstructural regions (presented in Figure 16) can be identified from the cut edge: newly formed martensite (1.), two-phase region (2.), and tempered original structure (3.).

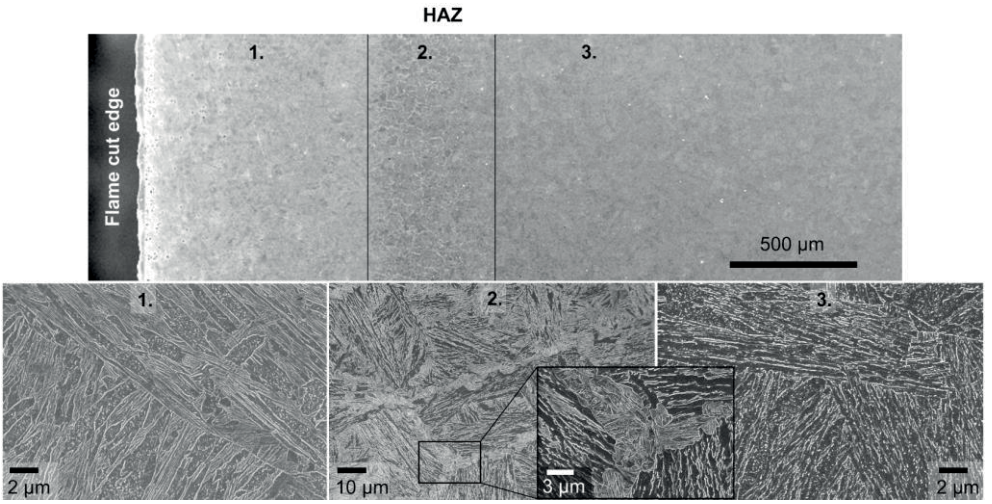

Figure 16. SEM micrographs of the heat affected zone (HAZ) showing the newly formed martensite region (1.), two-phase region (2.), and tempered original structure (3.).

The first region, closest to the cut edge, is fully austenized (temperature above A_{c3}) and during fast cooling transforms into martensite. The second region is partly austenized (temperature above A_{c1}) during the cutting process and in cooling the austenized regions transform into martensite while the rest of the structure is heavily tempered. The austenization in the two-phase region occurs heterogeneously in the prior austenite grain boundaries, which highlights the prior austenite grain morphology. The third region is the original structure, which undergoes elevated temperatures during flame cutting and is therefore tempered. The tempering effect gradually decreases while penetrating deeper into the subsurface. These regions not only create the transformation stresses but also affect the hardness profiles of the

cut edges (presented in Publications I, III, IV, V). Newly formed martensite has the highest hardness and the hardness is reduced in the two-phase region. Hardness starts to rise towards the end of the HAZ as the tempering of the cut edge gradually decreases.

The martensite transformation near the cut edge is accompanied by volume expansion. This volume expansion relieves the thermal tensile stress state (shown in Figure 15) near the cut edge and produces compressive stress state. The amount of compressive stresses produced depends on the thermal stress state before the transformation. The less thermal tensile stresses before martensite transformation, the more compressive stresses after martensite transformation. The compressive stress state changes to tensile stress in the two-phase region and the tensile stress peak is formed in the tempered region.

How to affect residual stress formation in flame cutting

Temperature differences (causing thermal stresses) and microstructural transformations (causing transformation stresses) can be affected in flame cutting by different flame cutting parameters. As previously described, thermal stresses can be reduced by choosing the cut parameters which create low temperature differences between the cut edge and the cold interior. As Figure 15 showed, the lower cutting speed produced less thermal tensile stresses than the faster cutting speed. If the whole plate were at the same temperature during flame cutting, there would be no thermal stresses as the volume expansion and contraction would be harmonized. However, this is practically impossible, so the best way is to aim for the lowest possible thermal stress state during cutting. Thermal stresses can be reduced by lowering the cutting speed and applying preheating before flame cutting. Both of these actions lower the temperature difference between the cut edge and the interior, and therefore generally result in higher and wider compressive stress region and lower tensile stress peak. Preheating is preferable to a lower cutting speed as the tensile stresses are generally lower in preheated samples. Figure 17a shows the experimentally measured residual stress states of the most generally applied flame cut parameters: slow cutting speed (150 mm/min), fast cutting speed (300 mm/min), and cutting with preheating (300 mm/min with 250 °C preheating). In addition, Figure 17b presents the extreme ends of flame cut parameters: 500 mm/min and 150 mm/min with 200 °C preheating. Figure 17 shows that the highest compressive stress state can be achieved by decreasing the cutting speed and applying preheating.

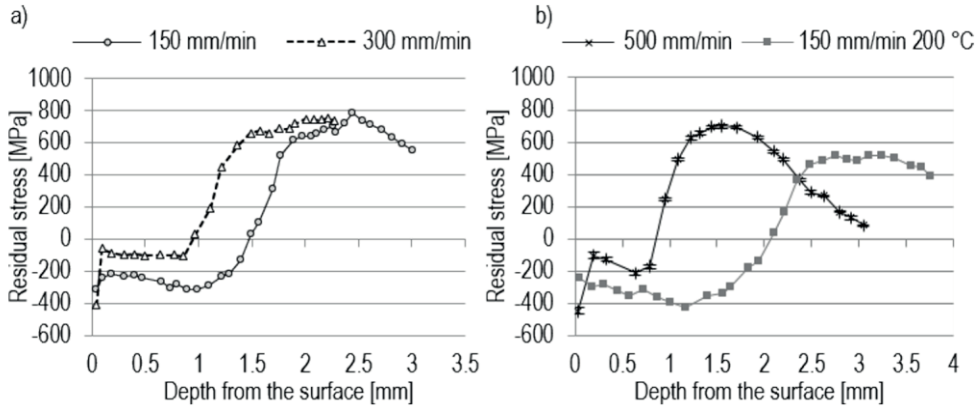

Figure 17. Effect of different flame cut parameters on residual stress formation: (a) Residual stresses of generally applied cutting parameters and (b) extreme ends of flame cut parameters (modified from Publications I and II).

In addition, the width of different microstructural regions in the HAZ can be affected by the flame cutting parameters, which also affects the width of the residual stress regions. The wider the newly formed martensite region, the wider the compressive stress region. In addition, the wider the two-phase region, the less pronounced the change from compressive stress to tensile stress. The width of the microstructural regions can be increased by raising the heat input during flame cutting, which can be achieved with a lower cutting speed and preheating. To generate the optimal residual stress state (i.e., higher and wider compressive stress region and lower tensile stress peak) during flame cutting, it is recommended to combine a low cutting speed and preheating. Figure 18 shows the effect of the preheating temperature on residual stress formation in flame cutting. Increasing the preheating temperature creates more compressive stresses and less tensile stresses. However, it should be noted that preheating also reduces the hardness of the plate.

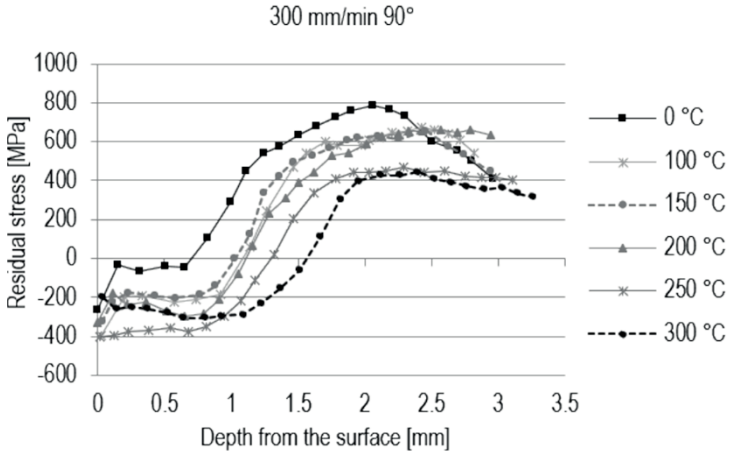

Figure 18. Effect of preheating temperature on residual stress formation in flame cutting.

4.2 Effect of microstructure on residual stress and crack formation

The manufacturing of wear-resistant steel plates generally aims at a martensitic microstructure and certain hardness, in this case 400 HV. However, the hardness level can also be reached with a microstructure that is a mixture of martensite and bainite, as shown in Publication III. In addition, manufacturing methods A (hot-rolled above 900 °C) and B (hot-rolled below 900 °C) resulted in different steel microstructures, presented in Figure 19.

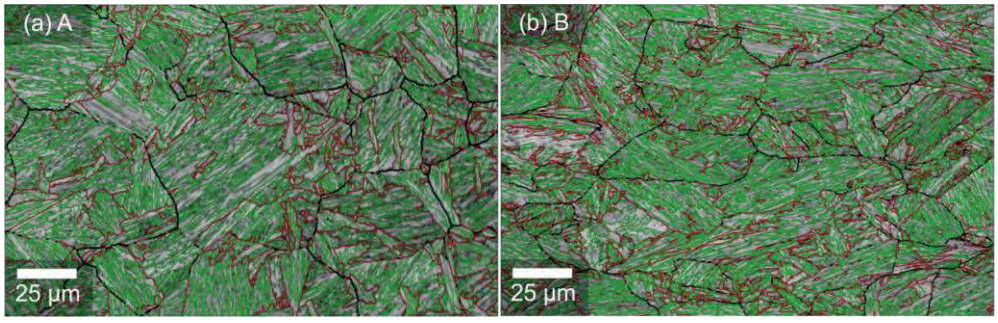

Figure 19. Reconstructed prior austenite grain boundary (PAGB) maps for samples (a) A and (b) B. PAGBs are superimposed on EBSD band contrast images as black lines. The red and green lines show the packet and block boundaries of martensite, respectively (Publication III).

The main difference between steels A and B lay in the prior austenite grain morphology. Steel A mainly consisted of equiaxed prior austenite grains with a few packet boundaries inside the grains. In contrast, steel B consisted of horizontally elongated prior austenite grains with more packet boundaries. Similar observations of the prior austenite grain morphology can be made from the two-phase regions of the samples, where the newly formed martensite highlights the prior austenite grain boundaries. Figure 20 shows examples of the two-phase regions of steels A and B, which were flame cut using a cutting speed of 300 mm/min.

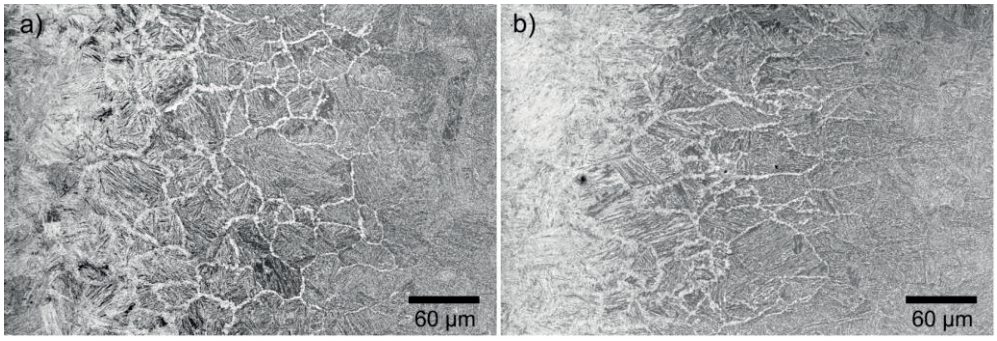

Figure 20. Two-phase regions of steels (a) A and (b) B flame cut at 300 mm/min. Chains of newly formed martensite highlight the prior austenite grain boundaries (modified from Publication III).

The prior austenite grain morphology seems to have an effect on the residual stress formation during flame cutting. Steel A generated lower tensile stress peaks during flame cutting compared to steel B, as shown in Figure 21. The residual stress results for steel A and steel B indicate that the equiaxed prior austenite grain structure produces less tensile stresses at the cut edge than the elongated prior austenite grain structure. It has been proposed [81] that the dislocation pile-ups existing in the vicinity of grain boundaries affect the local residual stress levels by creating a local stress peak in the grain boundary. In addition, it was noticed [81] that the residual stress levels monotonically decreased with increasing distance from the grain boundary. Therefore, one possible explanation could be that steel B has more prior austenite grain boundaries in the vertical direction compared to the equiaxed grain structure of steel A, which might create more local stress peaks in the structure. In addition, the elongated shape of the grains indicate that the structure contains more dislocations than the equiaxed prior austenite grain structure. As a result, the local stress peaks formed at the grain boundary level (type II residual stresses) might increase tensile stress state in the measured residual stress profiles (type I residual

stresses), thus creating higher tensile stress levels in steel B (elongated grain structure) compared to steel A (equiaxed grain structure).

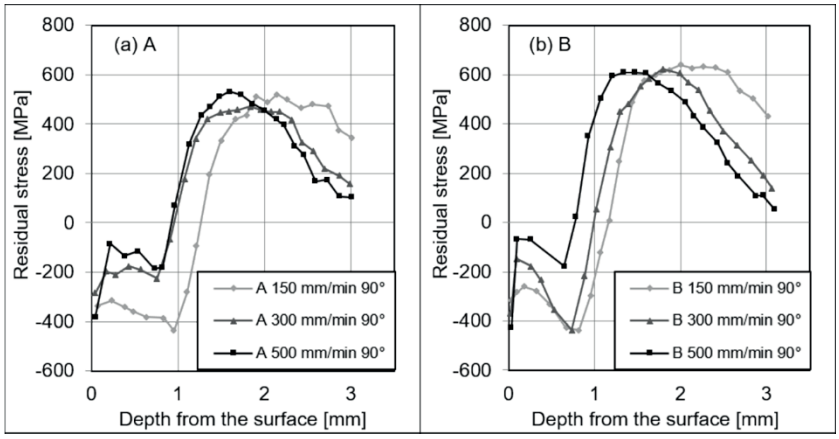

Figure 21. Residual stress profiles (thickness direction) measured for steel samples (a) A and (b) B at cutting speeds of 150, 300, and 500 mm/min (Publication III).

In addition, steel B is more susceptible to cracking than steel A as shown by the ultrasonic inspections in Figure 22. The reason for the higher cracking probability of steel B is the prior austenite grain morphology together with high residual tensile stresses. It has been shown [82] that the prior austenite grain boundaries are the most effective barriers for crack propagation as they have relatively high angle boundaries compared to other boundaries. It was also observed [82] that the crack changed direction as it encountered the prior austenite grain boundary. However, the horizontally elongated prior austenite grain boundaries in steel B create more potential crack paths through the structure instead of acting as obstacles and preventing crack propagation. In contrast, the equiaxed prior austenite grain structure of steel A has more vertical boundaries, which can act as barriers to horizontal crack propagation.

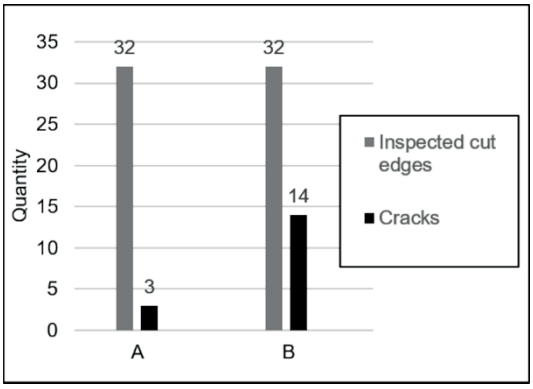

Figure 22. Ultrasonic inspected flame cut samples of steels A and B (modified from Publication III).

4.3 Effect of steel plate thickness on residual stress and crack formation

The cooling of different plate thicknesses produces different microstructures, as shown in Publication IV. Fast cooling is more uniform along the thickness direction with thin plates and therefore the produced microstructure is martensitic. However, with thicker plates the cooling in the middle section can be much slower compared to the upper and lower edge of the plates. Fast cooling at the edges results in a martensitic microstructure but slower cooling in the middle section produces a mixture of bainite and martensite. With increasing plate thickness, the bainite portion increases and the martensite portion decreases from the plate edges towards the middle section. In addition, thicker plates contain larger areas with segregated elements compared to thinner plates. Figure 23 presents the hardness profiles in the thickness direction of the plates, which shows both microstructural mixing of martensite and bainite and the amount of segregation (hardness peaks). The regions having the lowest hardness possess a mostly bainitic structure. Therefore, the amount of bainite is increased with increasing plate thickness as cooling is slower in the middle section.

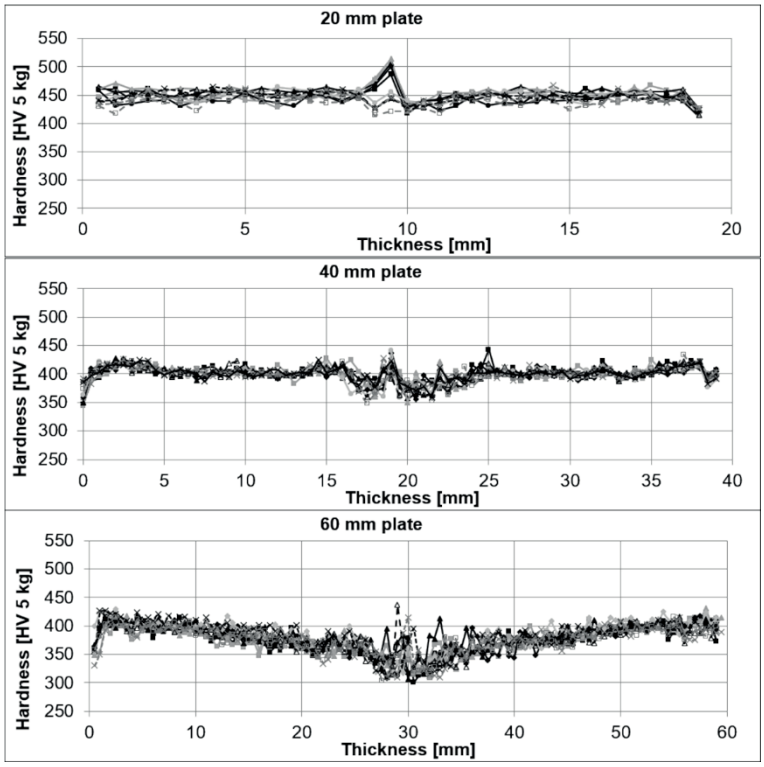

Figure 23. Hardness profiles (HV 5 kg) in the thickness direction in the studied plate thicknesses: 20, 40, and 60 mm (note the different thickness scale in each hardness profile) (Publication IV).

Flame cutting of different plate thicknesses produced similar regions, as presented in section 4.1: newly formed martensite, two-phase region, and tempered original structure. However, the tempered region was different depending on whether the original structure was martensite or a mixture of martensite and bainite. The tempering of bainite does not produce similar changes to the hardness as tempering of martensite and therefore the effect of tempering is somewhat milder in regions consisting mostly of bainite. In addition, the width of these regions was not significantly affected by the thicknesses of the plates. However, the thickness affects the residual stress formation during flame cutting of the plates, as can be seen in Figure 24. The following observations can be made on the residual stress profiles:

- Residual compressive stresses increase with decreasing plate thickness.
- Residual compressive stresses increase with decreasing cutting speed (40 and 60 mm).

- 20 mm plate produces less residual tensile stresses with 150 mm/min cutting speed than faster cutting speed (300, 500, 700 mm).
- Residual tensile stresses are not clearly affected by the plate thickness.
- Preheating produces more compressive stresses (40 and 60 mm) and a lower tensile stress peak (60 mm).

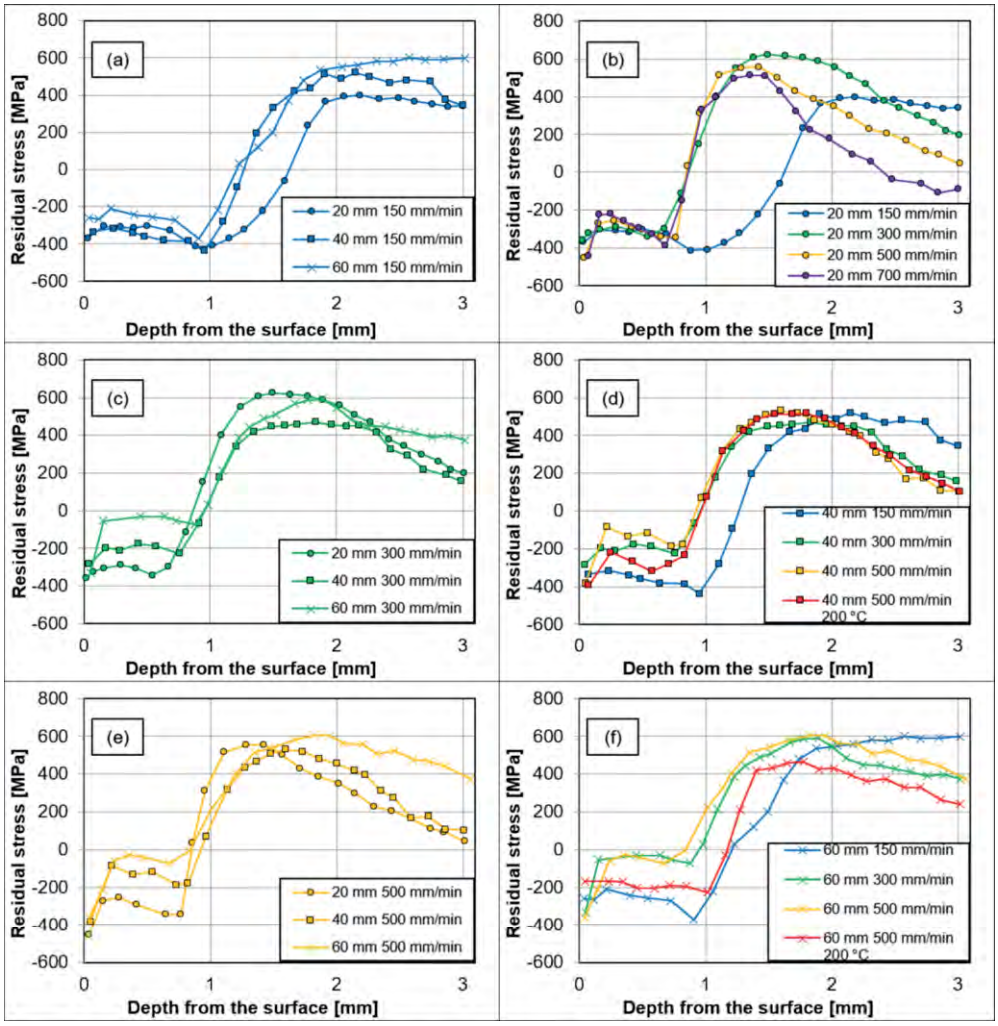

Figure 24. Residual stress profiles in the thickness direction (90°). The effect of thickness in residual stress profiles at cutting speeds of (a) 150, (c) 300, and (e) 500 mm/min. The effect of cutting parameters in residual stress profiles with certain steel thicknesses: (b) 20, (d) 40, and (f) 60 mm (Publication IV).

Based on the results, the thickness of the plate does not have any clear effect on residual tensile stress formation. However, it is still recommended to use preheating and lower cutting speeds based on the residual stress results. The difference in the compressive stress regions of the different plate thicknesses can be explained by the heat from the heating flame. The heating flame acts similarly to preheating in thin plates as its raises the temperature at the cut edge before cutting. With increasing plate thickness, the preheating effect of the heating flame decreases. Figure 25 depicts the preheating effect of the heating flame. The heat from the heating flame decreases the temperature difference between the cut edge and interior and therefore decreases the proportion of thermal stresses.

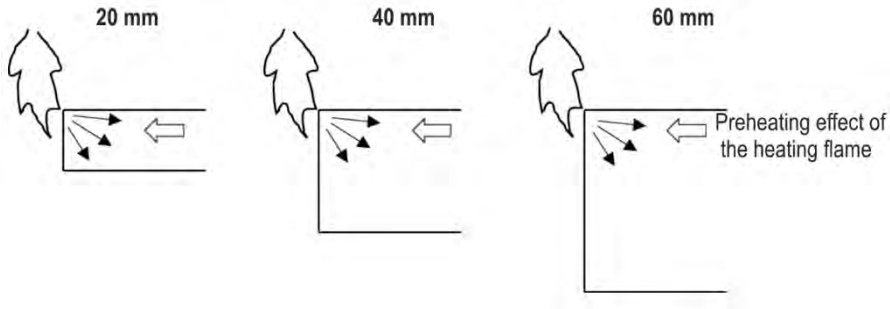

Figure 25. Preheating effect of the heating flame. The heating flame heats the cut edge more in thinner plates.

The impact test results from 60 mm plates, shown in Figure 26, reveal the main challenges of thick plates. The results are quite different depending on the depth in the thickness direction. Figure 26 clearly shows that the transverse and longitudinal impact toughness in the middle section of the plate is significantly worse than the results from the ¼ depth. Especially alarming are the results from the samples of 60 mm plate made in the thickness direction. These results were the worst and clearly show that the middle section of the thick plates has decreased toughness, being the same location as where the cracks are formed. In addition, it was shown (Publication IV) that segregations have even lower toughness compared to the surrounding regions, which indicates that the segregations are the weakest link of the structure.

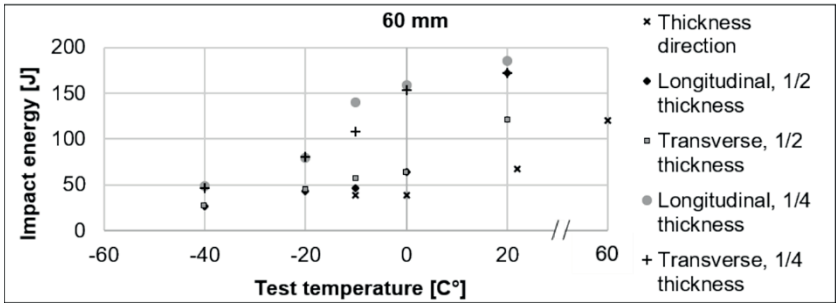

Figure 26. Charpy V-notch impact test results in longitudinal, transverse, and thickness directions for the 60 mm plate (modified from Publication IV).

The cracking probability increased with increasing thickness as shown by the ultrasonic inspections of the plates (Figure 27). The number of cracks was not high because the studied samples were from steel A, which was less prone to cracking, as shown in Figure 22. However, the tensile stress peaks were quite similar between the studied samples, which indicates that the 20 mm plate structure can withstand the residual tensile stresses caused by flame cutting. It was shown in Publication IV that 20 mm plates had a smaller prior austenite grain size and less segregations than thicker plates, both of which are beneficial factors from the cracking point of view. However, on some occasions, in the 40 and 60 mm plates, the structure failed to endure the residual stress state and a crack was formed in flame cutting. Therefore, the risk of cracking increases in proportion to the amount of segregations, whereas the amount of segregation is higher with thicker plates.

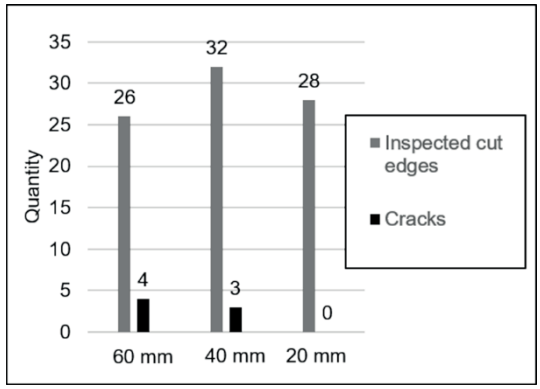

Figure 27. Ultrasonic inspection result from the flame cut samples with different thicknesses: 60, 40, and 20 mm (Publication IV).

4.4 Cracking characteristics of steel plates in flame cutting

The location of the cracks are in the tempered region below the cut edge, which is shown in Figure 28. The crack is located in a locally harder and more brittle region compared to the surroundings. This further confirms that cracks are formed in segregations, creating local hardness peaks in the structure.

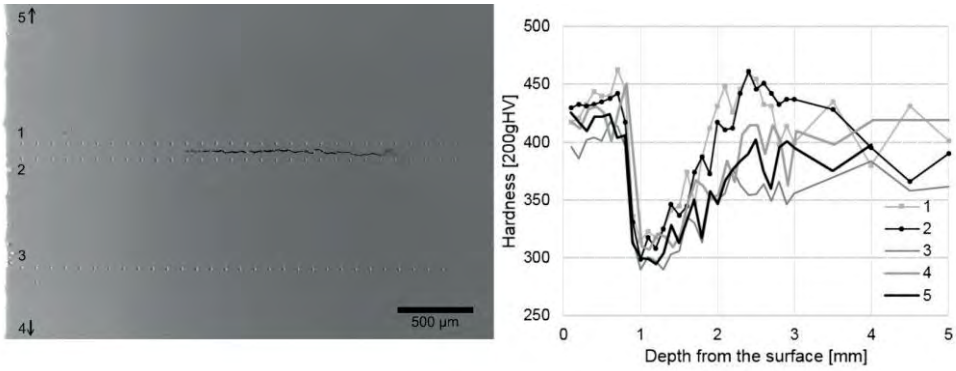

Figure 28. Hardness measurements from the cut edge of the cracked 40 mm plate (steel B) (Publication V).

The location of the cracks also ruled out the involvement of hydrogen in crack formation. As has previously been shown [83], in welding hydrogen cracking occurs in the regions that are austenized during welding. Hydrogen has a high diffusion coefficient in ferrite and higher solubility in austenite. Therefore, hydrogen build-up occurs in the austenized region, which is transformed into martensite during cooling with elevated levels of hydrogen in the structure. This hydrogen inside the structure causes the cracking of the steel. [83] For this reason, if the cracking in flame cutting were caused by hydrogen, the cracks should be located in the newly formed martensite region. However, the cracking initiates in the tempered region, which would be an unlikely location for hydrogen as it would prefer the austenized (newly formed martensite) region closer to the cut edge.

Segregations are the weak link in the structure of thicker plates, as shown in the previous chapter. So, what does the segregation consist of or why are segregations weaker than the surrounding structure (matrix)? Our results confirmed that the cracks were formed in the tempered region in the locally harder segregations, which are formed horizontally, and are worm-like regions generally in the middle section of the steel plates. Considering the size of the segregations, they can be classified as

microsegregations. The microstructure of the segregations was martensite whereas the surrounding structure was mostly bainite. The martensitic structure indicates that the hardenability of the segregation is higher than the surroundings. In addition, the segregations contained inclusions and precipitates. Examples of segregations, inclusions, and precipitations are shown in Figure 29. Segregations contained elevated amounts of Si, P, V, Cr, Mn, and Mo compared to the matrix or the nominal composition (OES). The inclusions had the same elements but even more Mo and P than the segregations. The precipitations were Ti- and N-rich, which indicates that they were titanium nitrides. Figure 30 presents the EDS results of the segregations, inclusions, close to the crack, and matrix, which are compared to the nominal composition (OES) of the steel. In Figure 30, the bar shows the average value of the EDS measurements and the error bars show the maximum and minimum values of the measurements. In addition, Figure 30 shows the carbon equivalents (CE) of each location, calculated by Ito and Besseoy, which covers low ranges of carbon (<0.18 wt%)[7]:

$$CE = W_C + \frac{W_{Si}}{30} + \frac{W_{Mn}+W_{Cu}+W_{Cr}}{20} + \frac{W_{Ni}}{60} + \frac{W_{Mo}}{15} + \frac{W_v}{10} + 5W_B\ Wt\% \quad (3)$$

Commonly, steels having over 0.4 wt% CE are difficult to weld because of their increased tendency to form martensite. [7] It can be seen that the CE of inclusions and segregations are over the critical value of 0.4 wt%. In addition, the CE of the "close to crack" location is precariously close to the critical value. However, the CE of the matrix and nominal composition are below the critical value.

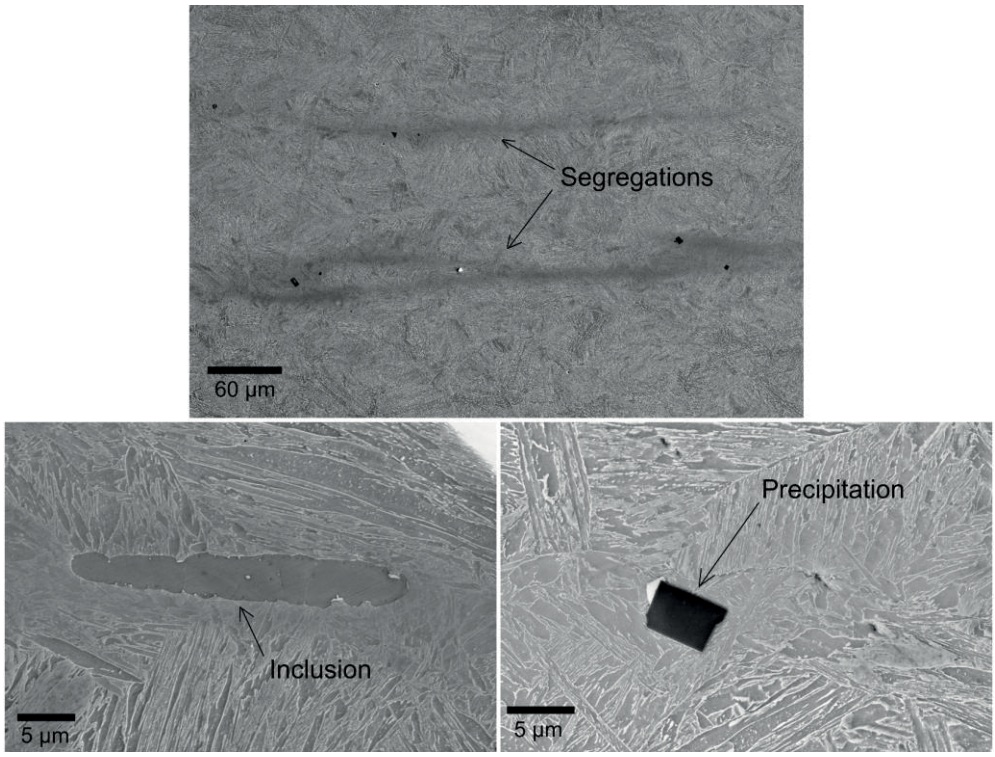

Figure 29. Micrographs from segregations, inclusion, and precipitation (Publication V).

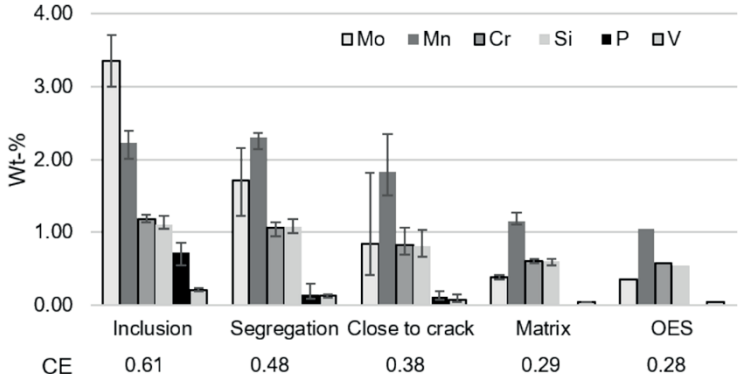

Figure 30. Comparison of Si, P, V, Cr, Mn, and Mo content between inclusion, segregation, close to crack, matrix, and nominal composition (OES). In addition, the carbon equivalents (CE) of each location are given (Publication V).

The enrichment of the alloying elements explains the increased hardness and hardenability of the segregations. In addition, most of these elements (Si, V, Cr, Mo) are known to have an effect on the tempering behavior of segregations by stabilizing the tetragonality of the martensite and also hindering the formation and coarsening of the cementite (Si, Cr, Mo). [7] Therefore, the segregation regions effectively maintain their hardness in tempering during flame cutting while the surrounding structure becomes softer and more ductile. In addition, the segregations contain inclusions and precipitations that can create harmful discontinuities and stress concentrations in the segregation regions.

The mechanical properties of the tempered region were simulated by heat-treated samples. Samples were heat-treated for 70 minutes at 300 °C (ht300) and 600 °C (ht600), which resembles the tempered region in flame cutting and are also the most critical temperatures considering the embrittlement phenomena. The results showed (Figure 31) that both impact and fracture toughness was lower in the heat-treated samples compared to the original samples, indicating that tempering weakens the structure. In addition, the fracture surfaces of the test samples were compared to the opened, flame-cut cracks (Figure 32). It can be seen that the 300 °C heat-treated samples have a transgranular fracture surface (Figure 32a), which is typical of tempered martensite embrittlement (TME). However, the 600 °C heat-treated samples and flame cut cracks both have a similar intergranular fracture surface (Figure 32b and 32c), which is typical [3; 7] of temper embrittlement (TE), thus lowering prior austenite grain boundary cohesion.

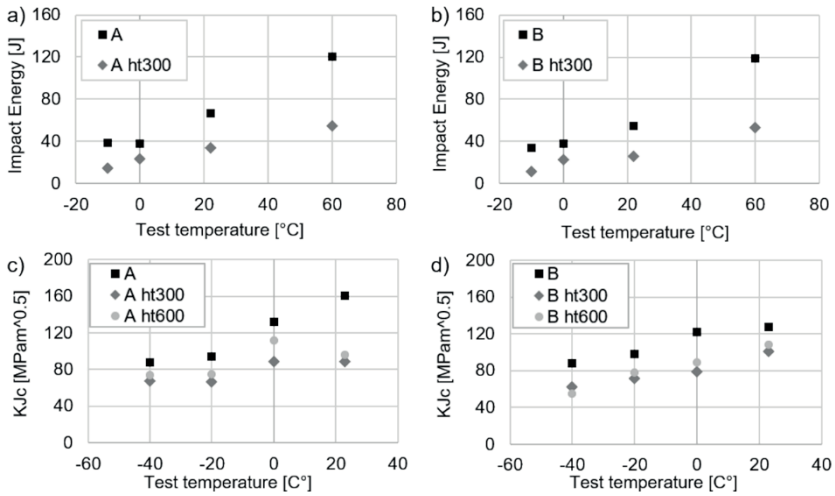

Figure 31. (a, b) Charpy-V impact and (c, d) fracture toughness test results of original (A and B) and heat-treated (A ht300, A ht600, B ht300, B ht600) samples of 60 mm plates (Publication V).

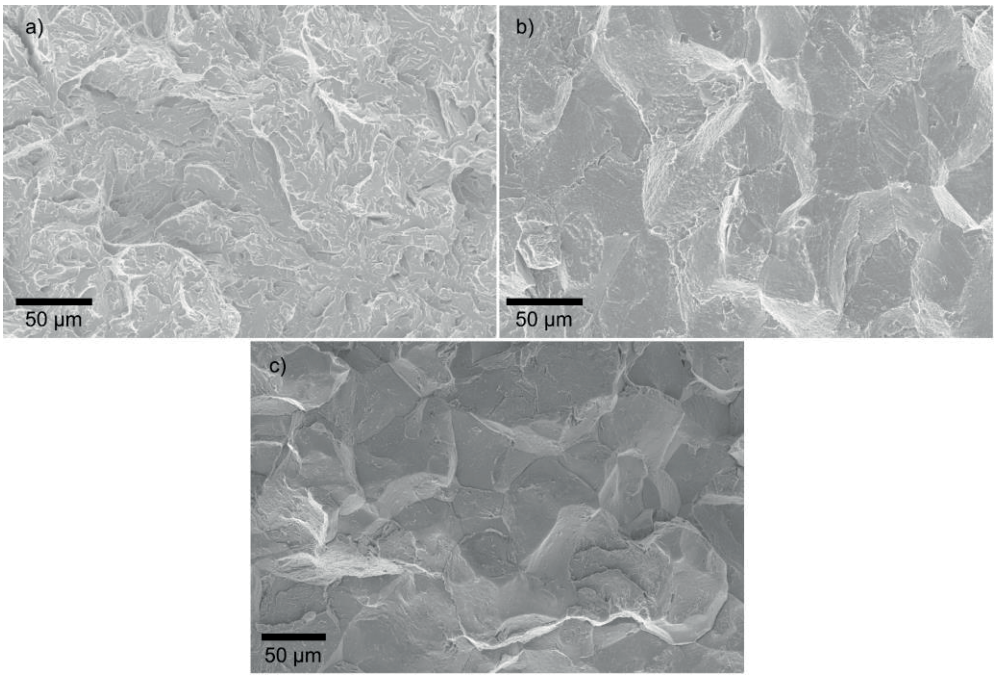

Figure 32. Fracture surfaces of fracture toughness test samples showing (a) transgranular fracture, (b) intergranular fracture, and c) opened flame-cut crack surface (Publication V).

The reduced prior austenite grain boundary cohesion is typically caused in TE by the accumulation of impurity elements, such as P, at grain boundaries. However, TE is also highly affected by the other alloying elements that can interact with P and affect the grain boundary cohesion. For example; P and Mn, Cr, Mo enhance the segregation of each other. Mn and Cr strongly co-segregate with P, increasing the risk of TE. Moreover, Mn also increases the embrittling potency of P [84]. In addition, Si increases the risk of TE [3] although it has a repulsive interaction with P [84]. However, the risk of TE is partially reduced by adding 0.7 wt% Mo, as it inhibits the segregation of P to grain boundaries and increases the grain boundary cohesion. On the other hand, larger additions are inefficient as the Mo is incorporated into cementite [84]. In addition, the nature of C and P is competitive with regard to iron, and generally C depresses the accumulation of P. However, the C content cannot be measured accurately enough by EDS and therefore the C content in the segregations is unknown and can only be speculated. On the other hand, if the segregation contains C, it also contains strong carbide-forming elements, such as Cr, Mo, or V, which can lower the solubility of carbon and therefore promote the segregation of P. [3; 7; 84] It seems that the alloying elements in segregations have a complex interaction with each other and with prior austenite grain boundary cohesion. However, when a crack is formed, the sum effect of these elements create an environment that is suitable for crack formation. In addition, tempering during flame cutting increases the weakening of the grain boundaries in segregations even further. The grain boundary cohesion reduced by these elements does not withstand the residual stress state caused by flame cutting. Figure 33 summarizes the cracking phenomenon in flame cutting.

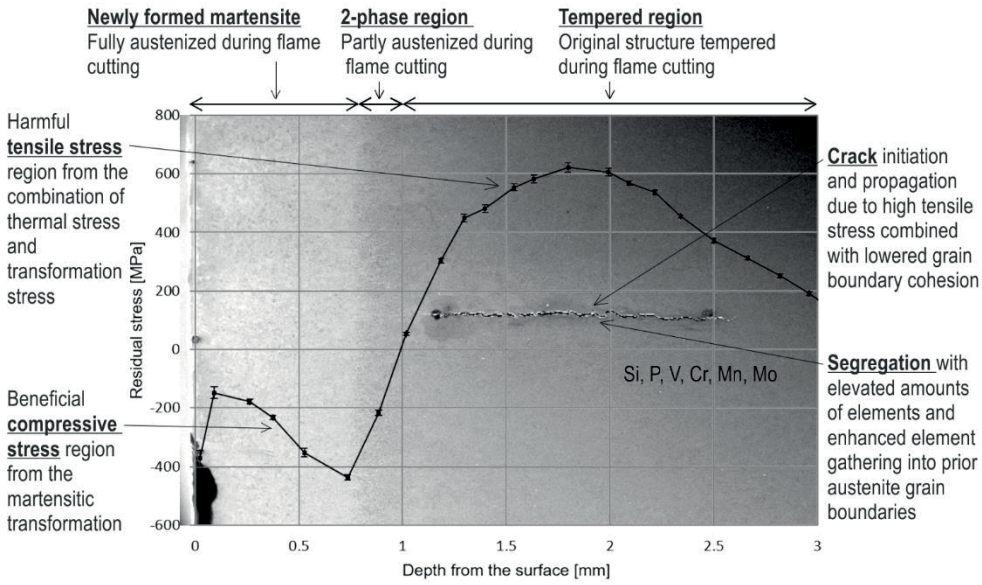

Figure 33. Microstructural regions, residual stress profile, and crack location at flame cut edge at a cutting speed of 300 mm/min.

4.5 How to avoid cracking of thick steel plates in flame cutting

There are two possible ways to avoid or at least lower the susceptibility to cracking in flame cutting: by lowering the residual stresses generated during flame cutting or by producing plates with a microstructure that lowers the cracking probability. It may be easier to concentrate on applying the optimal parameters in the flame cutting process and on aiming at the lowest possible residual stress state in the cut edge. The proposed methods are:

- Apply preheating → higher preheating temperature lowers the residual tensile stress peaks and increases the compressive stress state. However, a higher preheating temperature also reduces the hardness of the plate.

- Use a low cutting speed → not as effective as preheating but also generally lowers residual tensile stresses and increases compressive stress state.

- Combine preheating and low cutting speed → the most effective way to produce the highest compressive stress and the lowest tensile stress state.

A low cutting speed generally produces a more beneficial stress state, but in some cases the tensile stress peaks are still quite high. In addition, some occasions cracks has been detected from samples that were cut using a lower cutting speed. However, no cracks were detected from the preheated samples, which indicates that preheating is the most effective way to avoid the cracking related to the flame cutting process. Combining preheating and a low cutting speed produces the most beneficial stress state by increasing the compressive stress state and lowering the tensile stress peaks. It is also recommended to avoid long retention periods in temperatures of 600 °C and 300 °C as they lower the mechanical toughness of the steel. However, totally avoiding these temperatures during flame cutting is quite complicated, so it is recommended to concentrate more on lowering the residual stress state.

The other aspect to avoid cracking is to optimize the manufacturing process and the microstructural characteristics of the thick wear-resistant steel plate. This can be achieved by the following:

- Manufacture segregation-free plates or at least aim to reduce the amount and severity of segregations.

- Reduce the phosphorus, manganese, chromium, and silicon content of the plate, which would also decrease the amount of these elements in the segregations.

- Produce an equiaxed prior austenite grain structure, which is not as prone to cracking as an elongated grain structure. An equiaxed prior austenite grain structure has more vertical grain boundaries to inhibit crack propagation, which commonly occurs in horizontally formed segregations.

- Produce a structure that contains a small prior austenite grain size. As a result, the accumulation of alloying elements in the grain boundaries will be divided between more grain boundaries and therefore the weakening effect will be reduced.

At the moment, the manufacturing of segregation-free plate might be difficult. In addition, most of the elements found in the segregations also play an important role in steel in general such as an increase in hardness and hardenability. Therefore, these elements cannot be removed from the steel but it is recommended to aim for a more effective distribution of these elements. However, the last three points of the

previous list might be easier to achieve by slightly changing the manufacturing practices of thick plate. In addition, most of these properties are commonly desired and in most cases the manufacturing already aims at achieving them.

All of the described guidelines may not be the easiest to apply in practice. However, the end users of the plates, who cannot influence the manufacturing, should concentrate on the flame-cut process, whereas steel manufacturers should concentrate more on the manufacturing aspects. These manufacturing guidelines describe what kind of structural characteristics are favorable in steel. However, the actual methods for how to achieve them is left to manufacturing metallurgists, who have better knowledge of the actual manufacturing methods.

5 CONCLUDING REMARKS AND SUGGESTIONS FOR FUTURE WORK

In this chapter, the two research questions are revisited and answered based on the results of this work and the related five publications.

1. What are the main factors contributing to the cracking phenomenon of thick wear-resistant steel plates in the flame cutting process?

Two main factors contribute to the cracking phenomenon of thick wear-resistant steel plates in flame cutting. The first factor is the residual stresses formed during the flame cutting process, especially the high residual tensile stress peaks which are formed just below the cut edge. These tensile stresses are harmful as they increase crack formation by tearing the structure apart. The higher the tensile stress peaks are formed during flame cutting, the higher the danger of cracking.

The second factor is the microstructural characteristics of wear-resistant steel plate. Thick plates contain segregations in the steel structure and the proportion of segregations is higher with thicker plates. Segregations contain elevated amounts of alloying elements such as silicon, phosphorus, vanadium, chromium, manganese, and molybdenum. Most of these elements increase the hardenability of the segregation bands, therefore resulting in a hard and brittle martensitic structure. In addition, most of these elements hinder the effect of tempering during flame cutting. Most crucially, the elements interact with each other and have a high tendency to accumulate in the prior austenite grain boundaries. The sum effect of this accumulation is the weakening of the grain boundaries and reduced grain boundary cohesion. These weakened prior austenite grain boundaries fail to endure the residual tensile stresses formed during flame cutting. The weakening effect increases with increasing grain size as the accumulation of alloying elements concentrate in a smaller grain boundary area. In addition, long, parallel prior austenite grain boundaries in the horizontal direction significantly increase the risk of cracking as they create potential crack paths inside the steel structure.

2. How can flame cutting practices and steel plate characteristics be optimized in order to avoid cracking and have an effective cutting process?

Development of flame cutting practices concentrates on selecting the most beneficial cutting parameters to produce more compressive stresses and less tensile stresses at the cut edge. The most effective way to achieve this is to combine preheating and a low cutting speed. In addition, separately applied preheating or low cutting speed generally results in a better residual stress state compared to a fast cutting speed. However, a low cutting speed is not totally safe as, on some occasions, it can create a high tensile stress peak at the cut edge. However, cracking probability is significantly reduced by applying the previously described cutting parameters and it is highly recommended to flame cut according to these guidelines.

As previously described, certain microstructural characteristics of the steel plates are beneficial and resist crack formation and propagation effectively. The manufacturing of thick wear-resistant steel plate should aim at a small and equiaxed prior austenite grain structure. In addition, creating vertical barriers such as grain boundaries in the microstructure effectively resists crack propagation in the vertical direction. Additionally, concentrating on reducing the amount of alloying elements that are typically found in segregations should decrease the cracking probability. However, most of these elements might have an important role regarding steel properties and cannot be removed or reduced. In that case, manufacturing should concentrate on the more effective distribution of these elements, therefore decreasing the amount and severity of the segregations in the structure. Achieving these microstructural characteristics does not necessarily demand major changes to existing manufacturing practices. Even small changes can lead to beneficial results by reducing the cracking probability during flame cutting.

Future work

This work revealed the main factors contributing to the cracking phenomenon of thick wear-resistant plate in flame cutting. One recommendation for future work is to study even smaller details of the flame cut edge. This could be done by small scale mechanical testing of the different regions formed during flame cutting, which would further increase knowledge of the phenomenon. In addition, crack opening and testing by Auger electron spectroscopy might reveal which are the most harmful elements of the segregation that affect crack formation. This kind of measurement

was originally planned for this work but the sample preparation failed and the tests were not included in the present study.

In addition, studying the effect of the manufacturing parameters on the steel microstructure might give more specific guidelines on how to achieve beneficial microstructure characteristics. Furthermore, studying the interaction of different alloying elements would provide information on which specific alloying element combination should be avoided during plate manufacture.

Studying the residual stresses of the plate directly after manufacturing could also be one issue to concentrate on in the future. Different manufacturing parameters may induce a residual stress state in the steel plate even before the flame cutting process. This stress state has an effect on the resulting stress state after flame cutting, which in turn has an effect on the plate cracking probability.

REFERENCES

[1] Raex, Abrasion resistant steel, http://www.raexsteel.fi/ (accessed 4/3/2019).

[2] Hardox, Wear plate for extreme abrasion resistance, https://www.ssab.com/products/brands/hardox (accessed 4/3/2019).

[3] G. Krauss, Steels: Processing, Structure, and Performance, 2nd edition, ASM International, 2015.

[4] G.E. Totten, J.L. Dossett, N.I. Kobasko, Quenching of steel, Heat Treating Fundamentals and Processes, Vol 4A ed., ASM International, ASM Handbook, 2013, pp. 91-156. doi:10.31399/asm.hb.v04a.a0005824

[5] Freepik, https://www.freepik.com/premium-photo/coal-mine-area-many-heavy-truck-excavator-machine-mining-industry_ 2183274.htm (accessed 3/23/ 2019).

[6] D.A. Porter, K.E. Easterling, (Ed.). Phase Transformation in Metals and Alloys. 2nd ed. Cheltenham, UK, Nelson Thornes Ltd, 1992.

[7] H. Bhadeshia, R. Honeycombe, Steels: Microstructure and Properties, 4th ed. Butterworth-Heinemann, 2017.

[8] G.F. Vander Voort (Ed.), Martensitic Structures, Metallography and Microstructures, Vol 9, ASM International, ASM Handbook, 2004, pp. 165-178. doi:10.31399/asm.hb.v09.a0003736

[9] J.L. Dossett, G.E. Totten, Hardness and Hardenability of Steels, Steel Heat Treating Fundamentals and Processes, Vol 4A, ASM International, ASM Handbook, 2013, pp. 26-59. doi:10.31399/asm.hb.v04a.a0005823

[10] M.J. Perricone, Bainitic Structures, In: G.F. Vander Voort (Ed.), Metallography and Microstructures, Vol 9, ASM International, ASM Handbook, 2004, pp. 179-185. doi:10.31399/asm.hb.v09.a0003739

[11] W.F. Smith, Structure and Properties of Engineering Alloys, McGraw-Hill, 1993.

[12] D.M. Stefanescu, R. Ruxanda, Fundamentals of Solidification, in: G.F. Vander Voort (Ed.), Metallography and Microstructures, Vol 9, ASM International, ASM Handbook 2004, pp. 71-92. doi:10.31399/asm.hb.v09.a0003724

[13] S. K. Choudhary, S. Ganguly, A. Sengupta, V. Sharma, Solidification Morphology and Segregation in Continuously Cast Steel Slab, J. Mater. Process. Technol. 243 (2017) 312-321. doi:10.1016/j.jmatprotec.2016.12.030

[14] N. Yang, C. Su, X. Wang, F. Bai, Research on Damage Evolution in Thick Steel Plates, J. Constr. Steel Res. 122 (2016) 213-225. doi:10.1016/j.jcsr.2016.03.014

[15] Y. Wang, X. Liu, Z. Hu, Y. Shi, Experimental Study on Mechanical Properties and Fracture Toughness of Structural Thick Plate and Its Butt Weld Along Thickness and at Low Temperatures, Fatigue Frac. Eng. Mater. Struct. 36 (2013) 1258-1273. doi:10.1111/ffe.12062

[16] T. Zhou, H. Yu, S. Wang, Effect of Microstructural Types on Toughness and Microstructural Optimization of Ultra-Heavy Steel Plate: EBSD Analysis and

Microscopic Fracture Mechanism, Mater. Sci. Eng.: A 658 (2016) 150-158. doi:10.1016/j.msea.2016.02.001
[17] Y. Wang, X. Liao, Y. Zhang, Y. Shi, Experimental Study on the Through-thickness Properties of Structural Steel Thick Plate and Its Heat-affected Zone at Low Temperatures, J. Zhejiang Univ. Sci. A 16 (2015) 217-228. doi:10.1631/jzus. A1400273
[18] A. Ghosh, Principles of Secondary Processing and Casting of Liquid Steel, Raju Primlani, 1990.
[19] J. Zollinger, D. Daloz, On the Sampling Methodology to Characterize Microsegregation, Mater. Charact. 62 (2011) 1058-1065. doi: 10.1016/j.matchar.2011.07.015
[20] M. Réger, B. Verő, Z. Csepeli, Á. Szélig, Macrosegregation in CC slabs, Materials Science Forum, Vol 508, Trans. Tech. Publ., 2006 pp. 233-238. doi:10.4028/ www.scientific.net/MSF.508.233
[21] G. Lesoult, Macrosegregation in Steel Strands and Ingots: Characterisation, Formation and Consequences, Mater. Sci. Eng.: A 413 (2005) 19-29. doi:10.1016/j.msea. 2005.08.203
[22] T. Pikkarainen, V. Vuorenmaa, I. Rentola, M. Leinonen, D. Porter, Effect of Superheat on Macrostructure and Macrosegregation in Continuous Cast Low-alloy Steel Slabs, IOP Conference Series: Materials Science and Engineering, IOP Publishing, 117 (2016) 012064. doi:10.1088/1757-899X/117/1/012064
[23] S.L. Semiatin (ed.), Oxyfuel Gas Cutting, Metalworking: Sheet Forming, Vol 14B ASM International, ASM Handbook 2006, pp. 74-95. doi:10.31399/asm.hb.v14b.a0005175
[24] A. O'Brien (ed.). Welding handbook, Welding processes, part 1. Vol 2, 9th edition, American Welding Society, 2004.
[25] L.R. Soisson, Oxyfuel Gas cutting, In: D.L. Olson, T.A. Siewert, S. Liu, G.R. Edwards (Ed.), Welding, Brazing, and Soldering, Vol 6, ASM International, ASM Handbook, 1993, pp. 1155-1165. doi:10.31399/asm.hb.v06.a0001483
[26] R. Thiébaud, J. Drezet, J. Lebet, Experimental and Numerical Characterisation of Heat Flow During Flame Cutting of Thick Steel Plates, J. Mater. Process. Technol. 214 (2014) 304-310. doi:10.1016/j.jmatprotec.2013.09.016
[27] J. Niemi, M. Aromäki, Teräslevyjen terminen leikkaus, MET, Tekninen tiedotus, 1985.
[28] Metallirakentajan käsikirja, Hämeen ammattikorkeakoulu, Hämeenlinna, 2008.
[29] A. Martín-Meizoso, J. Aldazabal, J.L. Pedrejón, S. Moreno, Resilience and Ductility of Oxy-fuel HAZ Cut, Frattura ed Integrita Strutturale 30 (2014) 14-22. doi:10.3221/IGF-ESIS.30.03
[30] D. Radaj, Heat Effects of Welding: Temperature Field, Residual Stresses, Distortion, Springer-Verlag Berlin Heidelberg, 1992.
[31] A.D. Wilson, Hardness Testing of Thermal Cut Edges of Steel, Eng. J. 27 (1990) 98-107.
[32] W. Wood, Heat-affected Zone Studies of Thermally Cut Structural Steels, Government Research Announcements and Index, 1994.
[33] H. Thomas, J. De Back, T.J. Bos, T. Muller, J.J.W. Nibbering, C.J.J.M. Verwey, R. Vonk, The Properties of flame-cut edges, Technical steel research, Netherlands Institute of Welding, Delft, 1980.
[34] H. Bhadeshia, R. Honeycombe, The Tempering of Martensite, Steels: Microstructure and Properties (Third Edition), Butterworth-Heinemann, 2006, pp. 183-208.

[35] D. H. Jack, K. H. Jack, Invited review: Carbides and Nitrides in Steel, Mater. Sci. Eng. 11 (1973) 1-27. doi:10.1016/0025-5416(73)90055-4
[36] A.K. Tingaev, R.G. Gubaydulin, I. Ilin, Study of the Effect of Thermal Cutting on the Microstructure and Chemical Composition of the Edges of Workpieces Made of Steel Brands S345, S390, 2016, Procedia Eng. 150 (2016) 1783-1790. doi:10.1016/j.proeng.2016.07.171
[37] E. Piraprez, Fatigue Strength of Flame-cut Plates, Fatigue of steel and concrete structures 37 (1982) 123-130.
[38] M.N. James, Residual Stress Influences on Structural Reliability, Eng. Fail. Anal. 18 (2011) 1909-1920. doi:10.1016/j.engfailanal.2011.06.005
[39] G.S. Schajer (ed.), Practical residual stress measurement methods. John Wiley & Sons, 2013.
[40] P. Withers, H. Bhadeshia, Residual stress. Part 1–Measurement techniques, Mater. Sci. Tech. 17 (2001) 355-365. doi:10.1179/026708301101509980
[41] P. Withers, H. Bhadeshia, Residual stress. Part 2–Nature and origins, Mater. Sci. Technol. 17 (2001) 366-375. doi:10.1179/026708301101510087
[42] J. Lu (ed.), Handbook of Measurement of Residual Stresses, Society for Experimental Mechanics, The Fairmont Press, Inc. 1996.
[43] A.J. Perry, J.A. Sue, P.J. Martin, Practical measurement of the residual stress in coatings, Surf. Coat. Tech. 81 (1996) 17-28. doi:10.1016/0257-8972(95)02531-6
[44] K. Sherafatnia, G.H. Farrahi, A.H. Mahmoudi, Effect of initial surface treatment on shot peening residual stress field: Analytical approach with experimental verification, Int. J. Mech. Sci. 137 (2018) 171-181. doi:10.1016/j.ijmecsci.2018.01.022
[45] S. Santa-aho, A. Sorsa, J. Wartiainen, P. Lundin, L. Suominen, T. Jokiaho, M. Honkanen, K. Leiviskä, and M. Vippola, Surface Layer Characterization of Shot Peened Gear Specimens, Materials Performance and Characterization 7 (2018) 807-826. doi:10.1520/MPC20170169
[46] M. Lindgren, Hitsatun teräsputken jäännösjännitykset, Licentiate thesis, 2001.
[47] M. Narazaki, G.E. Totten, Distortion of Heat-Treated Components, Steel Heat Treatment: Metallurgy and Technologies, 2006.
[48] L.E. Lindgren, A. Carlestam, M. Jonsson, Computational model of flame-cutting, J. Eng. Mater. Tech. 115 (1993) 440-445. doi:10.1115/1.2904243
[49] R. Thiébaud, J. Lebet, Experimental study of residual stresses in thick steel plates, SSRC Annual Stability Conference Proceedings. 2012. p. 18-21.
[50] Z.Y. Wei, Y.J. Liu, B. Zhou, Distributions and Influence Factors of Residual Stresses Induced by Oxygen Cutting Opening in Steel Structure, Adv. Mater. Res. 314-316 (2011) 437-447. doi:10.4028/www.scientific.net/AMR.314-316.437
[51] P.S. Prevey, X-ray diffraction residual stress techniques, ASM International, ASM Handbook, 10 (1986) 380-392.
[52] ASTM E837-13a, Standard Test Method for Determining Residual Stresses by the Hole-Drilling Strain-Gage Method, 2013.
[53] A. Magnier, B. Scholtes, T. Niendorf, On the reliability of residual stress measurements in polycarbonate samples by the hole drilling method, Polym. Test. 71 (2018) 329-334. doi:10.1016/j.polymertesting.2018.09.024
[54] E. Van Puymbroeck, W. Nagy, H. Fang, H. De Backer, Determination of residual weld stresses with the incremental hole-drilling method in tubular steel bridge joints, Procedia Eng. 213 (2013) 651-661. doi:10.1016/j.proeng.2018.02.061

[55] R. Winkler, E. Saborowski, G. Paczkowski, T. Grund, T. Lampke, Characterization of thermally sprayed copper and numerically supported residual stress determination by the incremental hole-drilling method, Surf. Coat. Tech., 2018. doi:10.1016/j.surfcoat.2018.12.018

[56] N. Tebedge, G. Alpsten, L. Tall, Residual-stress measurement by the sectioning method, Exp. Mech. 13 (1973) 88-96. doi:10.1007/BF02322389

[57] J.R. Shadley, E.F. Rybicki, W.S. Shealy, Application guidelines for the parting out step in a through thickness residual stress measurement procedure, Strain 23 (1987) 157-166. doi:10.1111/j.1475-1305.1987.tb00640.x

[58] C. Ruud, J. Josef, D. Snoha, Residual stress characterization of thick-plate weldments using X-ray diffraction, Stress 100 (1993) 87-91.

[59] W. Reimers, A. Pyzalla, M. Broda, G. Brusch, D. Dantz, T. Schmackers, K. Liss, T. Tschentscher, The use of high-energy synchrotron diffraction for residual stress analyses, J. Mater. Sci. Lett. 18 (1999) 581-583. doi:10.1023/A:1006651217517

[60] K. Tanaka, Y. Akiniwa, M. Hayashi, Neutron diffraction measurements of residual stresses in engineering materials and components, Mater. Sci. Res. Int. 8 (2002) 165-174. doi:10.2472/jsms.51.12Appendix_165

[61] W. Woo, V. Em, P. Mikula, G. An, B. Seong, Neutron diffraction measurements of residual stresses in a 50 mm thick weld, Mater. Sci. Eng. A 528 (2011) 4120-4124. doi:10.1016/j.msea.2011.02.009

[62] W. Woo, G. An, V. Em, A. De Wald, M. Hill, Through-thickness distributions of residual stresses in an 80 mm thick weld using neutron diffraction and contour method, J. Mater. Sci. 50 (2015) 784-793. doi:10.1007/s10853-014-8638-9

[63] J. Berglund, Cut Cost Calculation, Master's thesis, Luleå University of Technology, 2006.

[64] G. Krauss, Deformation and Fracture of Martensite before and after Tempering, Encyclopedia of Materials: Science and Technology, 2016 pp. 5193-5197. doi:10.1016/B978-0-12-803581-8.02880-0

[65] Y. Zhao, X. Ren, Z. Hu, Z. Xiong, J. Zeng, B. Hou, Effect of tempering on microstructure and mechanical properties of 3Mn-Si-Ni martensitic steel, Mater. Sci. Eng. A 711 (2018) 397-404. doi:10.1016/j.msea.2017.11.037

[66] S. Park, K. Lee, M. Kim, B. Lee, Effects of boundary characteristics on resistance to temper embrittlement and segregation behavior of Ni–Cr–Mo low alloy steel, Mater. Sci. Eng. A 561 (2013) 277-284. doi:10.1016/j.msea.2012.10.078

[67] L.E. Lindgren, A. Carlestam, An improved two-dimensional model of flame cutting, International Conference on Computer-Assisted Materials Design and Process Simulation, 1993, pp. 141-146.

[68] D. Stemne, T. Narström, B. Hrnjez, Welding Handbook: A guide to better welding of Hardox and Weldox, SSAB, 2010.

[69] H. Bhadeshia, Prevention of Hydrogen Embrittlement in Steels, ISIJ Int. 56 (2016) 24-36. doi:10.2355/isijinternational.ISIJINT-2015-430

[70] A. Nagao, C.D. Smith, M. Dadfarnia, P. Sofronis, I.M. Robertson, The role of hydrogen in hydrogen embrittlement fracture of lath martensitic steel, Acta Mater. 60 (2012) 5182-5189. doi:10.1016/j.actamat.2012.06.040

[71] Q. Liu, Q. Zhou, J. Venezuela, M. Zhang, A. Atrens, The role of the microstructure on the influence of hydrogen on some advanced high-strength steels, Mater. Sci. Eng. A 715 (2018) 370-378. doi:10.1016/j.msea.2017.12.079

[72] N. Saidani, A. Mihi, R. Benbouta, Fracture process of C–Mn steel embrittled by hydrogen, J. Assoc. Arab Univ. Basic Appl. Sci. 11 (2012) 16-20. doi:10.1016/j.jaubas.2012.01.001
[73] W.T. Becker, R.J. Shipley (ed.), Hydrogen Damage and Embrittlement, Failure Analysis and Prevention, ASM International, ASM Handbook, 2002, pp. 809-822. doi:10.31399/asm.hb.v11.a0003552
[74] EN 15305: Non-destructive Testing Method for Residual Stress analysis by X-ray Diffraction, 2008.
[75] M. Fitzpatrick, A. Fry, P. Holdway, F. Kandil, J. Shackleton, L. Suominen, Determination of residual stresses by X-ray diffraction, Meas. Good Practice Guide 52, 2005.
[76] R. Alkaisee, R.L. Peng, Influence of layer removal methods in residual stress profiling of a shot peened steel using X-ray diffraction, Adv. Mater. Res. 996 (2014) 175-180. doi: 10.4028/www.scientific.net/AMR.996.175
[77] T. Nyyssönen, M. Isakov, P. Peura, V.-T Kuokkala, Iterative Determination of the Orientation Relationship Between Austenite and Martensite from a Large Amount of Grain Pair Misorientations, Metall. Mater. Trans. A 47 (2016) 2587-2590. doi:10.1007/s11661-016-3462-2
[78] SFS-EN ISO 6892-1, Metallic materials. Tensile testing. Part 1: Method of test at room temperature, Mechanical Engineering and Metals Industry Standardization in Finland, 2016.
[79] SFS-EN ISO 148-1, Metallic materials. Charpy pendulum impact test. Part 1: Test method, Mechanical Engineering and Metals Industry Standardization in Finland, 2016.
[80] ASTM E1820 - 17a, Standard Test Method for Measurement of Fracture Toughness, 2017.
[81] I. Basu, V. Ocelík, J.T.M. De Hosson, Measurement of spatial stress gradients near grain boundaries, Scripta Mater. 136 (2017) 11-14. doi:10.1016/j.scriptamat.2017.03.036
[82] S. Li, G. Zhu, Y. Kang, Effect of substructure on mechanical properties and fracture behavior of lath martensite in 0.1C–1.1Si–1.7Mn steel, Journal of Alloys and Compounds, Vol. 675, 2016, pp. 104-115.
[83] K. Easterling, Cracking and fracture in welds, Introduction to the physical metallurgy of welding (2nd ed.), Butterworth-Heinemann, 1992, pp 191-260.
[84] T. Xu, Interfacial Segregation and Embrittlement, Reference Module in Materials Science and Materials Engineering, 2016, pp. 1-8. doi:10.1016/B978-0-12-803581-8.03232-X

PUBLICATIONS

PUBLICATION I

The Characterization of Flame Cut Heavy Steel–The Residual Stress Profiling of Heat Affected Surface Layer

T. Jokiaho, T. Saarinen, S. Santa-aho, P. Peura, M. Vippola

Key Engineering Materials, Vol. 674 pp. 103-108
https://doi.org/10.4028/www.scientific.net/KEM.674.103

Key Engineering Materials Vol. 674 (2016) pp 103-108
© (2016) Trans Tech Publications, Switzerland
doi:10.4028/www.scientific.net/KEM.674.103

Submitted: 2015-05-29
Revised: 2015-07-01
Accepted: 2015-07-01

The Characterization of Flame Cut Heavy Steel – The Residual Stress Profiling of Heat Affected Surface Layer

Tuomas Jokiaho[1,a*], Tuomo Saarinen[2,b], Suvi Santa-aho[1,c], Pasi Peura[1,d], Minnamari Vippola[1,e]

[1] Tampere University of Technology, Department of Materials Science, P.O. Box 589, 33101 Tampere, Finland.

[2] SSAB Europe Oy, Rautaruukintie 155, 92101 Raahe, Finland

[a]tuomas.jokiaho@tut.fi, [b]tuomo.saarinen@ssab.com, [c]suvi.santa-aho@tut.fi, [d]pasi.peura@tut.fi, [e]minnamari.vippola@tut.fi

Keywords: flame cutting, heavy steel plate, heat affected zone, residual stress, X-ray diffractometer

Abstract. Flame cutting is commonly used thermal cutting method in metal industry when processing thick steel plates. Cutting is performed with controlled flame and oxygen jet, which burns steel and forms cutting edge. Flame cutting process is based on controlled chemical reaction between steel and oxygen at elevated temperature. Flame cutting of thick wear-resistant steels is challenging while it can result in cracks on and under the cut edge. Flame cutting causes uneven temperature distribution in the plate, which can introduce residual stresses. In addition, heat affected zone (HAZ) is formed and there both volume and microstructural changes as well as hardness variations are taking place. Therefore flame cutting always causes thermal stress, shape changes and consequently residual stresses to the material. Material behaviour under thermal and mechanical loading depends on the residual stress state of the material. Due to this, it is important to be able to measure the residual stresses. The aim of this study was to examine residual stresses on the cutting edge as a function of flame cutting parameters. Also resulting microstructures and hardness values were verified. Varying parameters were the cutting speed, preheating and post heating procedures. Flame cut samples were investigated with X-ray diffraction method to produce residual stress profiles of the heat affected surface layer. Results indicated that different cutting parameters provide different residual stress profiles and that these profiles can be modified by changing the cutting speed and pre- or post-treatment procedures. Cutting parameters also affect the depth of the reaustenized region in the surface. The results correlate well with the actual industrial flame cutting and thus they provide an effective tool for optimizing the flame cutting process parameters.

Introduction

Thermal cutting processes are widely used in the steel industry. Flame cutting is based on the chemical reaction between oxygen and steel at elevated temperature. At first the cut metal is heated locally to its ignition temperature with flame obtained from the combustion of a specific fuel gas mixed with oxygen. After heating the metal is burnt by jet of pure oxygen creating a continuous chemical reaction between the oxygen and the metal. The iron oxide, which is formed during flame cut, is blown away by the jet of oxygen. [1] Flame cutting process is exothermic and the generated heat supports the continuation of metal oxidation as the cut is proceeding [2].

Flame cutting of thick wear-resistant steel plates is challenging with increasing probability of crack formation in the heat affected surface layer. This cracking tendency is found to increase with increasing hardness and thickness of flame cut steel. [3] It has also been reported that cracking is more probable when the residual tensile stresses are higher in the cut edge [4]. Therefore cracking probability can be reduced by preheating or using slower cutting speed [3].

Flame cutting produces heat affected zone (HAZ) adjacent to the cut. During flame cutting the temperature gradient is rather steep over the short distance and part of the cut edge exceeds transformation temperature. Cutting parameters affect the microstructure and width of the produced

HAZ. It has been investigated that in HAZ hardness variation and microstructural changes occur: Higher hardness values are observed closer to the cut edge and values decrease with the distance from the cut. [1,5] Wood [6] observed that faster cutting speed produced narrower HAZ and slower cutting speed created wider HAZ. In the study of Thomas et al. [7] HAZ of flame cut Fe52 plate contained martensitic layer and the thickness of the martensite layer was dependent on the plate thickness and cutting speed. Flame cutting with preheating produced very thin layer of martensite in the cut edge.

Flame cutting process causes also residual stresses to the cut edge of the plate. Residual stresses have a significant effect on the material's mechanical properties and they can cause also cracking on the cutting edge. [1,8] Residual stresses occur in the material without external load. They are formed due to uneven plastic strain which causes elastic response. Surroundings of the plastically deformed areas must maintain the dimensional continuity and for that reason the residual stresses are formed. [9] Usually the residual compressive stress is favourable and increases fatigue resistance and prevents cracking. The residual tensile stress is often unfavourable and decreases fatigue resistance of materials and increases the probability of cracking. [10,11] Residual stresses caused by thermal cutting consist of thermal and transformation stresses which are often related to large thermal gradients. Thermal stress is caused by inhomogeneous thermal expansion or shrinkage of the material and the transformation stress is caused by microstructural transformations of the material. [12]

There is not much reported experimental work on determining the residual stresses of flame cut heavy steels available. The earlier studies are mainly concentrated on modelling the flame cutting heat flow and the residual stress state of the cut edge [4,6,8,13,14]. The aim of this study was to determine residual stress profiles produced by different flame cutting procedures. Also microstructures and hardness profiles of flame cut edge were studied and the results were reflected to earlier studies and to industrial flame cutting.

Materials and methods

Materials. The studied samples were steel blocks which were flame cut from low-alloy hot rolled 400 HBW steel plates. The size of the samples was 40 mm x 150 mm x 150 mm (thickness x length x width). The chemical composition of the samples is presented in Table 1.

Flame cutting was done by using an oxyfuel propane gas flame. Used flame cutting parameters are gathered in Table 2. Cutting speeds for the flame cut samples were 150 mm/min and 300 mm/min. Also 250 ºC furnace preheating was used for sample 3 and 600 ºC post heating with flame was used for sample 4.

Table 1. *Chemical composition of steel.*

Amount of elements [Wt%]				
C	**Cr**	**Mn**	**Si**	**Mo**
0,132	0,887	0,969	0,617	0,270
Al	**Ni**	**Cu**	**Nb**	**B**
0,08	0,06	0,01	0,003	0,001
balanced with Fe				

Table 2. *Samples and flame cutting parameters.*

Sample number	Cutting speed [mm/min]	Preheating [ºC]	Post heating [ºC]
1	150	-	-
2	300	-	-
3	300	250	-
4	300	-	600

Experimental procedure. Residual stress measurements were done by X-ray diffraction method (XRD), which measures the spacing of the of lattice planes that are affected by the residual stress. The lattice plane spacing changes from stress-free value to some new value which depends on the magnitude of presenting residual stress. Measurements were performed by XStress 3000 equipment (manufactured by Stresstech Oy). The measurements were carried out by using modified Chi-method [15] and the used measurement parameters are described in Table 3. The principal of this measurement is to calculate, using Bragg's law, the interplanar lattice spacing of ferrite [211] plane from the 156° Bragg diffraction angle. The lattice spacing d of the sample is measured at different ψ tilts, where the ψ angle is the angle between the normal of the sample and the normal of the

diffracting plane. Using elastic constants and the slope obtained from a plot of lattice spacing d as a function of $\sin^2\psi$, the residual stress can be calculated.

Table 3. *The used measurement parameters for XStress 3000 equipment.*

Parameters:			
ϕ-rotations (measurement directions)	0° and 90°	**Modulus of elasticity**	211 GPa
collimator	3 mm	**Poisson's ratio**	0,3
ψ-tilt angles in one directions (side / side)	6 / 6	**Voltage**	30 kV
maximum tilt angle	40°	**Current**	6,7 mA
ψ-oscillation	5°	**Radiation**	CrKα

Residual stress depth profiles were done at two points (A and B) at the centre line of each plate sample. Above described measurement was carried out in two perpendicular measurement directions identified as 0° and 90°. Selected measurement directions on the flame cut sample correspond to the flame cut direction and plate thickness direction, which are the most critical orientations for crack formation. Measurement points and measurement directions are illustrated in Fig. 1a.

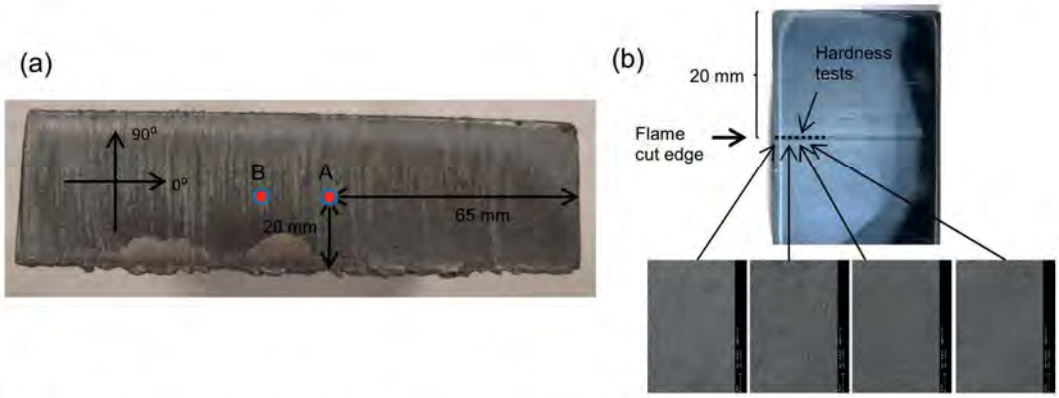

Fig. 1: (a) *Measurement points of X-ray diffraction method for the flame cut sample. 0° is the cut direction and 90° is the thickness direction.* ***(b)*** *Locations of hardness tests and microstructural characterization of flame cut samples.*

In each residual stress measurements the used X-ray diffraction radiation exposure time was 5 seconds. Between the residual stress measurements material layers were removed from measurement point with Movipol-3 (Struers) electrochemical polishing machine. Residual stress measurements combined with the layer removal enabled the measurements deeper from the cut surface. Polishing was done using electrolyte which was a mixture of 60% perchloric acid (A2-2), 65-85% ethanol, 10-15% 2-butoxyethanol and 5-15% water (A2-1). Polishing time was 45 second in a single polishing step and the used voltage in polishing was in range of 40-70 V. Polished and removed material depth was approximately 100-200 µm between the individual residual stress measurements. Material removal was verified with a dial indicator. The results of the XStress 3000 were analyzed with XTronic software and residual stress profiles were graphed from the analyzed results.

Also hardness depth profiles and microstructural characterization were done from the edge of the flame cut samples. Hardness measurements were carried out by Matsuzawa MMT-X7 microhardness tester with indentation load of 200 g. Microstructural characterization was performed with a scanning electron microscope (SEM), Zeiss ULTRAplus. The location of hardness depth profiles and SEM images are presented in Figure 1b.

Results and discussion

The hardness depth profiles of flame cut samples are described in Fig 2c. Slow cutting speed and fast cutting speed with preheating creates wider HAZ (increased hardness region in cut surface) than faster cutting speed. This observation is similar to earlier studies [5,6]. From Fig. 2c it can be seen that the high post heating temperature softens material too much compared to other cutting parameters. In each hardness profile (except 300 mm/min post heating 600 °C) there is a hard region in surface of the cut edge. Beyond this hard region the hardness values drop down and then start to rise slowly again. Hardness variations are dependent of the cutting parameters and thus can be affected by them.

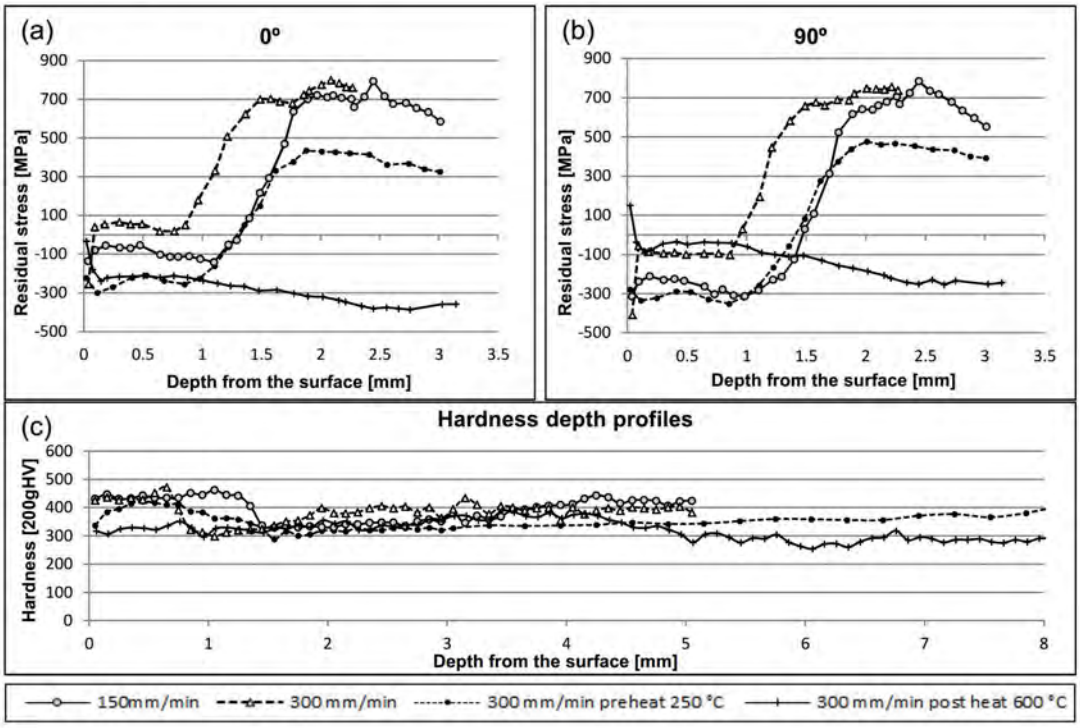

Fig. 2: ***(a)*** *The residual stress profiles of the flame cut samples in 0° measurement direction.* ***(b)*** *The residual stress profiles of the flame cut samples in 90° measurement direction.* ***(c)*** *The hardness depth profiles of flame cut samples.*

Fig. 2a and 2b describe the residual stress depth profiles of the flame cut samples in measurement directions of 0° and 90°. As it can be seen from Fig. 2a and 2b, change in flame cutting parameters produce different residual stress state in both measurement directions 0° and 90°. Very high post heating temperature (600°C) produced residual stress profile which was entirely different than other residual stress profiles, but it is not involved in further comparison with other cutting procedures due to the excessive softening of the cut edge. Cutting parameters 150 mm/min and 300 mm/min produced residual tensile stress peak which was around 700 MPa. Fast cutting speed combined with 250 °C preheating decreased the residual tensile stress peak to around 450 MPa. There were also differences in the residual compressive stress values which were created close to the cutting edge during flame cutting. Results indicate that with slow cutting speed or fast cutting speed combined with preheating more favourable residual stress state can be produced to the flame cut edge. Slow cutting or fast cutting with preheating produce more residual compressive stress and preheating also lowers the residual tensile stress peak which are beneficial against cracking. Same observations can be done on residual stress profiles in both 0° and 90° directions.

The shape of the residual stress profiles resemble a lot of earlier studied computer models [4]. The probability of cracking is known to be higher when faster cutting speeds are used and when preheating is not applied [4,14]. Present findings indicate that slow cutting speed and fast cutting speed with preheating produce more favourable residual stress profiles to the cut edge. Therefore when choosing optimized cutting parameters the cracking probability can significantly be reduced.

Fig. 3 presents the microstructure gradients in the cut edge from the flame cut steel samples with cutting speeds of 300 mm/min and 150 mm/min.

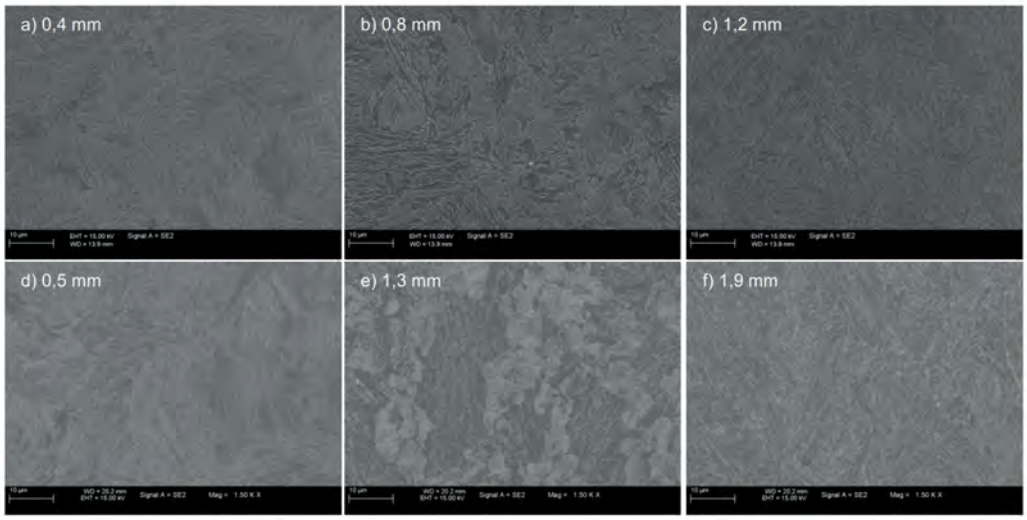

Fig. 3: *Micrographs from flame cut sample which is cut using cutting speed 300 mm/min.* ***(a)*** *0,4 mm from the surface.* ***(b)*** *0,8 mm from the surface presenting the two-phase region.* ***(c)*** *1,2 mm from the surface. Micrographs from flame cut sample which is cut using cutting speed 150 mm/min.* ***(d)*** *0,5 mm from the surface.* ***(e)*** *1,3 mm from the surface presenting the two-phase region.* ***(f)*** *1,9 mm from the surface.*

The original microstructure of the samples prior the flame cutting is martensitic. In flame cutting some metallurgical transformations occur near the cut edge due to the heat generation and cooling effect. In both samples three different regions can be discovered from the cut edge. First there is a region which is reaustenized during the flame cutting and martensite is formed to this region during the rapid cooling (high hardness near surface). After that there is a two-phase region (soft region) which is the mixture of newly formed martensite and tempered martensite. Microstructure changes to tempered martensite after two-phase region. Slow cutting speed is known to produce wider martensite layer to the cut edge than fast cutting speed [7]. Present study also indicates that slow cutting speed creates wider martensite layer. In martensite region the residual stress is compressive within slow cutting speed and near zero with fast cutting speed. In two-phase region residual stress profiles change from residual compressive stress to residual tensile stress as it can be seen from Fig. 2a and 2b. The residual tensile stress peaks are just beyond the two-phase regions. The present study shows that flame cutting parameters have a strong influence on HAZ microstructure, hardness and residual stresses and this agrees also well with the earlier studies [1,4,6,7,8] .

Conclusions

The investigated flame cut samples showed that mechanical properties, microstructure and residual stress state of the flame cut edge can be influenced by varying the flame cutting parameters. Residual stress depth profiling, hardness depth profiling and microstructural investigation were done to samples which were flame cut with slow and fast cutting speed and with preheating or post heating. Results indicate that slow cutting speed and fast cutting speed with preheating produce

more favourable residual stress state (greater residual compressive stress region and preheating also lowers residual tensile stress peak) in the cut edge than fast cutting speed without preheating. Fast cutting speed with preheating and post heating decreased hardness values in the cut edge more than slow or fast cutting speed. Slow cutting speed created wider hard martensite layer in cut edge than fast cutting speed. Results show that optimizing the cutting parameters, mechanical properties, microstructure and residual stress state of the flame cut edge can be improved and this way cracking probability of the thick steel plates can be reduced.

Acknowledgements

The work was funded mainly by the TUT's graduate school. The authors would like to thank FIMECC BSA programme from the additional financial support. Also we like to thank Dr. Essi Sarlin for the SEM work.

References

[1] R. Thiébaud, J. Drezet, J. Lebet, Experimental and numerical characterisation of heat flow during flame cutting of thick steel plates, J. Mater. Process. Tech. 214 (2014) 304-310.

[2] L.R. Soisson, Oxyfuel Gas cutting, Welding, Brazing, and soldering, Vol 6, ASM Handbook ASM International, 1993.

[3] HARDOX TechSupport, SSAB Oxelösund, 2007.

[4] L.E. Lindgren, A. Carlestam, M. Jonsson, Computational model of flame-cutting, J. Eng. Mater. Tech. 115 (1993) 440-445.

[5] A. Martín-Meizoso, J. Aldazabal, J.L. Pedrejón, S. Moreno, Resilience and ductility of Oxy-fuel HAZ cut, Frattura ed Integrita Strutturale 30 (2014) 14-22.

[6] W.E. Wood, Heat-affected zone studies of thermally cut structural steels. Publication No. FHWA-RD-93-015, U.S. Department of Transportation, Federal Highway Administration, 1994.

[7] H. Thomas, J. De Back, T.J. Bos, T. Muller, J.J.W. Nibbering, C.J.J.M. Verwey, R. Vonk, The Properties of flame-cut edges, Final report of Working Group 1913 of the Netherlands Institute of Welding, Technical steel research, Commission of the european communities, 1980.

[8] R. Thiébaud, J. Lebet, Experimental study of residual stresses in thick steel plates, Structural Stability Research Council, 2012.

[9] G.S. Schajer, (ed.); Practical residual stress measurement methods, Wiley, 2013.

[10] J. Lu, (ed.); Handbook of Measurement of Residual Stresses, Society for Experimental Mechanics Inc., The Farmont Press Inc.,1996.

[11] A.J. Perry, J.A. Sue, P.J. Martin, Practical measurement of the residual stress in coatings, Surf. Coat. Tech. 81 (1996) 17-28.

[12] D. Radaj, Heat effects of welding: temperature field, residual stresses, distortion; Berlin: Springer-Verlag, 1992.

[13] L.E. Lindgren, A. Carlestam, COMMP'93: International Conference on Computer-Assisted Materials design and Process Simulation, Nippon, Toshi Center, Tokyo, Japan, 1993, pp. 141-146.

[14] Z.Y. Wei, Y.J. Liu, B. Zhou, Distributions and Influence Factors of Residual Stresses Induced by Oxygen Cutting Opening in Steel Structure, Adv. Mat. Res. 314-316 (2011) 437-447.

[15] Non-destructive Testing. Test Method for Residual Stress analysis by X-ray Diffraction, SFS-EN 15305, Suomen Strandardisoimisliitto, SFS, Helsinki, 2008.

PUBLICATION II

Characterization of Flame Cut Heavy Steel – Modeling of Temperature History and Residual Stress Formation

T. Jokiaho, A. Laitinen, S. Santa-aho, M. Isakov, P. Peura, T. Saarinen, A. Lehtovaara, M. Vippola

Metallurgical and materials transactions B, Vol. 48, pp. 2891-2901
https://doi.org/10.1007/s11663-017-1090-x

Characterization of Flame Cut Heavy Steel – Modeling of Temperature History and Residual Stress Formation

T. Jokiaho[a,*,1], A. Laitinen[a], S. Santa-aho[a], M. Isakov[a], P. Peura[a], T. Saarinen[b,c], A. Lehtovaara[a], M. Vippola[a]

[a]Tampere University of Technology, Laboratory of Materials Science, P.O. Box 589, FI-33101 Tampere, Finland

[b]SSAB Europe Oy, Rautaruukintie 155, 92101 Raahe, Finland

[c]Sandvik Mining and Construction Oy, Pihtisulunkatu 9, 33330 Tampere, Finland[1]

*corresponding author

[1]tuomas.jokiaho@tut.fi

Abstract

Heavy steel plates are used in demanding applications that require both high strength and hardness. An important step in the production of such components is cutting the plates with a cost-effective thermal cutting method such as flame cutting. Flame cutting is performed with a controlled flame and oxygen jet, which burns the steel and forms a cutting edge. However, the thermal cutting of heavy steel plates causes several problems. A heat-affected zone (HAZ) is generated at the cut edge due to the steep temperature gradient. Consequently, volume changes, hardness variations and microstructural changes occur in the HAZ. In addition, residual stresses are formed at the cut edge during the process. In the worst case, unsuitable flame cutting practices generate cracks at the cut edge.

The flame cutting of thick steel plate was modeled by using the commercial finite element software ABAQUS. The results of modeling were verified by X-ray diffraction based residual stress measurements and microstructural analysis. The model provides several outcomes, such as obtaining more information related to the formation of residual stresses and the temperature history during the flame cutting process. In addition, an extensive series of flame cut samples was designed with the assistance of the model.

[1] Present address.

Keywords: flame cutting, heavy steel plate, finite element, heat-affected zone, temperature history, residual stress

Introduction

Flame cutting is a thermal cutting method generally used by steel manufacturers. It is an effective method for cutting thick wear-resistant steel plate, unlike mechanical cutting, which is both difficult and too slow for high production rates. Flame cutting is an exothermal process, which provides an advantage over other thermal cutting methods, because the heat generated from the cutting process supports the continuation of the flame cutting [1].

The flame cutting process consists of three steps. Firstly, the steel is heated locally to its ignition temperature by using a flame obtained from the combustion of a specific fuel gas mixed with oxygen. Secondly, the heated spot is burnt with a jet of pure oxygen, which creates a continuous chemical reaction between the oxygen and the steel. Thirdly, the oxygen jet not only burns the steel but also blows away the iron oxide that is formed during the cutting process. [2]

However, the flame cut edge is prone to cracking, which makes cutting of thick steel plate problematic. It has been shown [3] that an increase in both the hardness and thickness of the plate enhances the cracking tendency. Flame cutting produces a heat-affected zone (HAZ) at the cut edge of steel plate due to the generation of a steep thermal gradient during the cutting process. For example, Martín-Meizoso et al. [4] have reported that microstructural changes and hardness variations occur in the HAZ. Hardness values have been observed to be higher closer to the cut edge and decrease over a short distance from the cut edge [5]. In addition, the width of the HAZ decreases with increasing cutting speed [6]. Thomas et al. [7] found that flame cutting produces a martensitic layer on the steel edge. The thickness of the martensitic layer and the HAZ were observed to be dependent on the plate thickness and flame cutting speed.

The flame cutting process results in the formation of residual stresses in the cut edge of the steel. It has been reported [3] that high residual stresses in the cut edge promote crack formation. Residual stresses are formed by uneven plastic strains in the material which cause elastic strains. These elastic strains maintain the dimensional continuity in the vicinity of the plastically deformed regions [8]. The elastic strains and hence the residual stresses can be either compressive or tensile. Generally, residual compressive stresses are beneficial because they reduce the probability of cracking,

whereas residual tensile stresses are unfavorable because they enhance it. Large thermal gradients produced by flame cutting cause residual stresses consisting both of thermal stresses and transformation stresses. Thermal stress arises from the inhomogeneous thermal expansion and contraction of the material, while transformation stress is produced by microstructural transformations and their different volumetric expansions. [9]

Several studies have been carried out to determine and model the generation of residual stresses during flame cutting. Wei et al. [10] modeled the flame cutting of 10-mm-thick steel plate and the simulation results indicated that a slower cutting speed produced a wider HAZ and more compressive stress than a faster cutting speed. However, the cutting speed did not have any notable impact on the residual tensile stress maxima. Thiébaud and Lebet [11] used the section method to measure the residual stress distribution from 60-mm-thick steel plate. The results indicated that there was a tensile stress region close to the cut edge, which decreased rapidly with increasing distance from the edge, and was partly balanced by a compressive stress region deeper in the subsurface. Thomas et al. [7] studied 25 mm and 35 mm steel plates and discovered that, at a short distance (0.1 mm) below the flame cutting edge, the stresses are compressive and deeper (>1 mm), the stresses are tensile. Lindgren et al. [3] measured and modeled the residual stresses produced by flame cutting 50-mm-thick steel plates and the simulation results indicated the formation of a low compression stress region close to the cut edge, which was followed by a high residual tensile stress region. The residual tensile stress state was lower in preheated samples compared to samples which were cut without preheating. This model was verified by using a hole drilling strain gauge method to measure the residual stresses from certain locations of the cut edge. Despite the earlier studies, the residual stress formation in thick wear-resistant steel plates during the flame cutting process remains a fairly unknown phenomenon. The effect of different cutting parameters has been studied to some extent but further information related to this topic is required.

The aim of this study was to develop a model, which provides an effective tool for investigating the flame cutting process of a thick wear-resistant steel plate. In addition, modeling creates an opportunity to obtain information about the steel plate during the flame cutting process, which is almost impossible to obtain experimentally. The present model enables us to systematically study the effect of different flame cutting parameters, such as various flame cutting speeds, cutting preheated plate

and cutting steel plate of different plate thicknesses. In addition, with the assistance of the model we can design the flame cut parameters to be used in a comprehensive test series for future studies.

Material modeling and Experimental procedure

The modeling of the thick steel plate flame cutting process was carried out by using the commercial finite element software ABAQUS. The purpose of the modeling work was to simulate the behavior of a previously studied [12] low-alloyed wear-resistant steel, the composition of which is given in Table 1. In the preliminary study [12], the residual stress profiles were measured from some flame-cut thick wear-resistant steel plates. The modeled part here was a rectangular shape steel plate modelled as a two-dimensional plane strain section: the thickness (y-direction) was set to 40 millimeters and the width (x-direction) was defined as long enough that the body could be considered semi-infinite. The model was constructed with a mesh with over 33 000 four-node bilinear thermo-mechanically coupled elements (Fig.1). The mesh was designed to be denser (element size of 0.04 mm) in the middle section in order to ensure accurate results from the area of interest, which is the most critical for crack formation.

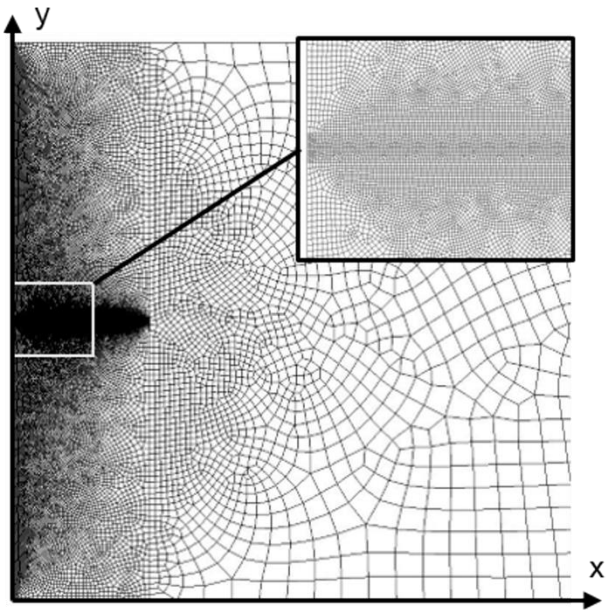

Fig. 1. *Finite element mesh with a zoomed view from the middle section.*

During the flame cutting process, every material point within the solid has its individual temperature history (i.e. maximal temperature, heating and cooling rate, etc.), which affects the material properties. For example, material properties during cooling depend on the maximum temperature

attained during heating. Accurate simulation of these history effects would require a very large number of experimental tests and a large number of material parameters in the model. Therefore, in the model presented here a simplification is made, i.e. most of the thermal and mechanical properties are assumed to be directly temperature-dependent without any history effects. The only exception is the thermal expansion coefficients, which have different values depending on the maximum temperature and whether the part is heating up or cooling down. As explained below, thermal expansion coefficients are used to model the effect of phase transformations on a specific material volume. Therefore, a history-dependent approach is needed for these material properties. In order to acquire the temperature-dependent yield strength properties of the material, a series of uniaxial compression tests was conducted in various temperatures using a Gleeble 3800 thermo-mechanical simulator. The strain rate in the test was set to 1 1/s to correspond to the actual cutting process and the specimen was heated to the target temperature at a heating rate of 250 °C/s. Loading was applied for 0.5-1.0 seconds after reaching the target temperature, thus minimizing excess temperature effects like tempering.

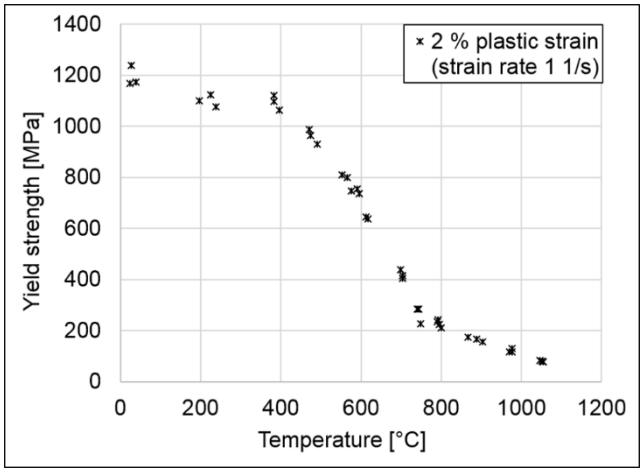

Fig. 2. *The results of the uniaxial compression tests using Gleeble: yield strength at 2 % plastic strain as a function of temperature.*

Fig. 2 shows that yield strength is a highly temperature-dependent material property and there is a significant drop in the yield strength values after the temperature rises above 400 °C. Acquiring correct values for yield strength as a function of temperature is important, since the yield limit decides whether the material reacts elastically or elastoplastically, which has a major impact on the stress distribution inside the steel plate. It should be noted that the yield strength values were measured for

the heating stage only and assumed to adequately represent the material behavior also during the cooling stage.

In order to work correctly, the model requires phase transformation temperatures for both austenite (A_{c3} and A_{c1}) and martensite (M_s and M_f) transformations. Both the austenite start temperature (A_{c1}) and the martensite start temperature (M_s) were obtained using the Andrews equations [13]:

$$A_{c1}(°C) = 723 - 10{,}7Mn – 16.9Ni + 29.1Si + 16.9Cr + 290As + 6.38W \quad (1)$$

$$M_s(°C) = 539 - 423C - 30.4Mn - 17.7Ni - 12.1Cr – 7.5Mo \quad (2)$$

where the chemical symbols denote the weight percentage of the element in question. However, a different approach was needed for the full austenitizing temperature (A_{c3}), due to the rapid heating characteristic of flame cutting. The A_{c3} was set to 1077 °C after comparing the temperature distribution obtained from the model with microstructures observed from SEM micrographs, such as Fig. 3.

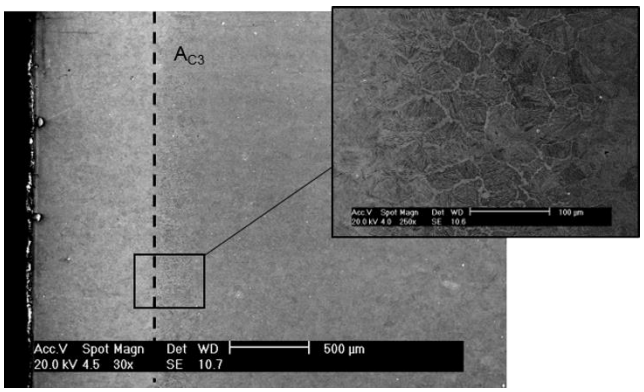

Fig. 3. *SEM micrograph from the cut edge of a 300 mm/min flame cut sample.*

In Fig. 3, the microstructural regions formed during the 300 mm/min flame cutting process can be seen. The fully martensitic region extends 0.8 mm from the flame cut edge of the sample. The M_f temperature was estimated to be 234 °C. According to Steven and Haynes [14], the M_f temperature can be approximated as 215 ± 15 °C below the M_s temperature. The phase transformation temperatures implemented in the model are shown in Table 2.

The thermal and phase transformation induced (austenite and martensite) volume changes were entered into the model as subroutines. The austenite phase fraction (f_a) was calculated using a modified Avrami function called Weibull's cumulative distribution function [15]:

$$f_a = f_{a_{final}} \left(1 - exp\left\{A\left(\frac{T - A_{c1}}{A_{c3} - A_{c1}}\right)^B\right\}\right), \quad (2)$$

where $f_{a_{final}}$ is the phase fraction at the end of the transformation, and A and B are material-dependent constants, set to -6 and 2, respectively [15]. The effect of austenite formation in the thermal axial expansion (∆L/L) was calculated using the following equation:

$$\frac{\Delta L}{L} = (f_a \alpha_a + (1 - f_a)\alpha_s)\Delta T, \quad (3)$$

where α_s is the thermal expansion coefficient of the parent steel and α_a is the austenite thermal expansion coefficient, set to 13 x 10^{-6} 1/K and 20 x 10^{-6} 1/K, respectively. The thermal expansion coefficient of the martensite (α_m) was the same as that of the parent steel. The martensitic phase fraction (f_m) was calculated by using the equation derived from Koistinen and Marburger [16]:

$$f_m = 1 - exp\{\beta(M_s - T)\}, \quad (4)$$

where a value of -0.04 was used for β, which was selected so that 50 per cent of the martensite transformation happens almost instantly. The axial expansion changes caused by the martensitic phase transformation were introduced to the model via thermal expansion subroutines, as shown in the following equation:

$$\frac{\Delta L}{L} = \left\{f_a\left((1 - f_m)\alpha_a + (f_m \alpha_m) + \left(\frac{\Delta x_m}{x_m}\Big/\left(M_f - M_s\right)\right)\right) + (1 - f_a)\alpha_s\right\}\Delta T, \quad (5)$$

where the $\Delta x_m/x_m$ is the axial expansion of the martensitic phase and was set to 0.75 per cent, which was evaluated to correspond to the real situation. The axial expansion can be converted to a volume expansion using the equation:

$$\frac{\Delta V}{V} = \left(1 + \frac{\Delta L}{L}\right)^3 - 1, \quad (6)$$

For simplification, the martensitic transformation was considered to be an isotropic volume expansion, which may not fully correlate with the actual martensitic transformation process.

The simulation of the flame is one step in the modeling of the flame cutting of a steel plate. From a modeling perspective, flame cutting is an extremely complex process with a large set of variables, which it is difficult to verify. However, the main purpose of this model was to study what occurs inside

the steel when it is subjected to a large amount of heat, rather than the perfect modeling of the flame. Consequently, some simplifications had to be made. Therefore, the flame was created as a time-dependent heat flux, which simulated the movement of the flame. In the three dimensional preliminary simulations the flame was modeled as a moving line heat flux on the surface (the cutting surface) of the plate. Based on the results of these preliminary studies the heat source was modelled in the actual two-dimensional simulations as a heat flux boundary condition (Fig. 4(a)) on the edge on the element mesh (the left edge of the model in Fig.1). The movement of the flame was simulated by changing the amplitude of the flux with respect to time. Similar method has previously been used by Lindgren et al. [3]. To represent the real flame cutting process, the heat flux applied to the part was not totally uniform, thus the upper (flame) side of the part was subjected to more heat since the flame has a greater impact there. In addition, we used a time-dependent amplitude distribution of the heat flux in our model to resemble a moving flame. The amplitude distribution for the 150 mm/min cutting speed heat flux (Fig. 4(b)) was created by studying the data obtained from a simulation based on a three-dimensional flame model.

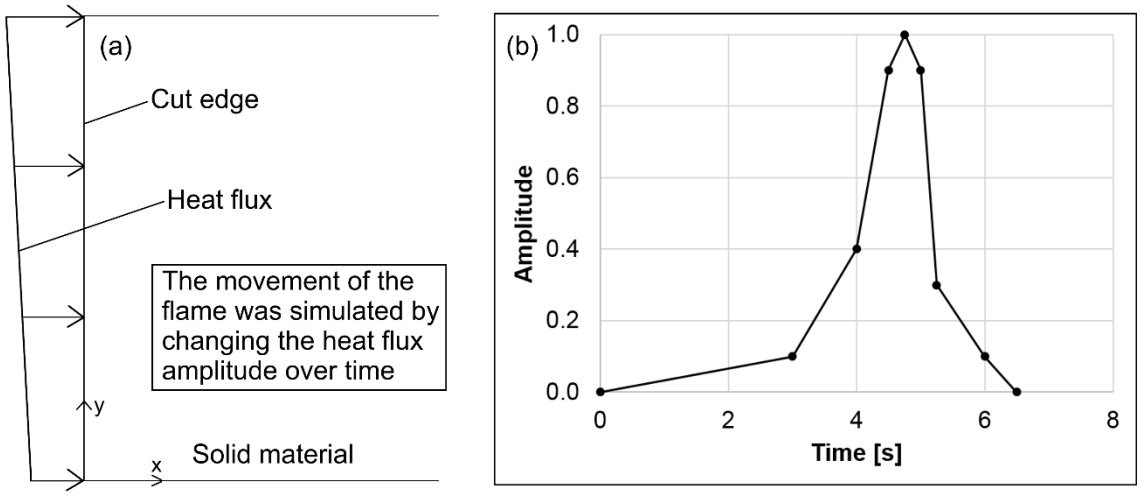

Fig. 4. *(a) Heat distribution along the cut edge (y-axis is the cutting depth). (b) The time-dependence of the heat flux amplitude for 150 mm/min cutting speed. It should be noted that the y-axis presents the magnitude of the heat flux relative to the maximum value.*

In Fig. 4(b), the time frame between 0 and 4.5 seconds simulates the heat transfer which occurs through conduction before the flame arrives. The period between 4.5 and 5 seconds simulates the moment when the flame is connected to the observed position. The time frame between 5 and 6.5 seconds represents the heat transfer to the observed position after the flame has passed. A similar

heat flux amplitude was used for other cutting speeds, although the periods were divided according to how fast the process was compared to the 150 mm/min cutting speed.

The heat input for the flame was determined by iterating the magnitude of the heat flux. The heat input (maximum amplitude with reference to Fig. 4(b)) for thermal analysis was 1.8 x 10^7 W/m^2 and it was selected so that the surface temperature at the center of the plate (i.e., x=0 and y=0.5 x thickness in Fig. 1) reached the melting point of 1520 °C. The heat input for the stress analysis of 150 mm/min and 300 mm/min cutting speeds was set to 1.65 x 10^7 W/m^2 and 2.37 x 10^7 W/m^2, respectively. The heat flux for stress analysis was selected so that the maximum temperature at the above-mentioned location (surface of the center of the plate) was just below the melting point. This was necessary in order to avoid the removal of elements or setting them to zero, which would have an undesired effect on the analysis of the stress curves in the surface region. Since the heat flux represents the net heat, the heat losses of the flame are ignored. In addition, the model was used to study the effect of preheating, as it has been observed to lower tensile stress maximum values in residual stress measurements. Preheating was simulated by setting the modeled part for different predefined temperature fields and the heat flux magnitudes were adjusted so that the surface elements would not exceed the melting temperature.

The results of the model were verified by residual stress measurements done with an XStress 3000 X-ray diffractometer (manufactured by Stresstech Oy) and the measurement method used is called the modified Chi method [17]. This method calculates, using Bragg's law, the interplanar lattice spacing of the ferrite [211] plane from the 156° Bragg diffraction angle. The lattice plane spacing changes from a stress-free value to some new value depending on the magnitude of the residual stress. With this method, the lattice spacing d of the sample is measured at different ψ tilts, where the ψ angle is the angle between the normal of the sample and the normal of the diffracting plane. The measured values provide a slope containing a plot of lattice spacing d as a function of $\sin^2 \psi$. This slope with elastic constants can be used to calculate the residual stress from the measured location. Residual stresses are calculated using the following equation [18]:

$$\sigma = \left(\frac{E}{(1+\nu)}\right) m, \qquad (7)$$

where the σ is the residual stress in the measured direction, E is the Young's modulus, v is the Poisson's ratio and m is the slope obtained from the lattice spacing d vs. $\sin^2 \psi$ curve. The parameters used are listed in Table 3.

Residual stresses, used for model verification, were measured from 40-mm-thick samples, which were flame cut using cutting speeds of 150 mm/min, 300 mm/min and 300 mm/min with preheating at 200 °C. Samples were measured from two locations (A and B) and in two perpendicular measurement directions: the flame cut direction (0°) and the thickness direction (90°). These selected directions are the most critical orientations for crack formation. The measurement locations and directions are shown in Fig. 5.

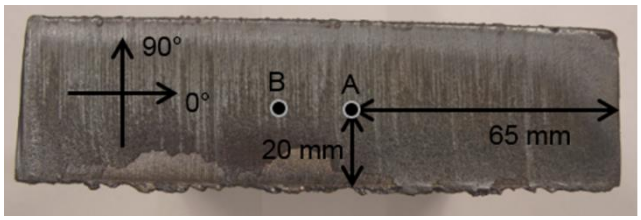

Fig. 5. *Residual stress measurement locations of X-ray diffraction method for a flame cut sample.*

Between the residual stress measurements, material layers were removed from the measurement location by electrochemical polishing. The polishing was done using Struers A2 electrolyte (a mixture of 60% perchloric acid, 65-85% ethanol, 10-15% 2-butoxyethanol and 5-15% water) and material removal was verified with a dial indicator. Residual stress measurement, combined with the layer removal method, provides residual stress depth profiles. The polished material depth was approximately 100-200 µm between each measurement. The measurement results were analyzed with XTronic software and residual stress profiles were plotted from the analyzed results.

Results and discussion

The model provided valuable information related to the temperature history of the part during the flame cutting process. Fig. 6 shows the modelled temperature profiles from different distances from the flame cut edge calculated at cutting speeds of 150 mm/min and 300 mm/min, respectively.

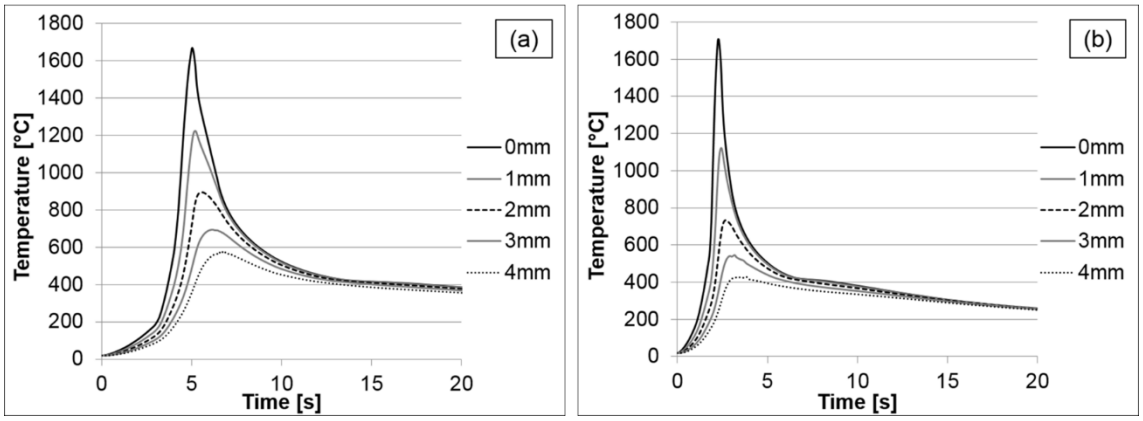

Fig. 6. *Temperature curves from different distances from the flame cut edge at (a) 150 mm/min and (b) 300 mm/min cutting speeds.*

Fig. 6 shows that the slower cutting speed creates more heat at the cut edge of the plate. In contrast, the faster cutting speed produces steeper thermal gradients compared to the slower cutting speed. With the slower cutting speed, the part has more time to heat up and the material has more time to adapt to the cutting situation. The shapes of the curves correspond to the experimental results of Thiébaud et al. [2].

One of the main purposes of the model was to reveal information on what occurs to the steel part during the flame cutting process. The uneven temperature distribution in the cut edge creates differing thermal expansion (and contraction) and consequently different residual thermal stresses. Fig. 7(a) shows the modeled thermal stress profiles (thickness direction) produced during the flame cutting process at cutting speeds of 150 mm/min and 300 mm/min. It should be noted that in general the maximum possible stress at a given temperature is limited by the current yield strength and fracture stress of the material, but in the simulations the plasticity of the material was taken into consideration. Therefore, the simulation results can be considered to indicate the best-case scenario, i.e. in reality, material fracture might take place at stress levels below those represented by the current simulations.

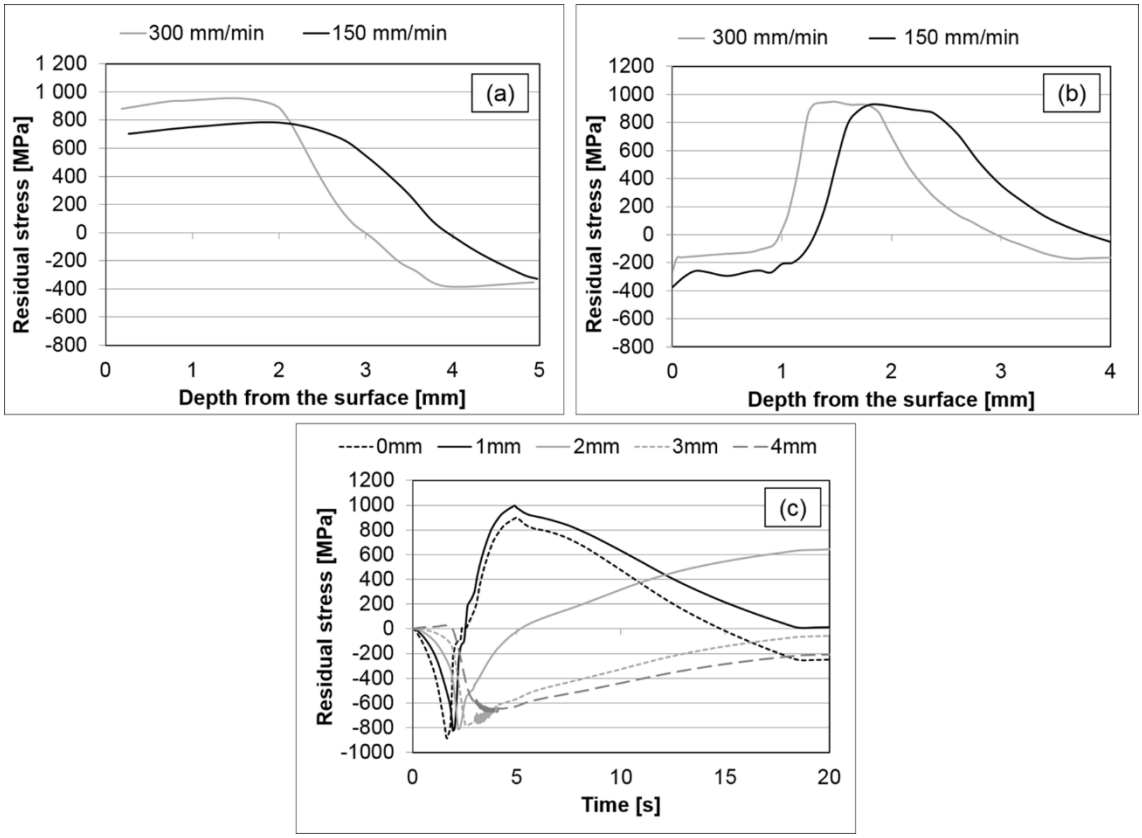

259

260 ***Fig. 7.*** *Simulated residual thermal stress profiles (thickness direction) of 150 mm/min and 300*
261 *mm/min flame cutting speeds (a) without phase transformations and (b) with phase transformations.*
262 *(c) Modelled residual stress formation during flame cutting with 300 mm/min cutting speed.*

263 The residual thermal stress state during the flame cutting process is very difficult to determine
264 experimentally; therefore, modeling is essentially the only tool capable of providing such information.
265 In addition, simulations allow us to separate the effects of pure thermal expansion from the effects of
266 phase transformations. This is illustrated in Fig. 7(a). Without the phase transformation, the residual
267 thermal stresses are due to the uneven thermal expansion and contraction that occurs during cutting.
268 The high temperature causes volume expansion in the cut edge, which is constrained by the cold
269 surroundings, thus creating a compressive stress near the cut edge. Consequently, as the
270 temperature increases and simultaneously the yield limit is lowered, the compressive stress exceeds
271 the yield limit and produces a plastically deformed (compressed) region near the cut edge. During
272 cooling, the contraction of the compressed region is restrained by the region without plastic
273 deformation. For this reason, residual tensile stress is generated in the deformed region near the cut
274 edge. The residual tensile stress is then balanced by the residual compressive stress deeper inside

the part. As we can see from Figs. 6(a), 6(b) and 7(a), the faster cutting speed produces steeper thermal gradients in the cut edge, consequently creating higher thermal stresses in the cut edge compared to the slower cutting speed. Therefore, rapid and significant temperature changes should be avoided in the flame cut edge.

In the actual case, martensitic phase transformation is also involved in the steel structure during the flame cutting process. Fig. 7(b) shows the modeled residual stress profiles produced by 150 mm/min and 300 mm/min cutting speeds, which also takes into account the phase transformation. The effect of the volume expansion caused by martensitic transformation on the formation of the residual stress profiles is clearly seen. The martensitic transformation relieves the residual thermal tensile stresses near the flame cut edge and produces a residual compressive stress. The shapes of both residual stress curves are quite similar, but the residual compressive stress area at the surface is larger at the cutting speed of 150 mm/min than at 300 mm/min. The reason for this is the higher heat input caused by the slower cutting speed. Therefore, the phase transformation regions are larger and more elements experience the expansion effect due to martensitic transformation. Fig. 7(a) and 7(b) show that a cutting speed producing lower thermal stress also produces more residual compressive stress during martensitic transformation. This result also indicates that steep thermal gradients should be avoided during the flame cutting process.

Fig. 7(c) summarizes the whole chain of events that takes place during the flame cutting process. At first, the heat from the flame produces compressive stress near the surface. The stress changes to tensile once the heat is no longer applied and the part begins to cool down after 3 seconds. The tensile stress peak value is highest at 5 seconds, when the part has reached the M_s temperature and martensite starts to form, leading to volume expansion and hence to a change in the local stress state from tensile into compression. After the martensite transformation, the stresses gradually set into the final state (Fig. 7(b)) as the temperature decreases towards room temperature. The above-mentioned effect of martensite nucleation can be seen from the 0 mm and 1 mm stress curves, which are located in the phase transformation regions. However, the 2 mm curve is not located in the phase transformation region, and therefore the tensile stress continuously increases until the part reaches room temperature. Similar changes take place deeper in the material, but the resulting residual stress levels are at a lower level. It is noteworthy that, as Fig. 7(c) shows, the stress state near the surface

changes during the cutting process (around 2.5 seconds in Figure 7c) from compressive stress to high tensile stress before changing back to compressive. This rapid change in the stress state takes place just prior to the martensitic transformation and might create potential sites for crack formation during the cutting process.

The model was used to predict residual stress formation with different flame cutting parameters and various plate thicknesses. Fig. 8 shows the residual stress curves for (a) different cutting speeds, (b) different plate thicknesses and (c) cutting at different preheating temperatures. The flame cutting speed of 300 mm/min was used in Fig. 8(b) and 8(c). The presented residual stress profiles are in the thickness direction of the modeled plate.

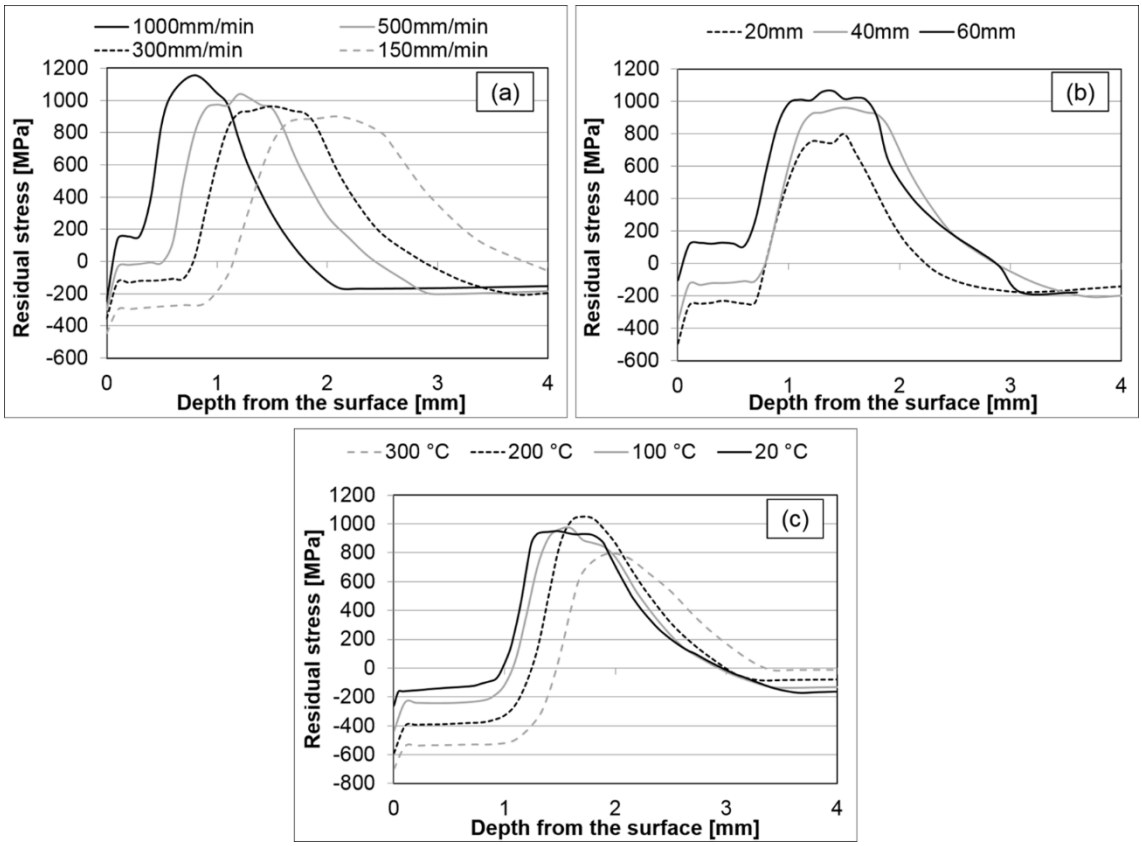

Fig. 8. *Simulation of the residual stresses (thickness direction) for different flame cutting processes: (a) cutting speed, (b) plate thickness, (c) preheating temperatures.*

Fig. 8(a) shows that there is a linear development in the residual stress profiles according to the cutting speed. The thermal shock effect from the flame is greater at faster cutting speeds; as a result, greater residual stress values are produced closer to the cut surface. The volume expansion of martensitic transformation is not enough to produce a residual compressive stress region on the

surface at faster cutting speeds. These results also indicate that rapid heating should be prevented during flame cutting.

Fig. 8(b) shows the effect of plate thickness on the formation of residual stresses at a cutting speed of 300 mm/min. The vertical deformation is not as restricted in thinner plates as it is in thicker plates. Consequently, the cutting of thicker plates causes higher residual tensile stresses in the cut edge. In addition, the residual compressive stress decreases near the cut edge as the plate thickness increases. Therefore, due to the residual stress state produced by flame cutting, thicker plates are more prone to cracking than thinner plates.

As can be seen from Fig. 8(c), preheating lowers the residual stresses produced during flame cutting. Lindgren et al. [3] discovered similar effects with preheating compared to flame cutting without preheating. Preheating of the sample increases the residual compressive stresses and decreases the residual tensile stresses. However, present studies indicate that preheating not only increases the compressive stress but also expands the compressive stress region deeper in the subsurface. This is because the part is at a uniform preheating temperature; therefore, material deeper in the plate reaches the phase transformation temperatures when the heat is applied to the cut edge. Higher preheating temperatures decrease the effect of thermal shock by lowering the temperature differences inside the part, and consequently sufficiently high preheating temperatures decrease the residual tensile stresses.

Fig. 9 shows the modeled residual stress curve (thickness direction) (a) of 150 mm/min, (b) 300 mm/min and (c) 300 mm/min with 200 °C preheating, compared to experimentally measured data from a similar sample.

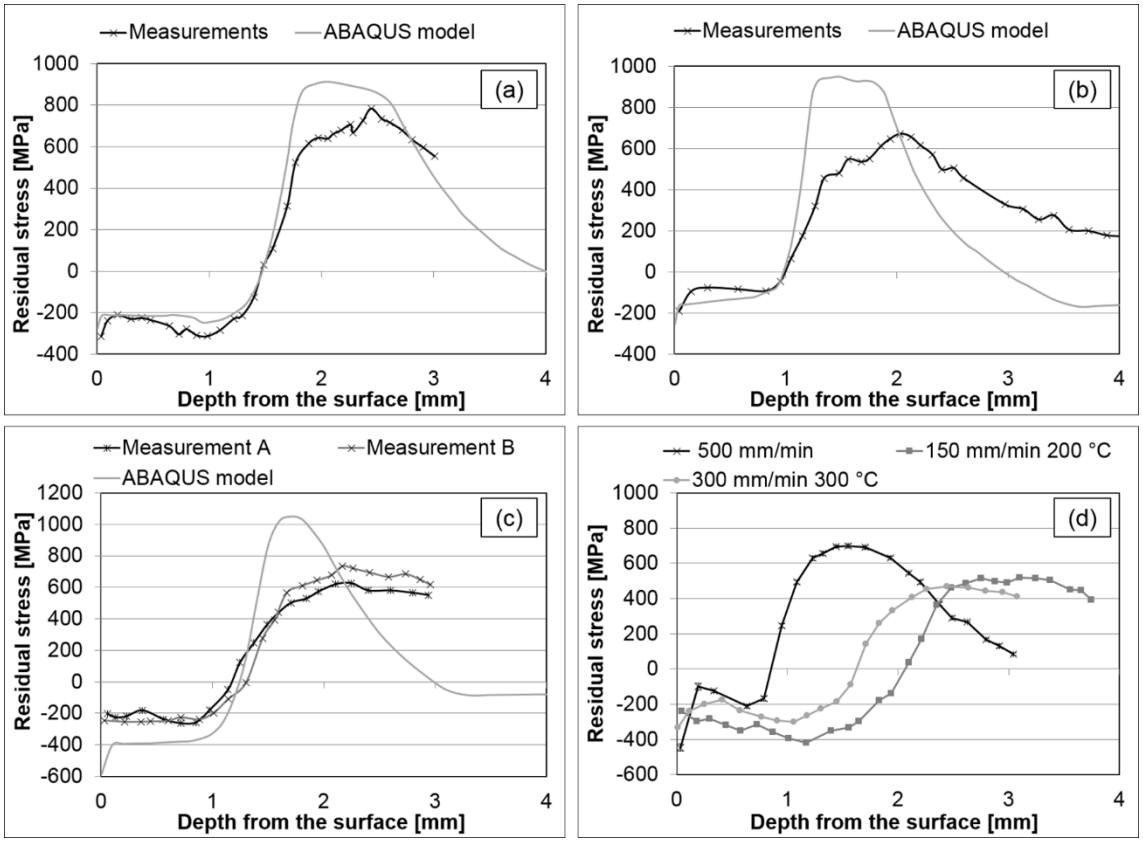

Fig. 9. *Comparison of modeled data with experimentally obtained data from (a) 150 mm/min, (b) 300 mm/min flame cutting speeds and (c) 300 mm/min cutting speed with 200 °C preheating. (d) Experimental measurements from samples which were flame cut using a cutting speed of 500 mm/min, 150 mm/min cutting speed with 200 °C preheating and 300 mm/min cutting speed with 300 °C preheating.*

Fig. 9(a) and 9(b) show that the compressive stress region is quite similar in both profiles; however, the residual tensile stress peaks are different. The tensile stress maximum is different in the model, which is to be expected, since the behavior of the material in the simulation is not totally equivalent to the behavior of steel in reality. The differences between the modelled and experimentally obtained residual stress curves of 300 mm/min (Fig. 9(b)) cutting speed are larger than for the 150 mm/min cutting speed (Fig. 9(a)). In the experimentally measured 300 mm/min flame cut sample, the tensile stress region is distributed to a larger area, which indicates that the material behavior and the heat load in the model are not fully accurate. Fig. 9(c) shows that preheating has a notable impact on the residual compressive stress region in both the modeled and measured profiles. However, there are differences, which can be explained by the slightly different cutting conditions in the actual flame cutting compared to the model. In addition, in the actual flame cutting, the tempering of martensite

also occurs, which is not taken into account in the model. In the preheated sample there is more tempering during the flame cutting compared to that without preheating, which may also be a reason for the difference between measured and modeled data. In addition, it has been noted [19] that diffraction based residual stress measuring method not only measures the type I residual stresses (macrostresses over large distances) but the type II residual stresses (microstresses over grain scale) can be also superimposed in the results. The purpose of this work was to study only the generation of long range (type I residual stresses) stresses during flame cutting by finite element simulations. This difference might also cause the deviation between modeled and experimental results.

Perfect modeling of the flame cutting process is a challenging task and there are many variables. Consequently, there are some simplifications in the model, which might have an effect on the results. It should be noted that the cracking was not taken into account in the modeling. In addition, two-dimensional modeling involves some restrictions. For example, in actual flame cutting, the moving flame not only heats one side of the part but it also simultaneously heats the part from both the cut and approach directions. Furthermore, in the actual cutting process the solid part is still intact in front of the cutting flame, which may have an effect on the formation of residual stresses. To summarize the differences of the model and experimental results (Fig. 9(a), 9(b) and 9(c)), the main discrepancy is seen at depths of 1.5 mm and deeper. Based on Fig. 6, the material temperature in this depth reaches the two-phase region and the resulting final microstructure is therefore a mixture of transformed and non-transformed material. From simulation point of view, this is the most demanding region because of the following reasons: 1) The actual microstructure in this region is very sensitive to the temperature history, thus highlighting any uncertainties in the simulated temperature field. 2) As noted previously, the simulations involved some simplifications in terms of material behavior, the most notable of which was the use of one yield strength – temperature –curve (Fig. 2) for all metallurgical states of the material. This means that the plastic-deformation behavior in the above mentioned two-phase region is probably oversimplified. In addition, the yield strength data obtained from the Gleeble experiments is from the heating stage only and at the maximum temperature, which is lower than in the actual flame cutting process. 3) Some phenomena, such as tempering of the martensite, were left outside the scope of the simulations, which most likely influences the results deeper in the material (the temperature deeper in the material is high enough for a long enough time so that some tempering may take place). The tempering of steel during flame cutting has an effect on the volume of the

388 tempered region. Therefore, the tempering also has an effect on the formation of residual stresses. In
389 this respect, the correspondence between the simulations and the measurements is considered good.

390 In addition to the modeled results, Fig. 9(d) shows experimentally obtained residual stress profiles
391 from samples which were flame cut using the following parameters: 500 mm/min cutting speed, 150
392 mm/min cutting speed with 200 °C preheating and 300 mm/min cutting speed with 300 °C preheating.
393 It clearly shows how the residual stress state can be affected by different cutting parameters. The 500
394 mm/min cutting speed produces a high residual tensile stress peak but only a small amount of
395 residual compressive stress near the cut edge. In contrast, the 300 mm/min cutting speed with 300 °C
396 preheating produced significantly more residual compressive stress near the cut edge compared to
397 cutting without preheating. The 150 mm/min cutting speed with 200 °C preheating also produced a
398 similar kind of compressive stress region near the cut surface, although the compressive stress region
399 extends deeper from the cut edge than the previous preheated sample. In addition, both preheated
400 samples have a much lower tensile stress peak compared to the sample that was cut without
401 preheating. These experimentally measured results confirm the predictions of the model: a slower
402 cutting speed produces more residual compressive stress, lowers the residual tensile stress peak and
403 preheating also has a similar effect on the residual stress state. In addition, the experimental
404 measurements show that the widest compressive residual stress region and a significantly lower
405 tensile stress peak can be produced by combining both a slow cutting speed and preheating. These
406 results also confirm that the developed model gives accurate trend lines for evaluating residual stress
407 formation during flame cutting.

408 **Conclusions**

409 Flame cutting of thick wear-resistant steel plates can be very problematic. It creates high residual
410 stresses and may cause cracking of the steel plate. Consequently, a model was developed to
411 investigate the problem and to study the flame cutting process. The model was created using the
412 finite element software ABAQUS and the input material was made to behave as similarly to the
413 studied steel as possible. The model takes into account the volume changes caused by thermal
414 expansion (contraction) and phase transformation (austenite and martensite). A variety of simulations
415 were computed using the model: flame cutting temperature histories, cutting at different cutting
416 speeds, cutting different plate thicknesses and cutting using different preheating temperatures. The

model enabled the study of residual stress formation during the flame cutting process, which would be extremely difficult or impossible to do experimentally. The results showed that the faster cutting speed produces steeper thermal gradients in the cut edge than the slower cutting speed and consequently higher residual tensile stresses. In addition, the slower cutting speed produced more residual compressive stress near the cut edge than the faster cutting speed. Therefore, rapid and large temperature variations during flame cutting should be avoided. In addition, the residual stresses vary quickly from compressive stress to tensile stress during the cutting process depending on the time and depth, which might create potential sites for crack formation. The results of the model also showed that varying the process parameters have an effect on the residual stress formation. The plate thickness also has an effect on the residual stress formation during the cutting process. Flame cutting of thinner plates created lower tensile stress maxima and more residual compressive stress than thicker plates. Therefore, the cracking tendency of thick plates is higher than thinner plates. The results also showed that preheating was an effective way to influence the residual stress formation during the cutting process. Flame cutting with preheating reduced the residual tensile stress and produced more compressive stress near the cut edge than cutting without preheating. In addition, the experimentally measured results confirmed the predictions of the model, as the slower cutting speed and preheating produced a wider residual compressive region and lowered tensile stresses. Additionally, the experimental results showed that combining both a slow cutting speed and preheating produced even more compressive stress and a significantly lower tensile stress peak. To conclude, the model produced valuable information about the flame cutting process and formation of residual stresses. In addition, the results of the model can be used as a basis for a new flame cut test series for future studies to reveal the comprehensive effect of microstructural features on residual stress and crack formation.

Acknowledgements

The funding for this work was mainly provided by the TUT graduate school. The authors would like to thank Mr. Juha Uusitalo from the University of Oulu for carrying out the Gleeble experiments.

References

[1] L.R. Soisson: 1993, ASM Handbook Online, ASM International, Vol. 6, pp. 1155-1165.

445 [2] R. Thiébaud, J. Drezet, J. Lebet: J. Mater. Process. Technol., 2014, vol. 214, pp. 304-310.

446 [3] L. Lindgren, A. Carlestam, M. Jonsson: J. Eng. Mater. Tech., 1993, vol. 115, pp. 440-445.

447 [4] A. Martín-Meizoso, J. Aldazabal, J.L. Pedrejón, S. Moreno: Frattura ed Integrita Strutturale, 2014,
448 vol. 30, pp. 14-22.

449 [5] A.D. Wilson: Eng. J., 1990, vol. 27, pp. 98-107.

450 [6] W. Wood: Publ. No. FHWA-RD-93-015, U.S. Department of Transportation, Federal Highway
451 Administration, Virginia, 1994.

452 [7] H. Thomas, J. De Back, T.J. Bos, T. Muller, J.J.W. Nibbering, C.J.J.M. Verwey, R. Vonk: Final
453 report of Working Group 1913 of the Netherlands Institute of Welding, Technical Steel Research,
454 Commission of the European Communities, Delft, 1980.

455 [8] G.S. Schajer: Practical Residual Stress Measurement Methods, 1 st. ed., John Wiley & Sons Ltd,
456 Chichester, 2013, pp. 1-3.

457 [9] D. Radaj: Heat effects of welding: temperature field, residual stresses, distortion, Springer-Verlag,
458 Berlin, 1992, pp. 7-9.

459 [10] Z.Y. Wei, Y.J. Liu, B. Zhou: Adv. Mat. Res., 2011, vol. 314-316, pp. 437-447.

460 [11] R. Thiébaud, J. Lebet: Experimental study of residual stresses in thick steel plates, Proceedings
461 of the Annual Stability Conference Structural Stability Research Council, Texas, USA, 2012, pp. 1-16.

462 [12] T. Jokiaho, T. Saarinen, S. Santa-Aho, P. Peura, M. Vippola: Key Eng. Mater. 2016, vol. 674, pp.
463 103-108.

464 [13] K.W. Andrews: J. Iron Steel Inst., 1965, vol. 203, pp. 721-727.

465 [14] W. Steven, A.G. Haynes: J. Iron Steel Inst., 1956, vol. 183, pp. 349-359.

466 [15] S. Kamamoto, T. Nishimori, S. Kinoshita: Mater. Sci. Technol., 1985, vol. 1, pp. 798-804.

467 [16] D.P. Koistinen, R.E. Marburger: Acta Metall., 1959, vol. 7, pp. 59-60.

468 [17] SFS-EN 15305, Non-destructive Testing - Test Method for Residual stress analysis by X-ray
469 Diffraction, 2008.

470 [18] M. Fitzpatrick, A. Fry, P. Holdway, F. Kandil, J. Shackleton, L. Suominen: International
471 Measurement Good Practice Guide No. 52, Crown, 2005.

472 [19] P.J. Withers, H.K.D.H. Bhadeshia: Mater. Sci. Technol., 2001, Vol. 17, pp. 355-365.

Fig. 1. *Finite element mesh with a zoomed view from the middle section.*

Fig. 2. *The results of the uniaxial compression tests using Gleeble: yield strength at 2 % plastic strain as a function of temperature.*

Fig. 3. *SEM micrograph from the cut edge of a 300 mm/min flame cut sample.*

Fig. 4. *(a) Heat distribution along the cut edge (y-axis is the cutting depth). (b) The time-dependence of the heat flux amplitude for 150 mm/min cutting speed. It should be noted that the y-axis presents the magnitude of the heat flux relative to the maximum value.*

Fig. 5. *Residual stress measurement locations of X-ray diffraction method for a flame cut sample.*

Fig. 6. *Temperature curves from different distances from the flame cut edge at (a) 150 mm/min and (b) 300 mm/min cutting speeds.*

Fig. 7. *Simulated residual thermal stress profiles (thickness direction) of 150 mm/min and 300 mm/min flame cutting speeds (a) without phase transformations and (b) with phase transformations. (c) Modelled residual stress formation during flame cutting with 300 mm/min cutting speed.*

Fig. 8. *Simulation of the residual stresses (thickness direction) for different flame cutting processes: (a) cutting speed, (b) plate thickness, (c) preheating temperatures.*

Fig. 9. *Comparison of modeled data with experimentally obtained data from (a) 150 mm/min, (b) 300 mm/min flame cutting speeds and (c) 300 mm/min cutting speed with 200 °C preheating. (d) Experimental measurements from samples which were flame cut using a cutting speed of 500 mm/min, 150 mm/min cutting speed with 200 °C preheating and 300 mm/min cutting speed with 300 °C preheating.*

Table 1. *Chemical compositon approximation of studied steel.*

Amount of elements [Wt%]			
C	**Cr**	**Mn**	**Si**
0.130	0.890	0.970	0.620
Mo	**Al**	**Ni**	**B**
0.270	0.08	0.06	0.001
balanced with Fe			

Table 2. *Phase transformation temperatures implemented in the model.*

Temperature	Value [°C]	Value [K]
A_{c3}	1077	1350
A_{c1}	745	1018
M_s	440	713
M_f	234	507

Table 3. *Measurement parameters used for XStress 3000 equipment.*

Parameters:			
ϕ rotations (measurement directions)	0° and 90°	**Modulus of elasticity**	211 GPa
Collimator	3 mm	**Poisson's ratio**	0.3
ψ tilt angles in one direction (side / side)	6 / 6	**Voltage**	30 kV
Maximum tilt angle	40°	**Current**	6.7 mA
ψ oscillation	5°	**Radiation**	CrKα

PUBLICATION III

Effect of Microstructural Characteristics of Thick Steel Plates on Residual Stress Formation and Cracking During Flame Cutting

T. Jokiaho, S. Santa-aho, H. Järvinen, M. Honkanen, P. Peura, M. Vippola

Materials Performance and Characterization, Vol. 7
https://doi.org/10.1520/MPC20170083

Materials Performance and Characterization

doi:10.1520/MPC20170083 / Vol. 7 / No. 4 / 2018 / available online at www.astm.org

Tuomas Jokiaho,[1] Suvi Santa-aho,[2] Henri Järvinen,[2] Mari Honkanen,[2] Pasi Peura,[2] and Minnamari Vippola[2]

Effect of Microstructural Characteristics of Thick Steel Plates on Residual Stress Formation and Cracking during Flame Cutting

Reference

Jokiaho, T., Santa-aho, S., Järvinen, H., Honkanen, M., Peura, P., and Vippola, M., "Effect of Microstructural Characteristics of Thick Steel Plates on Residual Stress Formation and Cracking during Flame Cutting," *Materials Performance and Characterization*, Vol. 7, No. 4, 2018, pp. 655–674, https://doi.org/10.1520/MPC20170083. ISSN 2379-1365

ABSTRACT

Thick wear-resistant steel plates are commonly used in demanding conditions, such as in the mining industry. In harsh environments, a high degree of both toughness and hardness is required, which extends the service life of the components but also makes the production of the plates difficult. Flame cutting is a generally applied cutting method in the heavy steel industry since it enables the cutting of thick steel plates at high production rates. However, flame cutting may cause cracks in the cut edge of the steel plates, leading to rejects for the steel industry and end-users. In addition, cutting generates a heat-affected zone at the cut edge, where volumetric and microstructural changes and hardness variations take place. A steep thermal gradient, generated during flame cutting, also produces high residual stresses on the cut edge. The goal of this study is to examine how microstructural features contribute to the residual stress formation and cracking probability of thick steel plates. Specific microstructural features can make the plates prone to cracking and tend to produce undesired stresses during the cutting process. The residual stress profiles of flame-cut specimens were measured using the X-ray diffraction method. In addition, the mechanical properties of steel plates were evaluated. The microstructures of the cut edge and the base material were characterized by electron microscopy. Results indicate that the shape of the prior austenite grains has an effect on both the cracking probability and residual stress

Manuscript received June 22, 2017; accepted for publication January 4, 2018; published online June 7, 2018.

[1] Tampere University of Technology, Laboratory of Materials Science, P.O. Box 589, FI-33101 Tampere, Finland (Corresponding author), e-mail: tuomas.jokiaho@tut.fi, https://orcid.org/0000-0002-6419-0582

[2] Tampere University of Technology, Laboratory of Materials Science, P.O. Box 589, FI-33101 Tampere, Finland https://orcid.org/0000-0002-0047-3268 (S.S.-A.)

formation. Longitudinally oriented prior austenite grain boundaries combined with a high residual tensile stress state provide potential sites for cracking.

Keywords

flame cutting, microstructure, residual stress, heat-affected zone, thick steel plate, X-ray diffractometer, electron microscopy

Introduction

High hardness and toughness are required for thick wear-resistant steel plates, but these properties are what make manufacturing difficult. Mechanical cutting of the plates is demanding and slow because the plates are almost as hard as the cutting tools. For this reason, thermal cutting methods are preferred. Flame cutting especially is a generally applied method in the steel industry for thick and wear-resistant plates. In addition, flame cutting is an exothermal process that generates large amounts of heat during the cutting process, which supports the continuum of the cutting process. Therefore, it enables the cutting of very thick plates and creates a major advantage compared to other thermal cutting methods [1].

The flame cutting process begins with heating a small area on the steel surface up to its ignition temperature using an oxyfuel gas flame. A jet of pure oxygen is then directed to the locally heated area, which causes rapid burning of the heated metal, thus creating a cut edge. In addition, the oxygen jet flushes the molten iron oxide away from the cut edge and exposes clean surfaces for cutting [2]. Consequently, a heat-affected zone (HAZ) is generated at the cut edge of the steel plate that is due to the formation of large thermal gradients during the flame cutting process. Martín-Meizoso et al. [3] reported that flame cutting of a 25-mm-thick steel plate produced higher hardness values near the cut edge that subsequently decreased toward the base material. Wilson [4] investigated thermal cutting of steel plates with thicknesses of 25.4, 50.8, and 101.6 mm, and it was shown that faster cutting speeds produced a narrower HAZ with higher hardness levels. In addition, richer chemistry steel plates tended to have broader and harder HAZ. Wood [5] noticed that flame cutting of 25-mm-thick low-carbon and low-alloy steel plates produced highest hardness close to the cut edge and decreased the hardness values toward the base material. The maximum hardness increased with faster cutting speeds [5]. High temperature and fast cooling during cutting produced a martensitic layer on the cut edge, which was followed by a region of tempered martensite [5]. As a common finding, hardness variations and microstructural changes take place in the HAZ, and it was noted in all studies that the hardness was greater near the cut edge and decreased toward the base material.

However, flame cutting may cause cracks in the cut edge of the steel plate. The size of the cracks can vary from micrometers to several centimeters. Generally, cracks are formed horizontally near the centerline of the steel plate, but cracks can also propagate in the vertical direction. The cracking tendency has been noticed to increase as the hardness and thickness of the steel increase [6]. In addition, flame cutting produces residual stresses (RSs) at the cut edge of the steel plate, and it has been reported [7] that high residual tensile stresses promote crack formation. RSs are internal stresses inside the material, and they are present even after all external forces have been removed. RSs originate from local misfits of the material, i.e., nonuniform plastic deformation that causes elastic strains to maintain

dimensional continuum [8]. In the case of flame cutting, the RSs can be divided into thermal stresses and transformation stresses. Thermal stresses arise from different thermal expansions and contractions of material during heating and cooling. Transformation stresses, in turn, arise from variations in volumetric sizes of different phases and microconstituents. [9]

RSs are often divided into three types (I, II, III) according to the scale over which they impact and self-equilibrate. Type I is a macrostress, which varies over large distances. This long-range stress is often referred to as the most important one because it equilibrates over a macroscopic distance, such as the scale of a structure. In contrast, Types II and III are microstresses, which vary in microscopic scale, thus making their influence difficult to predict. Type II stresses vary over the grain scale and nearly always exist in polycrystalline structures when the elastic and thermal properties are different between differently oriented neighboring grains. Type III stresses exist on atomic scale and are balanced within a grain, such as, for example, those stresses caused by dislocations and point defects. The measuring method has to be carefully considered as it depends on the stress type that is being measured. Typically, most material removal methods, i.e., hole drilling, measure only Type I stresses, as Types II and III stresses are averaged to zero in the sampled area. In diffraction-based measuring methods, the stress value is derived from a specific wavelength and diffraction condition. Therefore, the particular phase or grain orientation is sampled, and Type II stress can be recorded as superimposed on the Type I stress. [8]

Previous studies have been mainly focused on the modeling of RSs, and the simulation results have been verified by experimental measurements. Lindgren, Carlestam, and Jonsson [7] investigated and simulated the RS formation in the thermal cutting of thick steel plates. It was noticed that cutting produced a compressive stress area near the cut edge, and there was a tensile stress peak after the compressive stress region. RS values could be affected by changing the cutting parameters; for example, preheating produced more compressive stress and also lowered the tensile stress peak. Similar results were found in earlier studies [10,11] by the current author; the RS state was affected by the size of the specimen and cutting parameters. Preheating not only lowered the tensile stress but also increased the compressive stress area by shifting the tensile stress peak deeper in the subsurface. However, there is still a lack of knowledge on how RSs and crack formations are affected, e.g., by microstructural features. The aim of this study is to investigate the effect of microstructures on the RS formation and cracking probability and to identify the most suitable microstructural features from the flame cutting point of view.

Materials and Methods

The experimental procedure for understanding the effect of microstructural characteristics on RS and crack formation is presented schematically in **Fig. 1**. Firstly, the initial mechanical properties and microstructure of the studied steels (A and B) were examined. Then the steel plates were flame cut using different cutting speeds (150, 300, and 500 mm/min) and ultrasonically inspected after the cutting. After the ultrasonic inspection, the RSs were measured from the flame-cut specimens. The measured specimens were then sectioned for hardness measurements, electron microscopy analysis (SEM, transmission electron microscope (TEM)), and glow discharge optical emission spectroscopy (GDOES) measurements. Each of these experimental steps are described more precisely in the Materials and Experimental Procedure sections.

FIG. 1

Experimental procedure of the study.

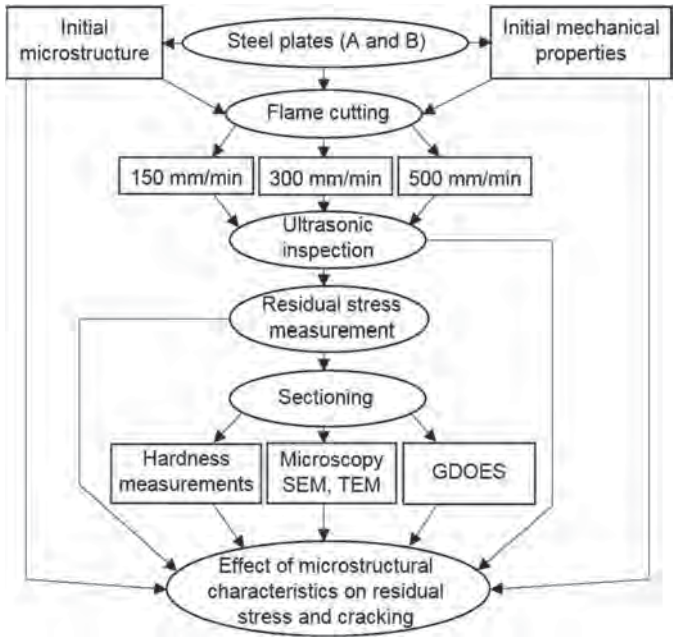

TABLE 1

Composition of studied steel types A and B.

Steel Plates	C %	Si %	Mn %	Cr %	B %	Mo %	Al %	Ni %	V %	Ti %
A	0.15	0.62	1.10	0.62	0.0015	0.42	0.048	0.20	0.042	0.017
B	0.14	0.55	1.05	0.57	0.0012	0.36	0.044	0.19	0.039	0.013

MATERIALS

The materials examined were hot-rolled, wear-resistant steel plates (A and B), of which steel plate A had a higher hot-rolling temperature (above 900°C) than steel plate B (below 900°C). The compositions of the studied steels are presented in Table 1. The dimension of the flame-cut specimens were 40 by 150 by 150 mm (thickness by width by length), and one side of each specimen was cut with an oxyfuel propane gas flame. The cutting speeds used for the specimens were 150, 300, and 500 mm/min, and the specimens were inspected using Phasor XS 16/16 Olympus ultrasonic equipment (General Electric, Boston, MA) with an MSEB 4 dual probe (4 MHz) after flame cutting. Ultrasonic inspection results were verified by repeating the inspections with two individual researchers and by sectioning a few specimens after inspection to confirm the existence of the defects.

EXPERIMENTAL PROCEDURE

The X-ray diffraction method (XRD) was used to measure the RSs from the flame-cut specimens. The measurement equipment was XStress 3000 (Stresstech Oy, Jyväskylä, Finland) and the measurement method used was the modified Chi method [12]. The principle of the method is the calculation of the interplanar lattice spacing of the ferrite [211]

plane from the 156° Bragg diffraction angle. Different Ψ tilts are used to measure the lattice spacing d (where the Ψ angle is the angle between the normal of the specimen and the normal with the diffracting plane). The RS can be calculated using the elastic properties of the material and the slope from a plot of measured lattice spacing d as a function of $\sin^2 \Psi$. Thus, RS can be calculated from a specific measurement location by using the following equation and [13]:

$$\sigma_\phi = \left(\frac{E}{1+\upsilon}\right) m \tag{1}$$

where σ_ϕ is the RS in the measurement direction ϕ, E is the Young's modulus, ν is Poisson's ratio, and m is the gradient of the measured d versus $\sin^2\Psi$ curve. The steeper the gradient m, the higher the RS level. The measurement parameters used are presented in **Table 2**.

RS measurements were performed at the centerline of the specimens, where the cracks are mostly formed during flame cutting. Measurements were carried out in two perpendicular measurement directions, 0° and 90°, which correspond to the cut direction and to the thickness direction of the specimen, respectively. The chosen directions are the most critical orientations for crack formation. The measurement locations and directions are shown in **Fig. 2a**.

An exposure time of 5 seconds was used in each RS measurement. To produce the RS depth profiles, the material layers were removed from the measurement location with an electrolytic polishing machine, Movipol-3 (Struers Inc., Cleveland, OH). The electrolyte used in polishing was A2 (60 % perchloric acid, 65–85 % ethanol, 10–15 % 2-butoxyethanol, and 5–15 % water). The removed material depths were approximately 100–200 µm between each measurement, and each polishing step was verified with a digital dial indicator. An example of the measured RS profile is presented in **Fig. 3**.

TABLE 2

Measurement parameters used for XStress 3000.

Parameter	Value/Unit	Parameter:	Value/Unit
ϕ rotations (measurement directions)	0° and 90°	Modulus of elasticity	211 GPa
Collimator	3 mm	Poisson's ratio	0.3
ψ tilt angles in one direction (side / side)	6 / 6	Voltage	30 kV
Maximum tilt angle	40°	Current	6.7 mA
ψ oscillation	5°	Radiation	CrKα

FIG. 2

(a) RS measurement location and directions and (b) hardness profile location.

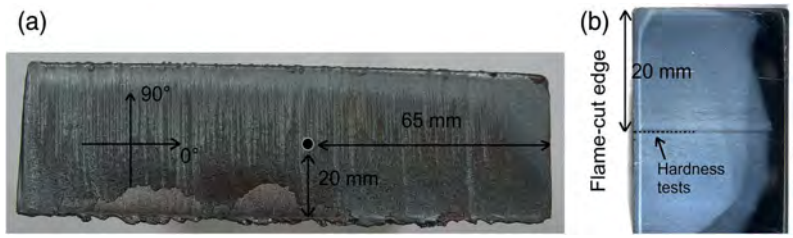

FIG. 3

RS profile from flame-cut specimen. RS and full width at half maximum in flame-cut direction (0°) and thickness direction (90°).

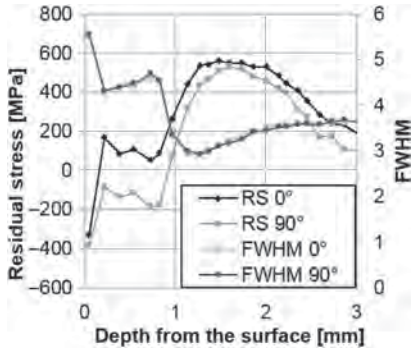

RS profiles include RSs and full width at half maximum values in both the flame-cut and thickness direction. However, as most of the cracks are formed in the flame-cut direction, the most critical RSs for crack formation are the ones formed in the thickness direction (90°) of the plates. For this reason, this study concentrates on the RS formation in the thickness direction of the plate.

Flame-cut specimens were sectioned from the centerline for microstructural analysis, which was carried out using scanning electron microscopes (SEMs). For microstructural analysis and hardness measurements, the specimens were ground using abrasive silicon carbide papers and polished with 3 and 1-μm diamond suspensions. After grinding, the specimens were etched with 4 % Nital solution. Hardness measurements of the original structure (HV 5 kg) were carried out using a DuraScan 80 (Struers Inc., Cleveland, OH) and the cross-section hardness profiles (HV 0.2 kg) from the flame-cut edge were performed with a MMT-X7 digital microhardness tester (Matsuzawa, Akita, Japan). The location of the hardness tests in relation to the flame-cut edge is presented in **Fig. 2b**. Tensile tests in the thickness direction were carried out with an MTS 250 kN and tests were performed according to SFS-EN ISO 6892-1, *Metallic Materials—Tensile Testing—Part 1: Method of Test at Room Temperature* [14]. In addition, GDOES profiles were measured from the flame-cut surfaces with a GDA 750/GDA 550 spectrometer (Spectruma Analytik GmbH, Hof, Germany). The microstructure characterization was carried out using a Philips XL-30 SEM (SEMTech Solutions, Billerica, MA) and an ULTRAplus field emission SEM (ZEISS, Oberkochen, Germany).

In addition, the specimens were analyzed in SEM with an HKL Premium-F Channel Electron Backscatter Diffraction (EBSD) system equipped with a Nordlys F400 detector (Oxford Instruments, Abingdon, United Kingdom). The specimens used in the EBSD measurements were sectioned and ground using abrasive silicon carbide paper and then polished with a colloidal silica suspension (0.04 μm). A step size of 0.1 μm and an acceleration voltage of 20 kV were used in the EBSD analysis of cross-sectional areas measuring 209 by 144 μm. The EBSD data obtained from the original microstructure was used as a starting point for reconstructing the grain boundaries of the prior austenite. The reconstruction was carried out using a MATLAB-based (MathWorks, Natick, MA) iterative algorithm originally developed by Nyyssönen et al. [15]. The algorithm determines an experimental orientation relationship between martensite and prior austenite and uses that information to reconstruct the grain boundaries of prior austenite. The script used was

supplemented with the MTEX texture and crystallographic analysis toolbox developed by Bachmann, Hielscher, and Schaeben [16]. A map revealing the grain boundaries was assembled from the EBSD orientation pixel map by using MTEX as described in Ref. [15]. A minimum grain boundary threshold value of 8° was applied. The prior austenite grain sizes (PAGS) were then measured from the reconstructed grain boundary maps by mean linear intercept.

A JEM-2010 TEM (Jeol Ltd., Tokyo, Japan) equipped with a Noran Vantage Si(Li) detector energy dispersive spectrometer (EDS; Thermo Fisher Scientific Inc., Raleigh, NC) was used to analyze precipitates before and after flame cutting. The TEM specimens were prepared using an extraction replica technique: the sectioned specimen was polished by a traditional metallographic method followed by etching (Nital 4 % solution) to remove the matrix so that the precipitates stood proud of the specimen surface. Then, a carbon film was evaporated on the specimen surface and scored into ~1 mm^2. After this, etching continued to dissolve the matrix and the squares of the carbon film carrying the precipitates with them were floated in distilled water and collected on copper TEM grids.

Results

SEM micrographs from the centerline of steel specimens A and B are presented in **Fig. 4**. The original structure of the specimens consists mainly of lath martensite (M, shown in **Fig. 4**). However, both microstructures may also contain a small amount of bainite (B, shown in **Fig. 4**), which is often difficult to distinguish from a martensite structure.

Some of the prior austenite grains can be distinguished in steel specimens A and B. However, the martensite and prior austenite grain structures are difficult to evaluate and compare from the SEM micrographs. For further investigation, an EBSD analysis was made for both steels, and the prior austenite grain boundaries (PAGBs) were constructed as previously described. The reconstructed PAGBs from the original microstructures of specimens A and B are presented in **Fig. 5**.

EBSD analysis and reconstruction of the prior austenite grains were used to calculate the PAGS and to evaluate the microstructures of the specimens using an 8° minimum grain boundary threshold. The PAGS of specimens A (**Fig. 5a**) and B (**Fig. 5b**) are 53 μm and 34 μm, respectively. Steel A has equiaxed prior austenite grains with few packet boundaries inside the grains. In contrast, the prior austenite grains in Steel B are elongated

FIG. 4 SEM micrographs of steel specimens (a) A and (b) B. Arrows indicate examples of martensite (M) and bainite (B).

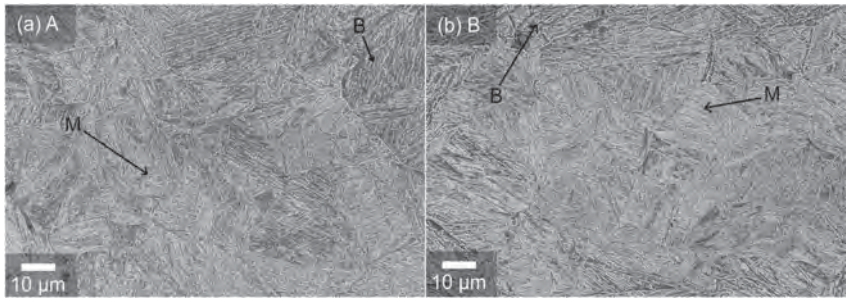

FIG. 5 Reconstructed PAGB maps for specimens (a) A and (b) B. PAGBs are superimposed on EBSD band contrast images as black lines. The red and green lines show the packet and block boundaries of martensite, respectively. (For interpretation of the references to color in these figures, the reader is referred to the web version of this article.)

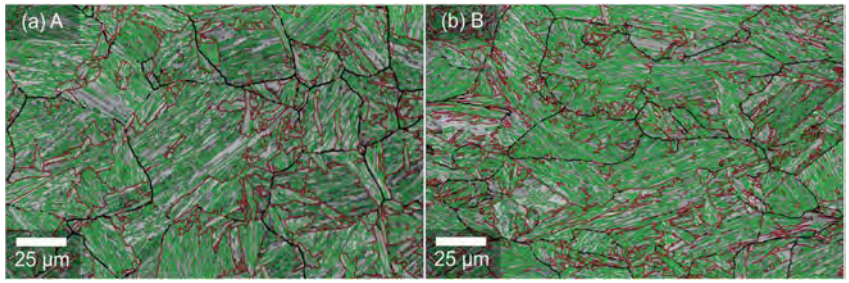

TABLE 3
Initial mechanical properties for Steels A and B. Tensile strength (R_m) corresponding to the maximum force and reduction of the area at fracture (Z %) in tensile tests. PAGS is expressed as the mean linear intercept (L_m) calculated from EPSD data.

Steel Grade	Hardness (HV 5kg)	R_m (MPa)	Z %	PAGS L_m (µm)
A	399	1,217	51	53
B	414	1,184	53	34

in the horizontal direction with more packet boundaries. In addition, Steel B has more block boundaries and a denser martensitic block structure compared to Steel A.

The initial mechanical properties of Steels A and B were tested by means of hardness measurements and tensile tests. The results presented in Table 3 show that there is only a small variation in hardness values and tensile properties between Steels A and B. To summarize, the mechanical properties of the original structures are similar for both steels. However, as noted previously, significant differences were observed in their microstructural features, especially in the prior austenite grain morphologies of Steels A and B.

FLAME CUTTING EXPERIMENTS

Steel specimens A and B were flame cut using three different cutting speeds: 150, 300, and 500 mm/min. Microstructural characterization showed that all the tested flame cutting speeds created a HAZ at the cut edge of the steel plate. In addition, three distinct microstructural regions (presented in Fig. 6) were identified from the HAZ in all the studied specimens a newly formed martensite region, a two-phase region, and the tempered original structure.

These regions have typical features that are present in all the studied flame-cut specimens. The region closest to the cut edge is fully austenized during the flame cutting and transforms into martensite during rapid cooling. An example micrograph of the martensite region formed close to the cut edge is presented in Fig. 7. The martensite region near the cut edge consists of martensite laths and autotempered martensite regions (indicated by arrows in Fig. 7), containing acicular-shaped cementite (Fe_3C) particles [17]. Martensite transformation occurs between the martensite start (M_s) and martensite finish (M_f) temperatures, which depend on the carbon content and alloying of the steel.

FIG. 6 SEM micrograph of the HAZ showing the newly formed martensite (1.), two-phase region (2.), and tempered original structure (3.).

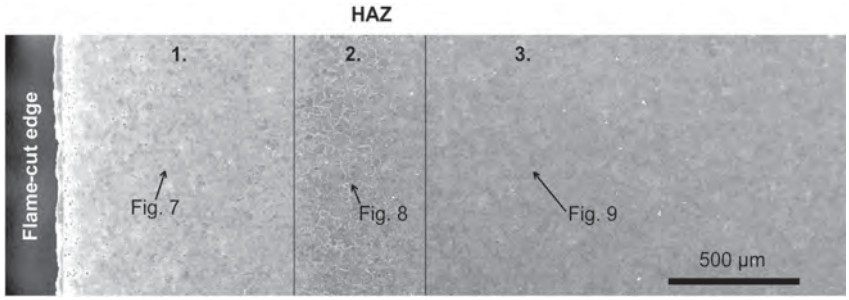

FIG. 7

SEM micrograph of a newly formed martensite region close to the cut edge. This region consists of a mixture of martensite laths and autotempered martensite (indicated by arrows) containing acicular-shaped Fe_3C.

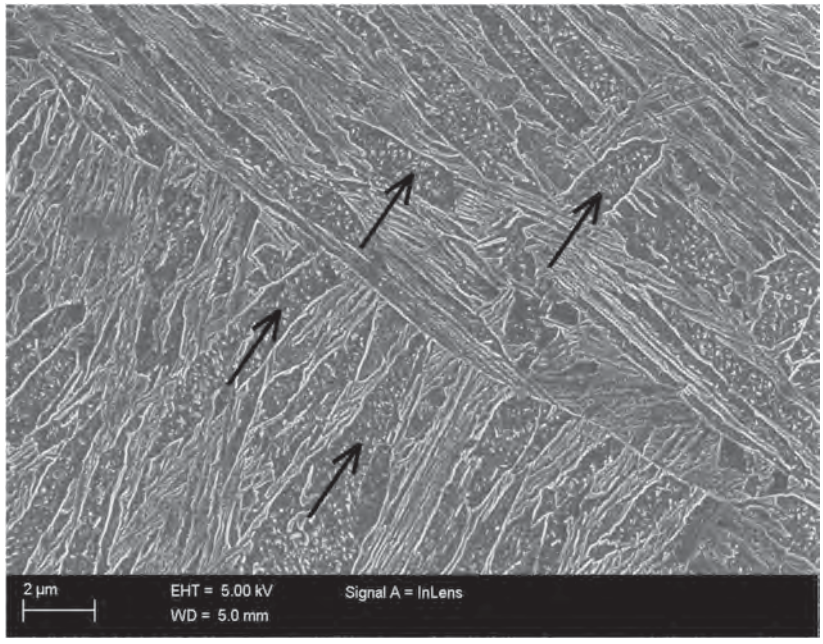

Therefore, the martensite that formed close to the M_s temperature is exposed to tempering conditions during the remaining quench cycle, which is called autotempering. The effect of autotempering increases with lower carbon content (lower carbon steels have a higher M_s) and a reduction in quench severity (increasing the time that fresh martensite is exposed to elevated temperatures) [18].

After the newly formed martensite, there is a two-phase region, which is a mixture of newly formed martensite and tempered original structure. An example structure of the two-phase region is presented in Fig. 8. The two-phase region is partly austenized during flame cutting and the austenization occurs heterogeneously at the PAGBs, while the rest of the structure is heavily tempered. During cooling, austenite forms a fine martensite lath

FIG. 8

SEM micrograph of the two-phase region containing both newly formed martensite and tempered original structure.

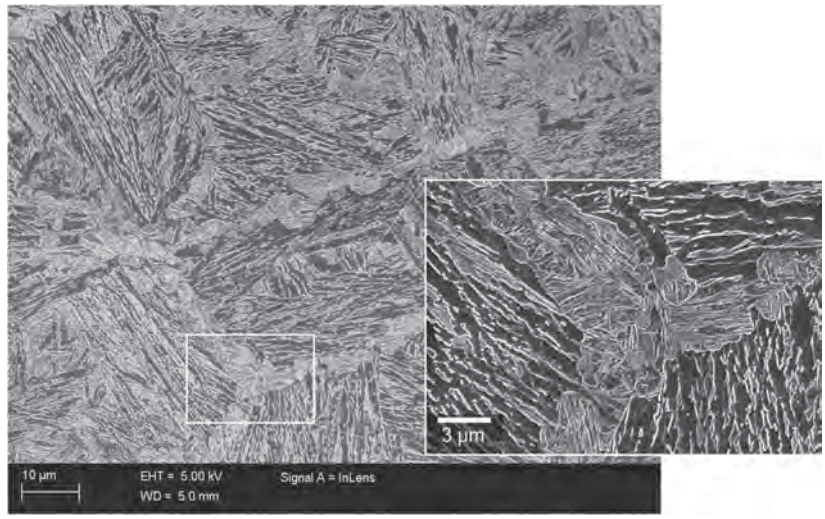

structure, which creates martensitic chains in the PAGBs while the original structure inside the prior austenite grains is tempered.

After the two-phase region, there is the tempered original structure, which is presented in Fig. 9. The original structure is the most tempered in the two-phase region that undergoes the highest temperatures during flame cutting without austenizing. The tempering effect

FIG. 9

SEM micrograph of tempered original structure containing fine dispersed Fe_3C particles (white dots).

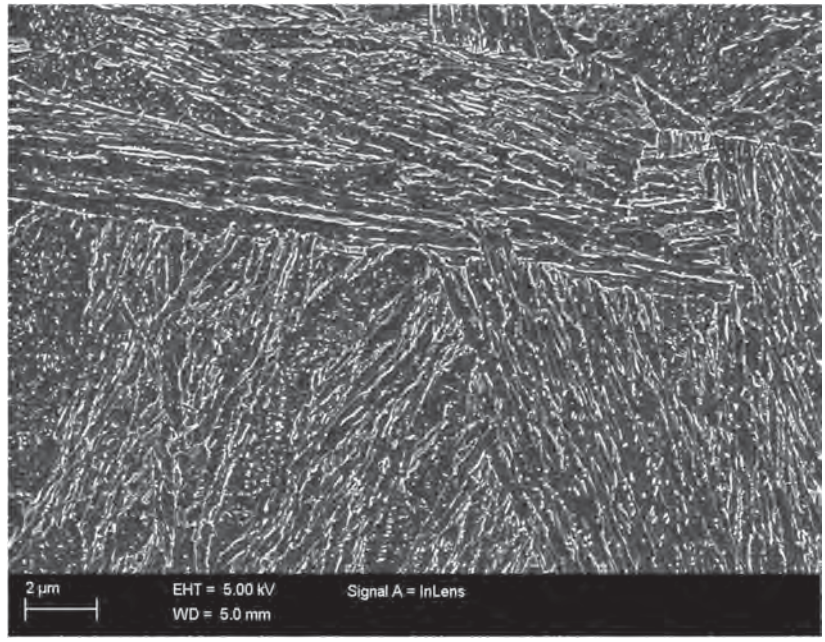

FIG. 10 Microstructural regions of the cut edge (newly formed martensite (1.), two-phase region (2.), and tempered region (3.)) from specimens A and B after 150, 300, and 500 mm/min of flame cutting. The measured RS profiles in the thickness direction are represented for each specimen.

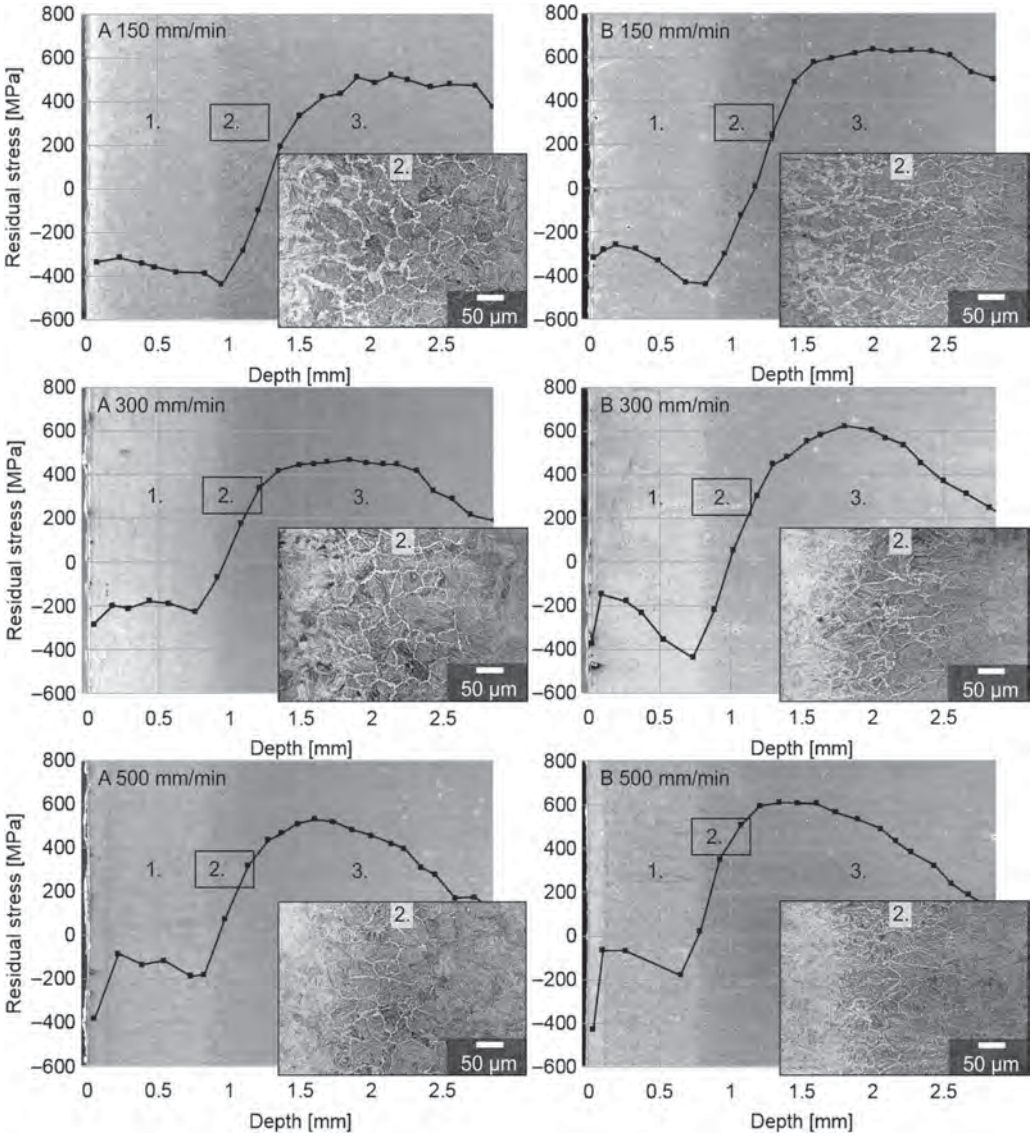

gradually decreases as it goes deeper into the subsurface. The fine structure of dispersed Fe_3C particles can be seen throughout the tempered region. The number of Fe_3C particles decrease deeper from the cut edge as the tempering of the structure decreases.

Microstructures of the cut edge and two-phase region are presented in Fig. 10 for specimens A and B after flame cutting was performed at speeds of 150, 300, and 500 mm/min. Additionally, Fig. 10 shows the measured RS profiles in the thickness direction for each specimen.

The microstructures of the flame-cut edges (Fig. 10) indicate that the newly formed martensite region (1.) is wider near the cut edge at slower cutting speeds. As the cutting speed increases, the thickness of the newly formed martensite layer decreases. The heat input is higher at slower cutting speeds and, for this reason, the fully austenized region reaches deeper into the subsurface compared to faster cutting speeds. Similar observations can be made for the two-phase regions (2.), which are presented in Fig. 10. The two-phase region is the widest at a cutting speed of 150 mm/min while a cutting speed of 500 mm/min produces the narrowest two-phase region. Additionally, the two-phase regions of the specimens highlight the prior austenite grain structure (martensite formation at the PAGBs) and similar observations can be made from both the two-phase region and the reconstructed EBSD images (Fig. 5). The two-phase regions of Steel A consist of prior austenite grains with equiaxed morphology, while the same regions of Steel B contain prior austenite grains with clearly elongated morphology. In addition, Fig. 10 plainly shows the generation of RSs in different microstructural regions of the cut edge. The martensite transformation occurring near the cut edge (1.) creates compressive stress. After that, the RS values start to increase and transform into tensile stress within the two-phase region (2.). The highest RS values are attained in the tempered region (3.).

The RS profiles shown in Fig. 10 are collected in Fig. 11 for further comparison. In flame cutting, the RSs are caused by the thermal shock (thermal stresses) and microstructural changes (transformation stresses) that are produced by the high temperatures and fast cooling during the cutting process.

As previously mentioned, martensite transformation creates a compressive stress region near the cut edge of the steel plates (Fig. 11). The extent and the values of the compressive stress region depend on the cutting speed. A slow cutting speed produces a wider compressive stress region (it shifts the tensile stress peaks deeper into the subsurface) and more compressive stress compared to faster cutting speeds. After the compressive stress region, the RS levels start to increase and finally form tensile stress peaks in the tempered region. As can be seen in Fig. 11, the tensile stress peaks generated in Steel A are smaller in comparison with Steel B. In Steel B (Fig. 11b), the tensile stress

FIG. 11 RS profiles (thickness direction) measured for steel specimens (a) A and (b) B at cutting speeds of 150, 300, and 500 mm/min.

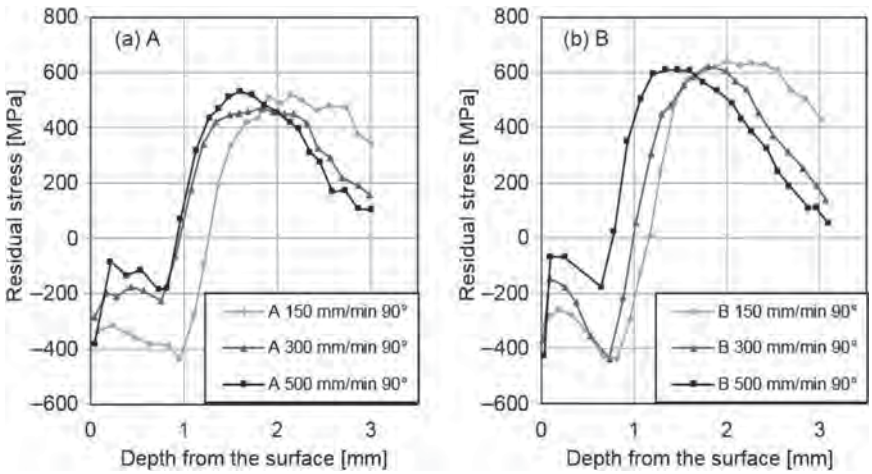

FIG. 12 Hardness profiles (HV 0.2 kg) from the cut edges of specimens (a) A and (b) B at cutting speeds of 150, 300, and 500 mm/min.

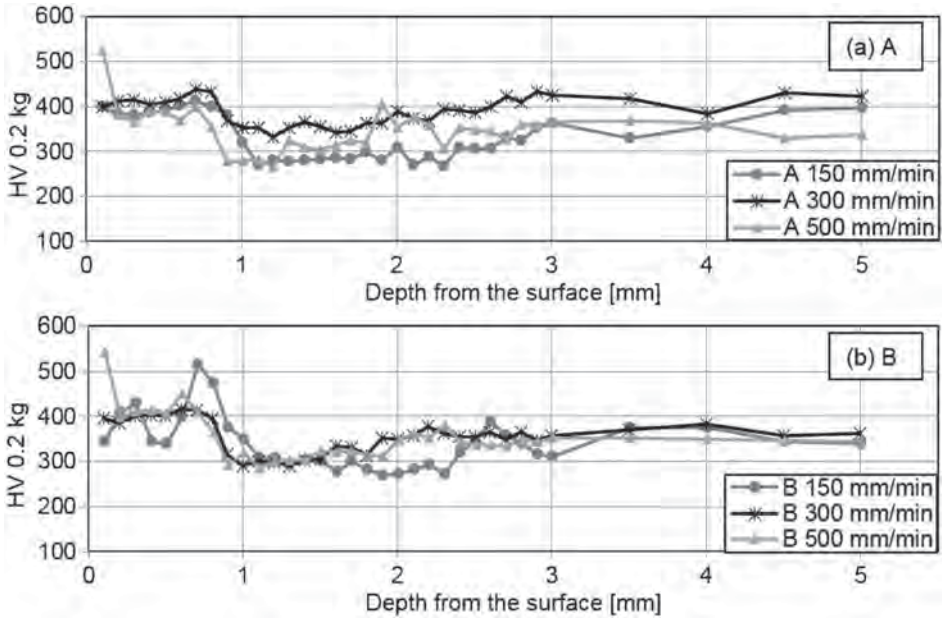

peak values are approximately 600 MPa in all the specimens. In contrast, the tensile stress peak values of Steel A (Fig. 11a) are approximately 100–150 MPa lower than in Steel B.

Fig. 12 presents the measured hardness profiles from the flame-cut edges of specimens A and B at cutting speeds of 150, 300, and 500 mm/min. The newly formed martensite region has the highest hardness levels near the cut edge in both steels. As the two-phase region starts, the hardness values gradually reduce as the content of newly formed martensite decreases and the fraction of tempered structure increases. The lowest hardness values are attained at the end of the two-phase structure where the original structure is the most tempered. After that, the hardness values start to increase toward the original hardness values. Fig. 12 indicates that the cutting speed has a role in determining the width of the area of the martensite region near the cut edge in both specimen materials. A faster cutting speed produces a narrower martensite region than slower cutting speeds. For this reason, hardness values start to decrease deeper in relation to the cut edge (as the two-phase region starts) at a cutting speed of 150 mm/min. In Steel A (Fig. 12a) there is some scatter in the hardness values in the tempered region and the 300 mm/min cutting speed shows higher values than those at cutting speeds of 150 and 500 mm/min. This might be due to segregation occurring in the hot rolling of the steel plates. Segregation can locally increase the hardness values and may create local hardness peaks in the hardness profiles. Similar hardness fluctuations can also be seen in Steel B, which is flame cut at 150 mm/min (Fig. 12b). The hardness changes from low (350 HV 0.2 kg) to high values (500 HV 0.2 kg) rapidly over a short distance.

GDOES profiles and SEM micrographs from the cut surfaces of Specimens. A and B are presented in Fig. 13. Both specimens were flame cut at a cutting speed of 300 mm/min. The GDOES profiles show that a thin iron oxide layer is formed in the cut surface during flame cutting. In addition, the cut surface is partly melted during the flame cutting process

FIG. 13

GDOES measurement and SEM micrographs from the cut surfaces of specimens (a) A and (b) B, which were flame cut using a cutting speed of 300 mm/min.

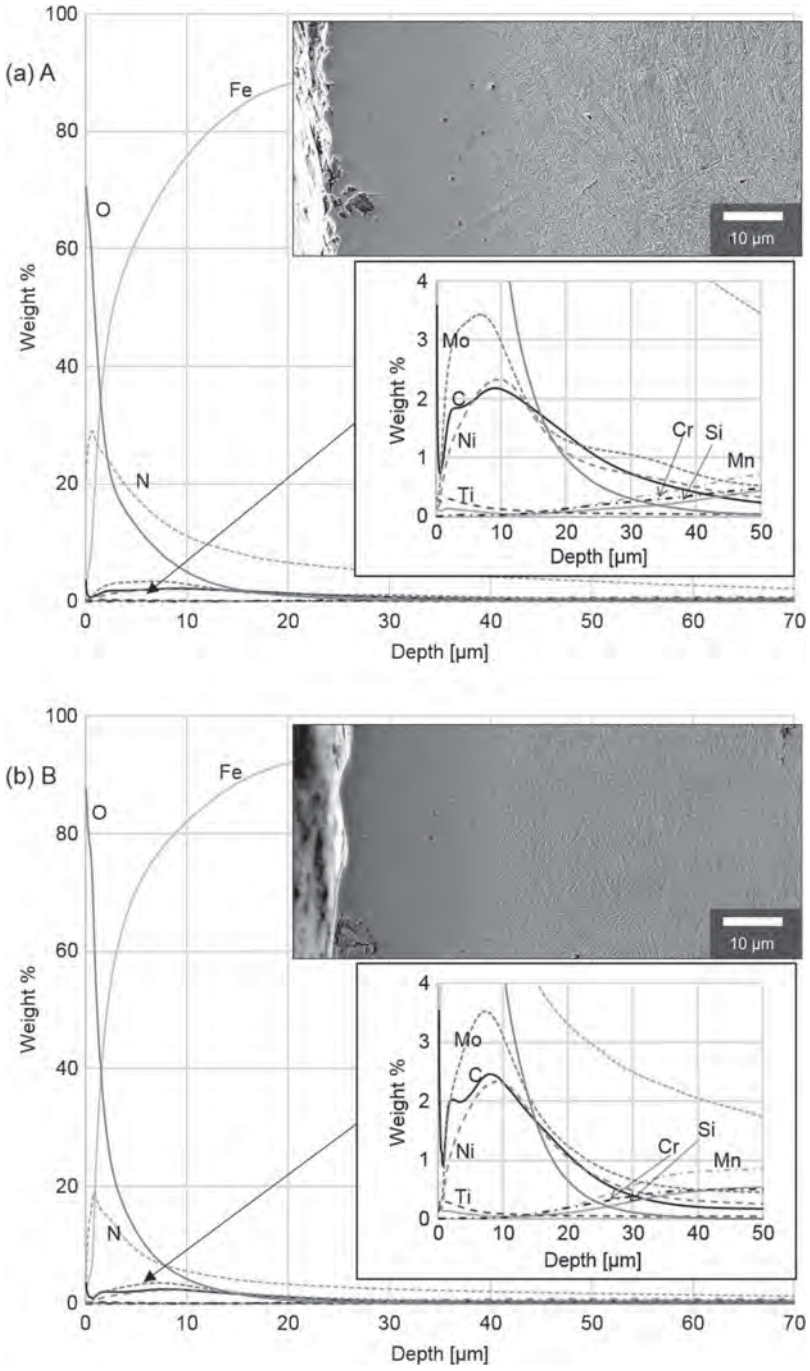

because of heat conduction and the molten region is enriched with carbon, molybdenum, and nickel. In addition, a small content of enriched titanium is present in the cut surface. However, results show that manganese, chromium, and silicon are burnt out from the cut

surface during the flame-cut process. A relatively high content of nitrogen, obtained in the cut surface, is most likely the result of diffusion from the atmosphere. The SEM micrographs in Fig. 13 show the partly molten surface region (grey areas in the cut surface without a clear microstructure). In general, the GDOES profiles from Specimen A and B are quite similar. The oxygen content near the cut edge is higher in Specimen B than in Specimen A. In contrast, the nitrogen level is lower in Specimen B compared to Specimen A.

The characterization of carbon extraction replicas was carried out for both as-received and flame-cut specimens. The carbon extraction replicas showed that both the original and the flame-cut specimens contained evenly distributed precipitates in the size range of 10–60 nm. The total investigated area was 136 μm^2 in each specimens. Steel specimen A contained 18 precipitates per 10 μm^2, Specimen B contained 17 precipitates per 10 μm^2, and flame-cut steel contained a similar amount of precipitates. This result indicates that precipitates were already formed during the manufacturing process and are not affected by flame cutting. The EDS analyses performed for individual precipitates indicate that they are titanium-rich precipitates. TEM micrographs and selected area electron diffraction (SAED) pattern of extraction replica specimen from steel A are presented in Fig. 14. SAED patterns indicate that the structure of the precipitates is a cubic rock salt structure (space group $Fm\bar{3}m$) which is a common structure for titanium carbides, titanium nitrides, and titanium carbonitrides (International Centre for Diffraction Data [ICDD], PDF-4+ 2015 database, 00-031-1400, 00-038-1420, 00-04201488).

After flame cutting, the specimens were inspected with ultrasound by two individual researchers, and the results are presented in Fig. 15. The ultrasonic inspection results clearly show that Steel B has a higher cracking tendency than Steel A. With the same amount of inspected cut surfaces (total cut edge length 4,800 mm), Steel A has 3 cracks (1 crack/1,600 mm) and Steel B has 14 cracks (1 crack/350 mm). The cracks located horizontally in the tempered region below the cut surface are according to the ultrasonic inspection results and the analysis of a few sectioned cracked specimens.

Discussion

Wear-resistant steel plates with two different microstructures were investigated to study the effect of microstructural features on the RS formation and cracking that was due to

FIG. 14

TEM analyses for the extraction replica specimen from Steel A. The amount of precipitates was not reduced or changed during flame cutting.

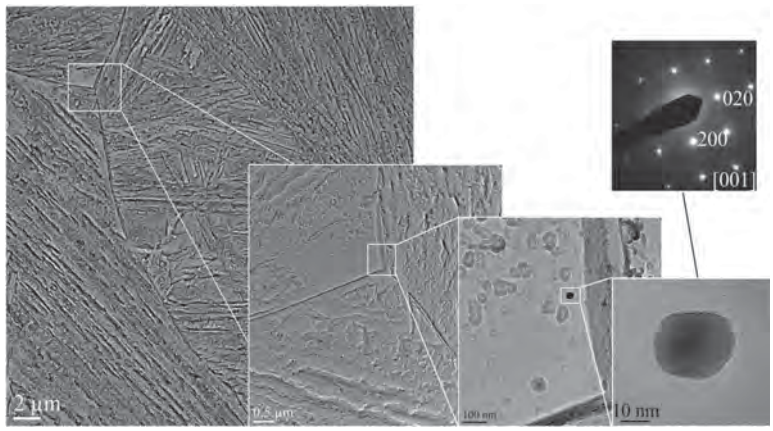

FIG. 15

Ultrasonic-inspected flame-cut specimens of Steels A and B.

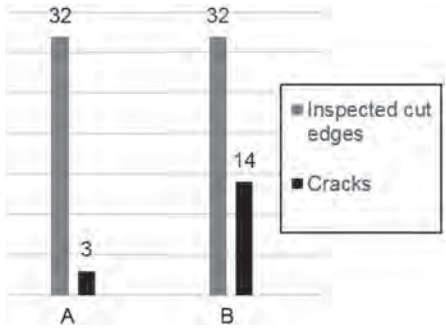

flame cutting. The chemical compositions and initial mechanical properties were approximately the same between the studied steels. As the microstructural analysis showed, the main difference in the studied steels was the prior austenite grain structure that was due to the different production histories. Steel A (equiaxed steel) consisted mainly of equiaxed prior austenite grains with few packet boundaries inside the grains, whereas the Steel B (elongated steel) contained elongated prior austenite grains in the horizontal direction with more packet boundaries. In addition, elongated steel had more block boundaries and a denser martensitic block structure compared to equiaxed steel. Generally, the martensite packet and block size are determined by prior austenite grains [19,20]. Additionally, the denser martensite blocks and packets in elongated steel compared to equiaxed steel may be caused by the bainite transformation that has taken place before martensite transformation. The formation of bainite refines subsequent martensitic packets and blocks, which has been reported [21] to increase the barriers to crack propagation. From the crack propagation point of view, it has been found [22] that existing boundaries in the martensitic structure are beneficial because they act as obstacles to crack propagation. Although both packet and block boundaries act as obstacles, it has been observed that packet boundaries deflect more cleavage cracks than block boundaries. The reason for this is the crystallographic misorientations of packet boundaries, which are bigger than block boundaries, and the fact that more energy is needed for the crack to cross packet boundaries. [22] However, PAGBs have been shown [19] to be the most effective barriers for crack propagation because they have a relatively high angle compared to other boundaries; in fact, a crack was observed to change direction as it encountered a PAGB. In the present study, the PAGS is larger in equiaxed steel than in elongated steel, which has more grain boundaries. However, the horizontally elongated PAGBs may act as potential paths for crack propagation rather than obstacles. Despite the bigger grain size, the equiaxed prior austenite grains would create more obstacles in the vertical direction in comparison with grain boundary chains as in elongated steel.

Flame cutting created three types of microstructural regions in the HAZ of the cut edge. A martensite region was formed closest to the cut edge. This region was fully austenized during flame cutting and, during cooling, formed martensite. After the martensite region, there was a two-phase region that partly austenized during flame cutting. The austenitization in the two-phase region occurred heterogeneously in the PAGBs, while the rest of the structure was tempered by the heat from the flame-cut process. After the

two-phase region, there was a tempered original structure in which the tempering effect gradually decreased as it went deeper into the subsurface. Generally, tempering is divided into four stages [23]. The first stage (<250°C) includes the redistribution of carbon atoms and precipitation of transition carbides such as ε ($Fe_{2.4}C$). However, it has been stated [24] that in low-alloy steels only the redistribution of carbon occurs in the first stage of tempering without ε-carbide formation. In the second stage (200°C–300°C), decomposition of retained austenite occurs. The third stage (200°C–350°C) involves the formation of Fe_3C particles, which most likely nucleate in ε-iron carbide interfaces and in both the interlath boundaries of martensite and the PAGBs. In the fourth stage (>350°C), Fe_3C particles coarsen and spheroidize. [23] However, in the present study, the tempering process could take place only for a very short time at high temperatures near the cut edge during flame cutting. The migration of trapped carbon atoms occurs within a short period of time. As the carbon content of the studied steel is low, it is assumed that ε-carbide precipitation does not occur. Fe_3C formation, in turn, starts as the temperature rises above 200°C. However, it seems that there is not enough time for any significant coarsening of Fe_3C particles, which leads to a fine, dispersed Fe_3C structure.

The martensite region had the highest hardness of all three regions; however, it started to decrease in the two-phase region. The lowest hardness values were in the tempered region, which followed the two-phase region, and after that, the hardness gradually increased deeper into the subsurface. According to Wood [5], the hardness of the surface region increases with faster cutting speeds. This was explained by the HAZ microstructures that were identified as a bainite with a slower cutting speed and as a martensite with a faster cutting speed. The present study shows that the hardness values in the surface region (>0.8 mm) were approximately the same with all studied cutting speeds. The reason for this is that the cooling conditions with all used cutting speeds produce similar kinds of martensite structures close to the cut edge.

According to a study by Lindgren, Carlestam, and Jonsson [7], flame cutting created a compressive or low tensile stress region (>1 mm) near the cut edge, which was followed by a tensile stress peak (2–3 mm below the surface). It was also stated that RS can be affected by chancing the cut parameters, for example, by using preheating. Similar results were also found in earlier studies by the current author [10,11], which state that the RS levels could be affected by using different cutting parameters, such as cutting speed. The present study shows that the shape of the RS profiles (compressive region near the cut edge followed by tensile stress peak) are similar to those in the previous studies [7,10,11]. In addition, it can be clearly seen how RS levels are chanced depending on the microstructural region in the HAZ. The martensite region produced residual compressive stress near the cut edge, and the RS changed from compressive to tensile stress in the two-phase region. The highest tensile stress values were in the tempered region following the two-phase region. As the cutting speed increases, the width of the martensite and two-phase region decreases because of the lower heat input created by the flame cutting process. In addition, a slower cutting speed produced more residual compressive stress in the cut edge compared to a faster cutting speed. According to the author's earlier study [11], the reason for this is that a fast cutting speed produces higher temperature differences in the cut edge during flame cutting compared to a slow cutting speed. The heating stage creates a thermal shock, which causes high thermal tensile stress (that is caused by uneven plastic strain due to the thermal expansion and contraction that occurs during flame cutting) close to the cut edge. The thermal shock is greater at faster cutting speeds and, for this reason,

produces more thermal tensile stress in the surface. During cooling, the austenized surface region forms martensite, leading to the structural expansion of the surface area, which is partly restrained by the inner structure. The expansion caused by martensite formation changes the thermal tensile stresses that are in the surface to compression stresses. As the thermal shock (and thermal tensile stress) is higher at faster cutting speeds, the martensite expansion creates less compressive stress in the surface region than it would at a slower cutting speed.

Equiaxed steel produced lower tensile stress peaks compared to elongated steel. In elongated steel, the tensile stress peak values are approximately 600 MPa in all the specimens. In contrast, the tensile stress peak values of equiaxed steel are approximately 100–150 MPa lower than in elongated steel. The RS results indicate that the microstructural features of equiaxed steel produce less tensile stress in the cut edge compared to elongated steel. Studies have shown [25] that dislocation pileups exist in the vicinity of grain boundaries and affect the local RS levels. A dislocation pileup creates a local stress peak in the grain boundary, and the RS levels monotonically decrease with increasing distance from the grain boundary. Elongated steel has more high-angle grain boundaries present in the vertical direction compared to equiaxed steel, which might create local stress peaks in the structure. In addition, the elongated shape of the grains indicate that the structure contains more dislocations in comparison with equiaxed prior austenite grains. As a result, the local stress peaks that are formed in the grain boundary level (Type II RS) may be superimposed in the measured RS profiles (Type I RS) thus creating higher tensile stress levels in elongated steel compared to equiaxed steel.

The ultrasonic inspection results showed that elongated steel contained more cracks than those contained in equiaxed steel. The cracks were located in the tempered region below the cut surface, which also contained the highest residual tensile stresses. These results indicate that the combination of high residual tensile stress with the microstructural features observed from elongated steel led to an enhanced cracking tendency in comparison with equiaxed steel. The results of this study indicate that the horizontally elongated grain structure is unbeneficial in both RS and crack formation points of view. The elongated prior austenite grain–structured steel produced higher tensile stress peaks during flame cutting compared to steel, which consisted of equiaxed prior austenite grains. In addition, elongated prior austenite grain structures create long parallel grain boundary chains, which can act as possible paths for crack formation. The susceptible microstructure of elongated prior austenite grains associated with the high residual tensile stresses formed during flame cutting make the steel plate vulnerable to crack formation.

Conclusions

Wear-resistant steel plates with two different microstructures were investigated to study the effect of microstructural features on the RS formation and cracking that is due to flame cutting. The following conclusions can be made from this study:

(1) The flame cutting process creates three types of microstructural regions in the HAZ of the cut edge: the martensite region, two-phase region, and tempered original structure. The depth of these regions was shown to depend on the cutting speed.

(2) Different microstructural regions have different hardness and RS values. The martensite region closest to the cut edge is the hardest and tends to produce compressive RS. In the two-phase region, the hardness values decrease, and RS values start to increase as the newly formed martensite region is mixed with the tempered original structure. The original structure, which is tempered during the flame cutting process, has both the lowest hardness values and the highest residual tensile stress values.
(3) Equiaxed prior austenite grains produced lower tensile stress peaks compared to steel with horizontally elongated prior austenite grains.
(4) Elongated prior austenite grain–structured steel was more prone to cracking compared to equiaxed steel. Horizontally elongated PAGBs can act as potential paths for crack propagation. Equiaxed prior austenite grains created more obstacles in the vertical direction in comparison with grain boundary chains found in elongated prior austenite grain structures.
(5) Prior austenite grain structures have an effect on both the RS formation and the probability of cracking. The combination of elongated prior austenite grains and high-residual tensile stresses makes steel plates more prone to crack formation during the flame cutting process.

ACKNOWLEDGMENTS

The funding for this work was mainly provided by the Tampere University of Technology graduate school. The authors would like to thank Mr. Petri Jussila (SSAB) for carrying out the GDOES experiments.

References

[1] Soisson, L. R., "Oxyfuel Gas Cutting," *ASM Handbook Volume 6: Welding, Brazing, and Soldering*, ASM International, Materials Park, OH, 1993, pp. 1155–1165.
[2] Thiébaud, R., Drezet, J., and Lebet, J., "Experimental and Numerical Characterisation of Heat Flow during Flame Cutting of Thick Steel Plates," *J. Mater. Process. Technol.*, Vol. 214, No. 2, 2014, pp. 304–310, https://doi.org/10.1016/j.jmatprotec.2013.09.016
[3] Martín-Meizoso, A., Aldazabal, J., Pedrejón, J. L., and Moreno, S., "Resilience and Ductility of Oxy-Fuel HAZ Cut," *Frattura ed Integrita Strutturale*, Vol. 30, 2014, pp. 14–22.
[4] Wilson, A. D., "Hardness Testing of Thermal Cut Edges of Steel," *Eng. J. Am. Inst. Steel Constr.*, Vol. 27, No. 3, 1990, pp. 98–105.
[5] Wood, W. E., *Heat-Affected Zone Studies of Thermally Cut Structural Steels, Report No. FHWA-RD-93-015*, Federal Highway Administration, McLean, VA, 1994, 92p.
[6] HARDOX TechSupport, SSAB Oxelösund, Stockholm, Sweden, 2007, 2p, http://www.aemach.com/hardox/pdf/016_TS_Hardox_Cutting_of_Hardox_wear_plate_UK.pdf
[7] Lindgren, L., Carlestam, A., and Jonsson, M., "Computational Model of Flame-Cutting," *J. Eng. Mater. Technol.*, Vol. 115, No. 4, 1993, pp. 440–445, https://doi.org/10.1115/1.2904243
[8] Withers, P. and Bhadeshia, H., "Residual Stress. Part 1—Measurement Techniques," *Mater. Sci. Technol.*, Vol. 17, No. 4, 2013, pp. 355–365, https://doi.org/10.1179/026708301101509980
[9] Withers, P. and Bhadeshia, H., "Residual Stress. Part 2—Nature and Origins," *Mater. Sci. Technol.*, Vol. 17, No. 4, 2013, pp. 366–375, https://doi.org/10.1179/026708301101510087
[10] Jokiaho, T., Saarinen, T., Santa-Aho, S., Peura, P., and Vippola, M., "The Characterization of Flame Cut Heavy Steel—The Residual Stress Profiling of Heat Affected Surface Layer," *Key Eng. Mater.*, Vol. 674, 2016, pp. 103–108, https://doi.org/10.4028/www.scientific.net/KEM.674.103

[11] Jokiaho, T., Laitinen, A., Santa-aho, S., Isakov, M., Peura, P., Saarinen, T., Lehtovaara, A., and Vippola, M., "Characterization of Flame Cut Heavy Steel: Modeling of Temperature History and Residual Stress Formation," *Metall. Mater. Trans. B*, Vol. 48, No. 6, 2017, pp. 2891–2901, https://doi.org/10.1007/s11663-017-1090-x

[12] EN 15305, *Non-Destructive Testing—Test Method for Residual Stress Analysis by X-Ray Diffraction*, German Institute for Standardization, Berlin, Germany, 2008, https://standards.globalspec.com

[13] Fitzpatrick, M., Fry, A., Holdway, P., Kandil, F., Shackleton, J., and Suominen, L., *Determination of Residual Stresses by X-Ray Diffraction, Measurement Good Practice Guide No. 52*, National Physical Laboratory, Teddington, UK, 2005, 77p.

[14] SFS-EN ISO 6892-1, *Metallic Materials—Tensile Testing—Part 1: Method of Test at Room Temperature*, Finnish Standards Association, Helsinki, Finland, 2016, www.iso.org

[15] Nyyssönen, T., Isakov, M., Peura, P., and Kuokkala, V.-T., "Iterative Determination of the Orientation Relationship between Austenite and Martensite from a Large Amount of Grain Pair Misorientations," *Metall. Mater. Trans. A*, Vol. 47, No. 6, 2016, pp. 2587–2590, https://doi.org/10.1007/s11661-016-3462-2

[16] Bachmann, F., Hielscher, R., and Schaeben, H., "Texture Analysis with MTEX—Free and Open Source Software Toolbox," *Solid State Phenom.*, Vol. 160, 2010, pp. 63–68, https://doi.org/10.4028/www.scientific.net/SSP.160.63

[17] Järvinen, H., Isakov, M., Nyyssönen, T., Järvenpää, M., and Peura, P., "The Effect of Initial Microstructure on the Final Properties of Press Hardened 22MnB5 Steels," *Mater. Sci. Eng., A*, Vol. 676, 2016, pp. 109–120, https://doi.org/10.1016/j.msea.2016.08.096

[18] Rudnev, V., Fett, G. A., and Semiatin, S. L., "Tempering of Induction-Hardened Steels," *ASM Handbook Volume 4C: Induction Heating and Heat Treatment*, ASM International, Materials Park, OH, 2014, pp. 130–159.

[19] Li, S., Zhu, G., and Kang, Y., "Effect of Substructure on Mechanical Properties and Fracture Behavior of lath Martensite in 0.1C–1.1Si–1.7Mn Steel," *J. Alloys Compd.*, Vol. 675, 2016, pp. 104–115, https://doi.org/10.1016/j.jallcom.2016.03.100

[20] Zhang, C., Wang, Q., Ren, J., Li, R., Wang, M., Zhang, F., and Sun, K., "Effect of Martensitic Morphology on Mechanical Properties of an As-Quenched and Tempered 25CrMo48V Steel," *Mater. Sci. Eng., A*, Vol. 534, 2012, pp. 339–346, https://doi.org/10.1016/j.msea.2011.11.078

[21] Zhou, T., Yu, H., and Wang, S., "Effect of Microstructural Types on Toughness and Microstructural Optimization of Ultra-Heavy Steel Plate: EBSD Analysis and Microscopic Fracture Mechanism," *Mater. Sci. Eng., A*, Vol. 658, 2016, pp. 150–158, https://doi.org/10.1016/j.msea.2016.02.001

[22] Wang, C., Wang, M., Shi, J., Hui, W., and Dong, H., "Effect of Microstructural Refinement on the Toughness of Low Carbon Martensitic Steel," *Scr. Mater.*, Vol. 58, No. 6, 2008, pp. 492–495, https://doi.org/10.1016/j.scriptamat.2007.10.053

[23] Bhadeshia, H. and Honeycombe, R., "The Tempering of Martensite," *Steels: Microstructure and Properties*, 3rd ed., Butterworth-Heinemann, Oxford, 2006, pp. 183–208.

[24] Jack, D. H. and Jack, K. H., "Invited Review: Carbides and Nitrides in Steel," *Mater. Sci. Eng.*, Vol. 11, No. 1, 1973, pp. 1–27, https://doi.org/10.1016/0025-5416(73)90055-4

[25] Basu, I., Ocelík, V., and De Hosson, J. T. M., "Measurement of Spatial Stress Gradients Near Grain Boundaries," *Scr. Mater.*, Vol. 136, 2017, pp. 11–14, https://doi.org/10.1016/j.scriptamat.2017.03.036

PUBLICATION IV

Role of Steel Plate Thickness on the Residual Stress Formation and Cracking Behavior During Flame Cutting

T. Jokiaho, S. Santa-aho, P. Peura, M. Vippola

Metallurgical and Materials Transactions A
https://doi.org/10.1007/s11661-019-05314-w

Role of Steel Plate Thickness on the Residual Stress Formation and Cracking Behavior During Flame Cutting

TUOMAS JOKIAHO, SUVI SANTA-AHO, PASI PEURA, and MINNAMARI VIPPOLA

Thick wear-resistant steel plates are utilized in challenging applications, which require a high hardness and toughness. However, utilization of the thick plates is problematic as they often have nonuniform mechanical properties along the thickness direction due to the manufacturing-induced segregations. In addition, the processing of thick plates commonly involves flame cutting, which causes several challenges. Flame cutting forms a heat-affected zone and generates high residual stresses during the cutting process. In the worst case, flame cutting causes cracking of the cut edge. The aim of this study is to investigate the role of plate thickness on the residual stress formation and cracking behavior when utilizing flame cutting. Residual stress profiles are measured by X-ray diffraction, plates and cut edges and are mechanically tested and characterized by electron microscopy. The results show that thicker plates generate more unfavorable residual stress state during flame cutting. Thick plates also contain segregations, which have decreased mechanical properties. The combination of high residual tensile stresses and segregations increase the risk of cracking during flame cutting. To prevent the cracking, the residual stresses should be lowered by lower cutting speeds and preheating. In addition, manufacturing practices should be aimed at lowering segregation formation in thick plates.

https://doi.org/10.1007/s11661-019-05314-w

I. INTRODUCTION

THICK wear-resistant steel plates are utilized, for example, in the mining industry, where a high degree of hardness and toughness is required. In terms of properties and manufacturing, thick steel plates are more complex compared to thin plates. During solidification, liquid steel may cool unequally and the solidification process may proceed at different rates at different locations in the plate. The formation of segregation on the center plane of the plate is caused by the enrichment of alloying elements such as carbon, phosphorus, sulfur, and manganese near the center region of the thick steel plate. The rolling process compresses the regions enriched by alloying elements and nonmetallic inclusions into thin sheets or strips and results in a layered structure.[1,2] There have been several studies related to the mechanical properties of thick steel plates. Yang *et al.*[1] studied 100- and 120-mm-thick steel plates and noticed that the mechanical properties of plates vary depending on the test location in the thickness direction and generally that properties deteriorate toward the center region of the plate. Wang *et al.*[2] investigated steel plates with thicknesses of 60, 90, 120, and 150 mm, and the results indicated that yield strength, ductility, and fracture toughness values decline as the testing position is changed from the plate surface toward the centerline. Additionally, these properties become worse with increasing plate thickness. Wang *et al.*[3] studied 60-, 80-, 100-, 120-, and 150-mm-thick plates and indicated that the mechanical properties decrease as the plate thickness increases. It was noted that tensile strength, ductility, impact toughness, and fracture toughness were lower in both the transverse and thickness directions as the plate thickness increases. In addition, mechanical properties and impact strength in the thickness direction have been shown to be inferior to those in the horizontal directions (transverse or rolling direction).

The manufacturing of wear-resistant and thick steel plates includes cutting, which is difficult due to the hardness, toughness, and thickness of the plates. Mechanical cutting is slow and challenging because the plates are often as hard as the cutting tools. Therefore,

TUOMAS JOKIAHO, SUVI SANTA-AHO, PASI PEURA, and MINNAMARI VIPPOLA are with the Materials Science and Environmental Engineering, Faculty of Engineering and Natural Sciences, Tampere University, 33014 Tampere, Finland. Contact e-mail: tuomas.jokiaho@tuni.fi

Manuscript submitted November 7, 2018.

Published online: 17 June 2019

thermal cutting is a commonly utilized method in the steel industry for cutting thick wear-resistant steel plates. In particular, flame cutting is preferred as it is suitable for thick plates and high production rates. The flame cutting process is exothermal and generates large amounts of heat during the cutting. The generated heat supports the continuity of the cutting process and enables the cutting of very thick steel plates.[4] The flame cutting process includes three stages: First, the steel is locally heated to its ignition temperature by using an oxyfuel gas flame. Second, a jet of pure oxygen is directed to the locally heated area. The oxygen jet causes rapid burning of the steel, thus, cutting through the steel plate. Third, the oxygen jet blows away the iron oxide from the cut edge and exposes clean surfaces for further cutting.[5]

Due to the inherent characteristics of the flame cutting process, a notable heat-affected zone (HAZ) is formed near the cut edge of the steel plate. In the HAZ, hardness variations and microstructural and specific volume changes take place. Wood[6] studied 25-mm-thick, low-carbon and low-alloy steel plates and noticed that flame cutting produced a higher hardness region close to the cut edge and the hardness values decreased with increasing distance from the cut edge. Similar findings were reported by Martín-Meizoso *et al.*,[7] who also studied the flame cutting of 25-mm-thick steel plates. Wilson[8] studied the flame cutting of 25.4-, 50.8-, and 101.6-mm-thick plates and indicated that a higher cutting speed generated narrower HAZ and higher hardness. It was also reported that plates with an increased amount of alloying elements tend to produce harder and broader HAZ. In addition, in an earlier study,[9] it was confirmed that the flame cutting process creates three types of microstructural regions in the HAZ: a martensite region, two-phase region (mixture of newly formed martensite and tempered original structure), and tempered original structure. The region closest to the cut edge is fully austenized during the flame cutting, and during cooling, it transforms into martensite. Behind the newly formed martensite region, there is a two-phase region, which is partly austenized during flame cutting and during cooling forms martensite while the nonaustenized regions are tempered. The rest of the HAZ structure consists of the tempered original structure, and the tempering effect gradually decreases with increasing distance from the cut edge.

In addition to microstructural changes, flame cutting generates residual stresses near the cut edge of the plate. Residual stresses are internal stresses that exist in the component even after the external applied loads are removed. Residual stresses originate from a local misfit inside the solid body, such as local plastic deformation, which is balanced by local elastic strains.[10] In flame cutting, the residual stresses can be classified as thermal stresses and transformation stresses. Thermal stresses are caused by different thermal expansions and contractions that occur during heating and cooling. Local thermal expansion and contraction is restrained by the cold surrounding regions, leading to plastic deformation in restrained regions and residual stresses. Transformation stresses arise from local phase transformations, which cause volume changes in these regions. For example, martensite transformation includes volumetric expansion, which can be incoherent with the other microstructural regions and thus create residual stresses.[11] Often residual stresses are grouped into three types (types I, II, and III residual stresses) depending on the range they affect and over which they self-equilibrate. Type I is a macrostress, which varies over large distances, and equilibrates on a macroscopic scale. Types II and III are microstresses, which vary and equilibrate on a microscopic scale. Type II stresses exist in the grain scale, and they usually occur in polycrystalline structures. Type III stresses vary on atomic scale and often originate from dislocations and point defects. Usually, for example, in the hole drilling method, only type I residual stresses are measured as type II and III stresses are averaged to zero within the sampled area. However, it has been noted that in diffraction-based measuring methods, where a particular phase or grain orientation is sampled, type II residual stress can be superimposed on the type I stress.[10]

In the worst-case scenario, flame cutting leads to cracking of the cut edge. The crack size can be several centimeters long. Commonly cracks are formed in the horizontal (sheet) plane, but they may also propagate in the vertical direction. In an earlier study[9] by the current author, it was found that cracks are often formed just beneath the flame cut surface and for that reason they are difficult to detect. The cracking probability has been noticed[12] to enhance with increasing plate hardness and thickness. In addition, Lindgren *et al.*[12] reported that high residual tensile stresses promote crack formation. It was shown that a residual compressive stress area is formed close to the cut edge, which is followed by a high residual tensile stress area deeper in the component. It was also noted that a slower cutting speed and flame cutting with preheating produce a lower residual stress state in the cut edge. Similar results were obtained in other studies[13,14] by the author; the residual stress formation during flame cutting can be affected by the size of the sample and cutting parameters. In addition, preheating not only decreases the residual stresses in general but also increases the compressive stress region close to the surface by shifting the tensile stress region deeper into the subsurface.

This study is a continuation for previous studies by the current author. The first study[14] confirmed that the residual state of the flame cut edge can be affected by variating the cutting parameters. In another study,[13] a model was developed to investigate the flame cut process and residual stress formation. It was used for example to investigate the thermal histories and residual stress formation of the modeled sample during flame cutting. The combination of preheating and low cutting speed produced the most beneficial residual stress state with the most compressive stress and the lowest tensile stress peak. To obtain further knowledge of the flame cut process and cracking behavior, another study[9] was made to investigate the microstructural characteristics related to this topic. It was shown that a higher residual stress state was caused by elongated prior austenite

grains compared to an equiaxed prior austenite grain structure. In addition, the cracking probability is higher with an elongated prior austenite grain structure compared to equiaxed prior austenite grains. The elongated prior austenite grain structure is susceptible to cracking as it creates grain boundary chains, which can act as possible paths for crack formation. However, despite the studies mentioned earlier, there is still a considerable lack of knowledge on how the plate thickness affects the residual stress formation and cracking in flame cutting. The aim of this study is to determine the effect of the steel plate thickness on the residual stress formation and on the cracking probability. To achieve this goal, wear-resistant steel plates of varying thickness were mechanically tested, flame cut in controlled conditions, and inspected with ultrasound to evaluate the cracking tendency. After this the resulting residual stress state as well as the changes in the microstructure near the cut edge were characterized. The results of this study can be utilized to avoid the cracking of the plates during flame cutting and to improve the manufacturing of thick plate products.

II. EXPERIMENTAL PROCEDURE

The studied samples were aluminum-killed, hot-rolled, wear-resistant steel plates. The plate thicknesses of the examined samples were 20, 40, and 60 mm (width 150 mm, length 150 mm). One side of each sample was flame cut utilizing an oxyfuel propane gas flame. The flame cutting parameters applied are shown in Table I. The preheating at 200 °C (holding time ~ 1 h) of the 40- and 60-mm plates was performed in an industrial furnace under a normal air atmosphere, and the plate temperature was verified by a radiation thermometer. After flame cutting, the samples were inspected using Phasor XS 16/16 Olympus ultrasonic equipment with a MSEB 4 dual probe (4 MHz). The ultrasonic inspection results were verified by having two individual researchers repeat the inspections and by sectioning a few samples after inspection to confirm the existence of defects. The nominal composition of the studied sample material is presented in Table II, and the carbon equivalent is calculated with Ito and Besseyo (1), which covers low ranges of carbon (< 0.18 wt pct C). Steels with over 0.4 wt pct CE cannot be easily welded because of their increased tendency to form martensite.[15]

Table I. Flame Cutting Parameters of the Studied Samples

Flame Cutting Parameters		
Thickness (mm)	Cutting Speed (mm/min)	Preheating (°C)
20	150	—
20	300	—
20	500	—
20	700	—
40	150	—
40	300	—
40	500	—
40	500	200
60	150	—
60	300	—
60	500	—
60	500	200

Residual stress measurements were performed using an XStress 3000 X-ray diffractometer (manufactured by Stresstech Oy) by the modified Chi method.[16] The residual measuring method is described in more detail in previous studies.[9,13,14] The examination locations and directions of the residual stress measurements are described in Figure 1. As shown in the figure, measurements were performed at the centerline of the samples (where the cracks are mostly formed during flame cutting) in two perpendicular measurement directions: the rolling direction (0 deg) and the thickness direction (90 deg). The selected directions are the most important orientations from crack formation point of view.

Sectioned flame cut samples were analyzed using scanning electron microscopes (SEMs). Grinding of the samples were done with abrasive SiC papers and polishing with 3-μm and 1-μm diamond suspensions. After grinding and polishing, the samples were etched using 4 pct Nital solution. Microstructural characterization was performed using a Philips XL-30 SEM and a Zeiss ULTRAplus field emission SEM (FE-SEM). The prior austenite grain sizes (PAGS) were measured from the micrographs of the centerline and two-phase region by mean linear intercept (L_M). Hardness profiles (HV 5 kg) in the thickness direction of the plates were obtained using a Struers DuraScan 80, whereas the hardness depth profiles (HV 0.2 kg) from the flame cut edge were carried out using a digital microhardness tester Matsuzawa MMT-X7. The location of the hardness depth profiles in relation to the cut edge is presented in Figure 1. Tensile tests in the thickness direction for each plate were performed with an MTS 250 kN, according to the EN-ISO 6892-1 standard.[17] The samples were round bars with an original diameter (D0) of 6, 10, and 10 mm and parallel length (L_c) of 11, 22, and 42 mm for the 20-, 40-, and 60-mm-thick plates, respectively. Charpy V-notch impact tests were performed according to the EN-ISO 148-1 standard[18] with specimens sectioned into square bars with dimensions of 10 mm × 10 mm × 55 mm. The studied samples were in the longitudinal and transverse directions in relation to the rolling direction with test temperatures of − 40 °C, − 20 °C, − 10 °C, 0 °C, and 20 °C. In addition, samples from 40- and 60-mm plates were made from both the 0.5 and 0.25 thicknesses (longitudinal and transverse directions). The 60-mm plates were also tested with samples made in the thickness direction at temperatures of − 10 °C, 0 °C, 22 °C, and 60 °C. The impact test results presented in this study are an average of six repetitions. The test location and directions of this study are presented in Figure 1.

III. RESULTS

The mechanical properties of the steels under study were determined by means of hardness measurements and tensile tests. The results presented in Table III show that the average hardness (hardness profiles in the

Table II. Nominal Composition of the Studied Steel Plates and Carbon Equivalent (CE)[15] for Studied Material

C (pct)	Si (pct)	Mn (pct)	Cr (pct)	Mo (pct)	Ni (pct)	Cu (pct)	V (pct)	B (pct)
0.15	0.6	1.1	0.6	0.4	0.2	0.02	0.06	0.0016

$$\mathrm{CE} = W_C + \frac{W_{Si}}{30} + \frac{W_{Mn}+W_{Cu}+W_{Cr}}{20} + \frac{W_{Ni}}{60} + \frac{W_{Mo}}{15} + \frac{W_v}{10} + 5W_B \text{ wt pct} = 0.3 \quad (1)$$

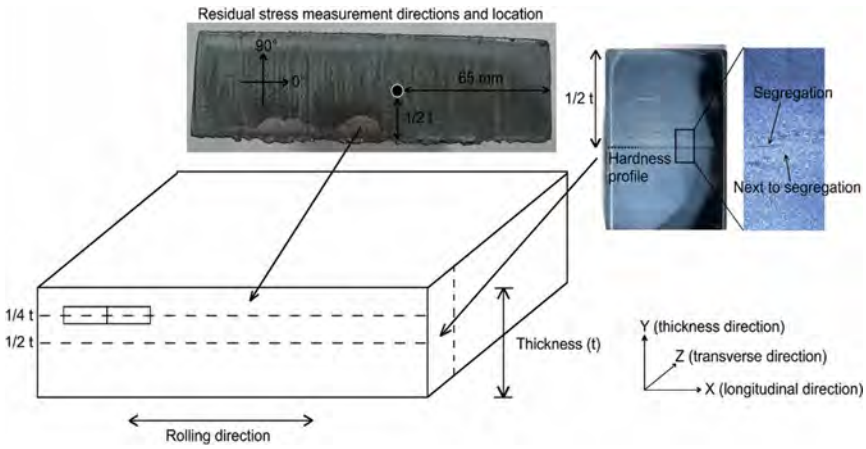

Fig. 1—Test and measurement locations and directions used in this study.

Table III. Initial Mechanical Properties of Studied Steels

Thickness	Hardness (HV 5 kg)	R_m (MPa)	Z (pct)	PAGS L_M (μm)
20 mm	448	1347	46	16
40 mm	399	1217	51	44
60 mm	378	1063	56	54

The average hardness values (HV 5 kg), tensile strength (R_m), and percentage reduction of the area at fracture (Z pct) in tensile tests (thickness direction). Prior austenite grain size (PAGS) is expressed as the mean linear intercept (L_m) calculated from the centerline micrographs of the studied steels.

thickness direction) of the plate decreases as the thickness increases. Similar observations can be made in the case of the tensile strength (R_m). The percentage reduction of the area fracture (Z pct) is the lowest in the 20-mm plate and the highest in the 60-mm plate. Furthermore, as is evident from the Z values, all the studied steels exhibit ductile behavior in the as-received state. In addition, Table III shows that the prior austenite grain size (PAGS) is the smallest with the 20-mm plate and increases with larger plate thicknesses.

SEM micrographs from the centerline of the steel plate samples are presented in Figure 2. The centerline structure of the 20-mm plate sample consists of lath martensite (Figure 2(a)). The structure of the 40-mm plate sample in the centerline consists of a mixture of bainite and lath martensite (Figure 2(b)). The centerline microstructure of 60-mm plates consists mainly of bainite (Figure 2(c)). However, there may also be a small amount of lath martensite in the centerline microstructure of the 60-mm plate.

The hardness values presented in Table III are an average of the hardness profiles measured in the thickness direction of the studied plates. Figure 3 presents the hardness profiles (ten profiles from each sample) along the thickness direction of the 20-, 40-, and 60-mm plates. Hardness profiles from the 20-mm plate indicate a few hardness peaks in the middle section of the plate. In the 40-mm plate, there is more fluctuation in the hardness values in the middle section compared to in the 20-mm plate hardness profiles. There are not only hardness peaks but also softer regions in the thickness range of 15 to 25 mm. The hardness profiles of the 60-mm plate show a steady decrease in hardness with increasing distance from either the top or the bottom surface of the plate toward the center of the plate. The center region (~ 25 to 35 mm) consists of low hardness regions with high hardness peaks. In general, the profiles

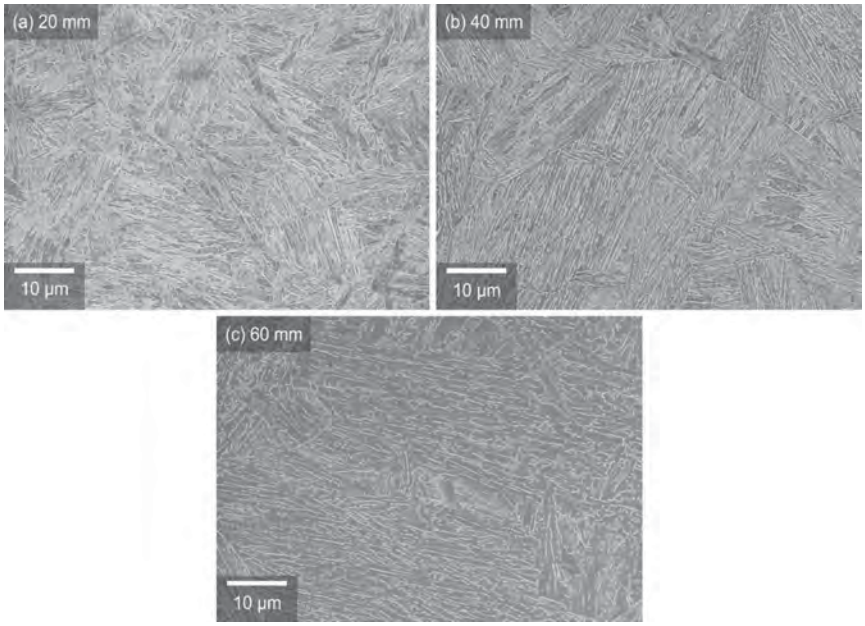

Fig. 2—SEM micrographs of steel plate samples (*a*) 20 mm, (*b*) 40 mm, and (*c*) 60 mm.

in Figure 3 show that the fluctuations in hardness values increase as the plate thickness increases.

Charpy V-notch impact tests were carried out to determine the impact toughness properties of the studied steel plates. As indicated in Figure 4, for all the tested steel plates, the results are similar between the longitudinal and transverse directions in relation to the rolling direction. However, the impact toughness values (longitudinal and transverse in 0.5 thickness) are higher in the 40-mm plates compared to in the 20-mm plates. A comparison of the 40- and 60-mm plates shows that the 40-mm plates have higher impact toughness values in 0.5 thickness, whereas in 0.25 thickness, the situation is reserved. In other words, in the tested cases, for the 40-mm plate, the highest impact toughness is measured at 0.5 thickness and for the 60-mm plate at 0.25 thickness. In addition, impact toughness tests were performed in the thickness direction for the 60-mm plates, and the results were much lower compared to the transverse and longitudinal directions (Figure 4).

The impact tests in the thickness direction were performed in two different notch locations (average of three repeats per notch location): in the segregation and next to segregation regions as shown in Figure 1 (the location of segregation was determined from the etched specimens). Figure 5 shows that the impact test location has an effect on the impact energy values. Samples that had a notch in the segregation region have somewhat lower impact toughness properties compared to samples that had a notch next to the segregation. Figure 6 shows SEM micrographs of the fracture surfaces at the segregation (a) and next to the segregation (b) at test temperatures of − 10 °C, 0 °C, 22 °C, and 60 °C. The fracture surfaces from both test locations have brittle fracture characteristics (examples are shown in Figure 6 with black arrows) such as cleavage planes and river patterns. In addition, in Figure 6(a), the fracture surface at the test temperature of − 10 °C contains an intergranular fracture region. With increasing test temperature, fracture surfaces contain an increasing amount of ductile fracture characteristics such as dimples (examples are shown in Figure 6 with white arrows). In addition, fracture surfaces at the segregation (Figure 6(a)) show more brittle fracture characteristics compared to fracture surfaces next to the segregation (Figure 6(b)).

Figure 7 presents the results of the residual stress measurements. It can be seen (Figures 7(a), (c), and (f)) that the 20-mm plates have the largest compressive stress region close to the cut edge (< 1 mm) and that the compressive stress values decrease as the plate thickness increases. In addition, the 20-mm plate has the lowest residual tensile stress values compared to the 40- and 60-mm plates at a cutting speed of 150 mm/minute. However, as the cutting speed increases to 300 and 500 mm/minute, the tensile stress peak values are almost identical, with only small variations between the studied plate thicknesses. The 20-mm plate has the highest tensile stress peak at a cutting speed of 300 mm/minute. Figures 7(b), (d), and (f) compare the residual stresses produced by different cutting parameters in the case of each plate thickness. It can be seen that 150 mm/minute produces the most compressive stresses at the cut edge and the lowest tensile stress region in the 20-mm plates. However, with regard to higher cutting speeds, a very high speed of 700 mm/minute causes the lowest tensile stress region. In addition, the tensile stress peak at 700 mm/minute is not as wide as the peaks at the 300-

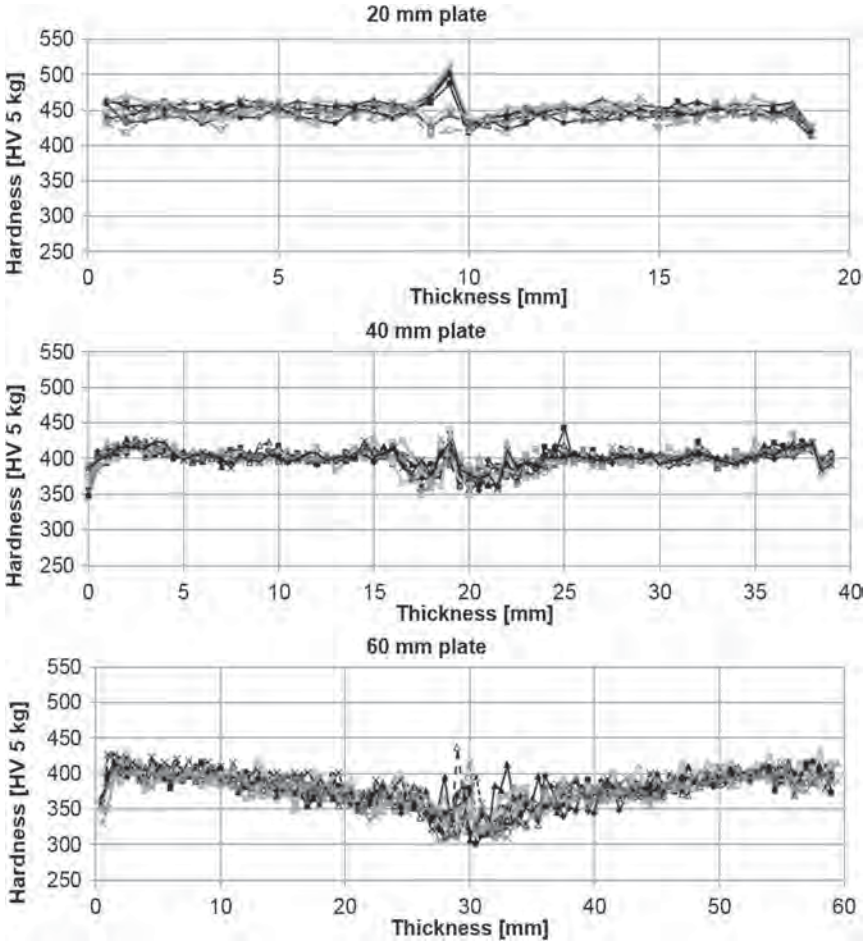

Fig. 3—Hardness profiles (HV 5 kg) in the thickness direction in the studied plate thicknesses: 20, 40, and 60 mm (note the different thickness scale in each hardness profile).

and 500-mm/minute cutting speeds. The low 150-mm/minute cutting speed produces the highest residual compressive stress in the 40-mm plates as well. However, the tensile stress values are similar at all cutting speeds. In the 40-mm sample, preheating produces more compressive stress in the surface region but does not affect the tensile stress peak. In the 60-mm plates, the 150-mm/min cutting speed also produces the most compressive stress in the surface. As in the case of the 40-mm samples, the tensile stress peak values are similar between the cutting speeds of 150, 300, and 500 mm/minute. However, in the 60-mm sample, preheating increases the compressive stress near the surface and lowers the tensile stress deeper in the plate.

Figure 8 presents the hardness profiles measured from the flame cut edges of the studied steel plates. Each flame cut sample produced a high hardness region near the cut edge, after which the hardness levels start to decrease around 0.7 to 0.9 mm from the cut edge. The lowest hardness values are located after the hardness drop, and subsequently, the hardness gradually increases toward the hardness of the original structure. However, after the lowest hardness values, the increase in hardness is less in the 40-mm plates than in the 20-mm plates and the hardness levels are almost constant in the 60-mm plates after the hardness drop. Figure 8 shows that a slow cutting speed produces a slightly wider high hardness region near the cut edge. As the cutting speed increases, the width of the high hardness region decreases. However, the differences are not significant between different cutting speeds.

Flame cutting creates an HAZ in the cut edge of thick wear-resistant steel plates with three distinct microstructural regions: a martensite region, two-phase region, and tempered original structure.[9] In addition, preheated samples had similar microstructural regions as samples that were flame cut without preheating. The region closest to the cut edge is fully austenized during flame cutting and forms martensite during rapid cooling. This region was similar for all the studied plate thicknesses. Figure 9 shows the martensite regions formed in the cut edge of the 20-, 40-, and 60-mm-thick plates using a

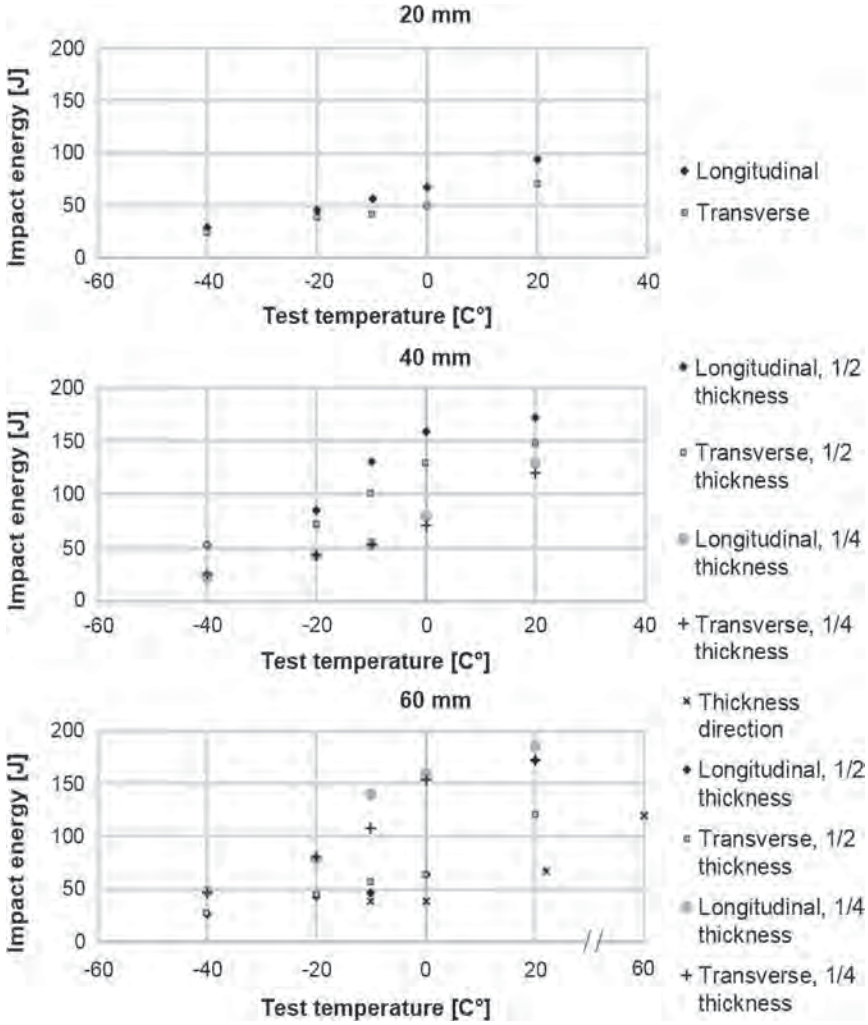

Fig. 4—Charpy V-notch impact test results in longitudinal and transverse directions in relation to the rolling direction. In addition, the 60-mm plate was also tested in the thickness direction (note different temperature scale in 60-mm results).

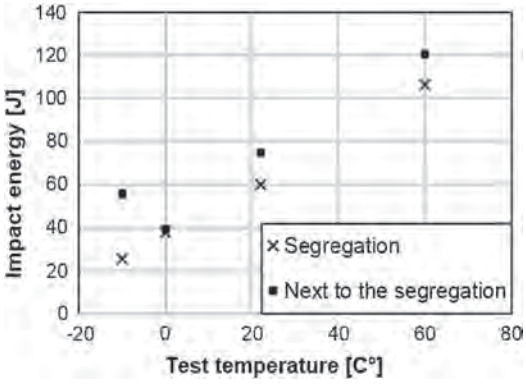

Fig. 5—Charpy V-notch impact tests in the thickness direction with specific notch locations (segregation and next to the segregation) of the 60-mm plate samples.

cutting speed of 300 mm/minute. The image locations were from the centerline of the sample and from a depth of 0.4 mm from the cut surface.

After the newly formed martensite, there is a two-phase region consisting of martensite and a tempered original structure. The austenization occurs heterogeneously in the grain boundaries of the prior austenite, and during cooling, the austenized regions form a fine martensite lath structure in the two-phase region. The rest of the structure, between the austenized regions, is tempered during the cutting process. Figure 10 shows the two-phase regions from the centerline of the studied 20-, 40-, and 60-mm plates produced by a cutting speed of 300 mm/minute.

After the two-phase region, the rest of the HAZ consists of the original structure, which is tempered during the cutting process. The tempering effect is gradually reduced while going deeper into the

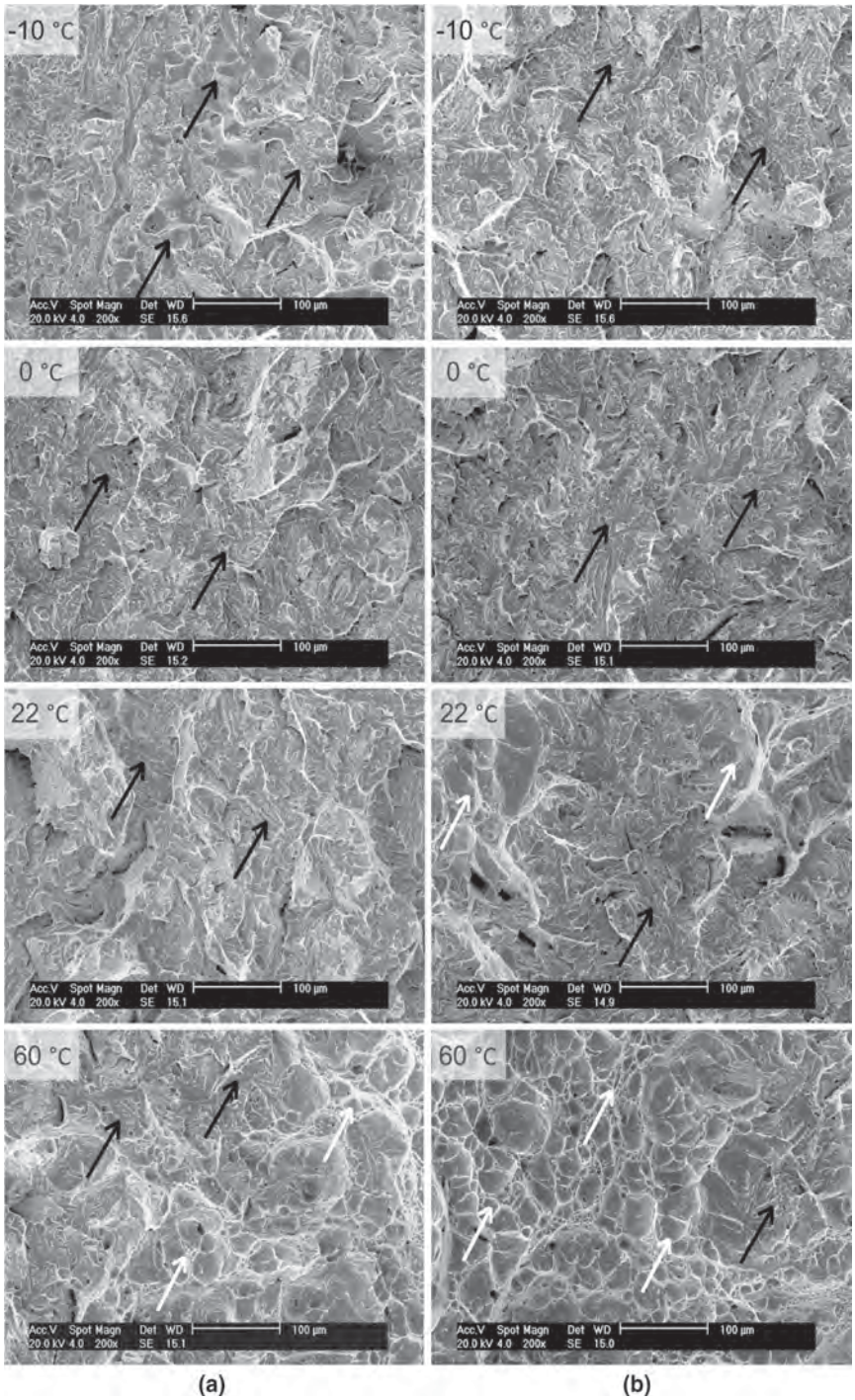

Fig. 6—Fracture surfaces of Charpy V-notch impact tests in the thickness direction of the 60-mm sample: notch location (*a*) at the segregation and (*b*) next to the segregation. Examples of brittle fracture and ductile fracture characteristics are marked in the images with black and white arrows, respectively.

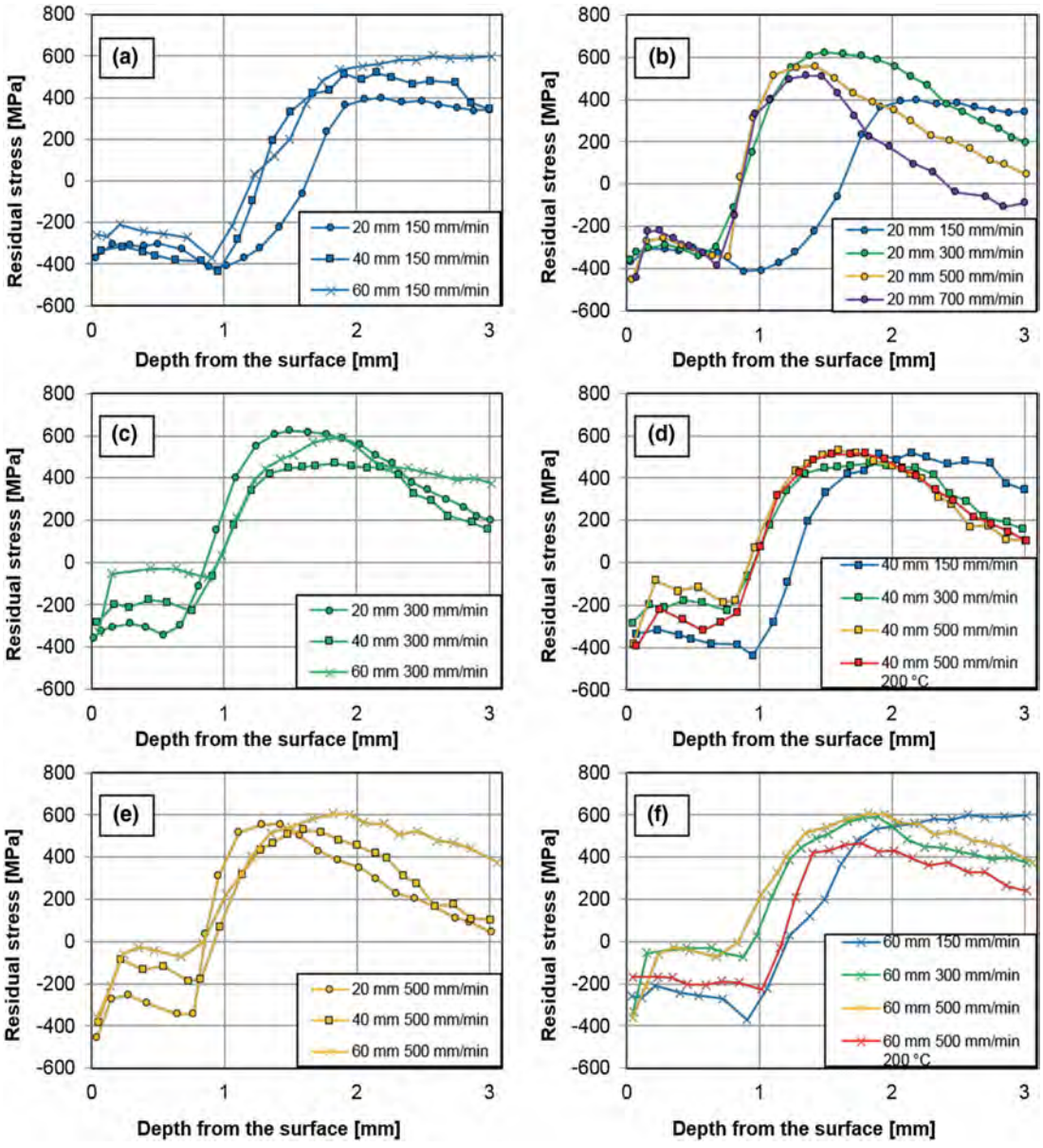

Fig. 7—Residual stress profiles in the thickness direction (90°). The effect of thickness in residual stress profiles at cutting speeds of (*a*) 150, (*c*) 300, and (*e*) 500 mm/min. The effect of cutting parameters in residual stress profiles with certain steel thicknesses: (*b*) 20, (*d*) 40, and (*f*) 60 mm. (For interpretation of the color references in these figures, the reader is referred to the web version of this article).

subsurface. Figure 11 shows the centerline micrographs of the studied 20-, 40-, and 60-mm plates from the tempered region (1.6 mm from the cut surface), which is formed using a 300-mm/minute cutting speed.

The samples were inspected by ultrasound after flame cutting. As presented in Figure 12, no cracks were detected in the 20-mm plates after flame cutting. However, the inspection revealed three (1 crack/1600 mm) and four cracks (1 crack/975 mm) in the 40- and 60-mm plates, respectively. It should also be noted that no cracks were detected in the preheated samples. The cracks that were found were located immediately below the cut surface in the center region (*i.e.*, near the midplane) of the plates. The crack normal was parallel to the thickness direction of the plate.

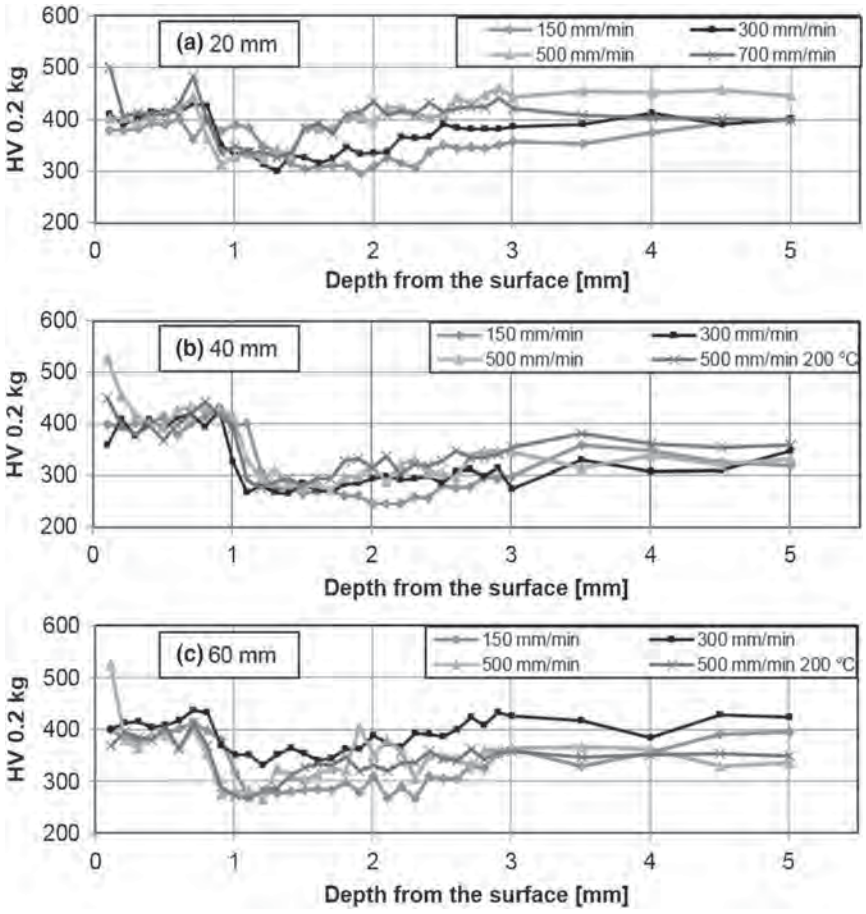

Fig. 8—Hardness depth profiles of studied plate thicknesses: (*a*) 20-mm, (*b*) 40-mm, and (*c*) 60-mm cut with different flame cutting parameters.

IV. DISCUSSION

Wear-resistant steel plates with thicknesses of 20, 40, and 60 mm were flame cut and characterized. The hardness and tensile strength properties were found to reduce as the thickness of the plates increases. The prior austenite grain size also increases with increasing plate thickness. The centerline microstructure of the 20-mm plates consists of lath martensite. However, the microstructure of the 40-mm plates consists of both bainite and martensite, and the 60-mm plates consist mainly of bainite (with a small amount of lath martensite). The microstructures of the studied plates derive from the cooling conditions during the fabrication process. The cooling of thick plates is not necessarily as uniform and fast as that of thinner plates due to the increased thickness. This results in a partially bainitic structure or mainly bainitic structure in the centerline of the thicker plates and the morphology of microstructures are different, depending on the distance from the upper surface of the plate. The effect of different microstructures can also be seen in the hardness profiles measured in the thickness direction. The profiles showed that the hardness levels were generally higher and smoother in the thinnest plate and that the thicker plates contained more fluctuation near the centerline of the plates. The fluctuations seen in the hardness profiles are most likely due to the segregation that occurred during the manufacturing of the plates.[1] The hardness results show that center segregation is the most severe in the 60-mm plates and reduces with decreasing plate thickness. The amount of segregations increases with increasing plate thickness.

The impact toughness values are smaller in the 20-mm plates than in the 40-mm or 60-mm plates (0.5 thickness). The explanation for this is the original microstructure on the centerline, which is lath martensite in the 20-mm plates, a mixture of bainite and lath martensite in the 40-mm plates, and mainly bainite in the 60-mm plates. It has been shown[19] that martensite has inferior impact toughness properties than bainite and that the increasing volume fraction of bainite in the bainite-martensite structure increases the impact toughness. Generally, a small prior austenite grain size is known to induce the refinement of martensitic packets and blocks and therefore simultaneously to enhance the impact toughness.[20] However, the formation of bainite

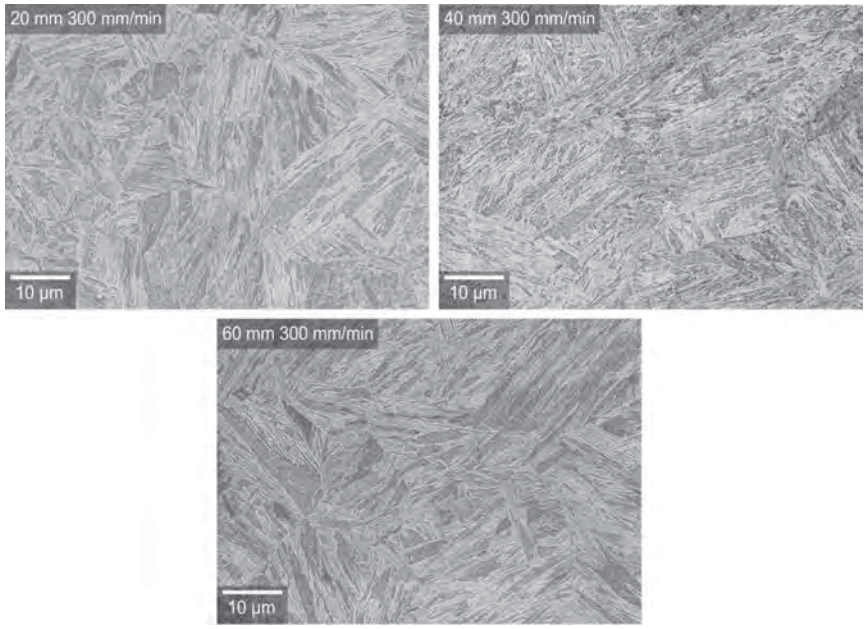

Fig. 9—Newly formed martensite regions of the 20-, 40-, and 60-mm plates produced by a 300-mm/min flame cutting speed. The images were from the centerline of the samples at a depth of 0.4 mm.

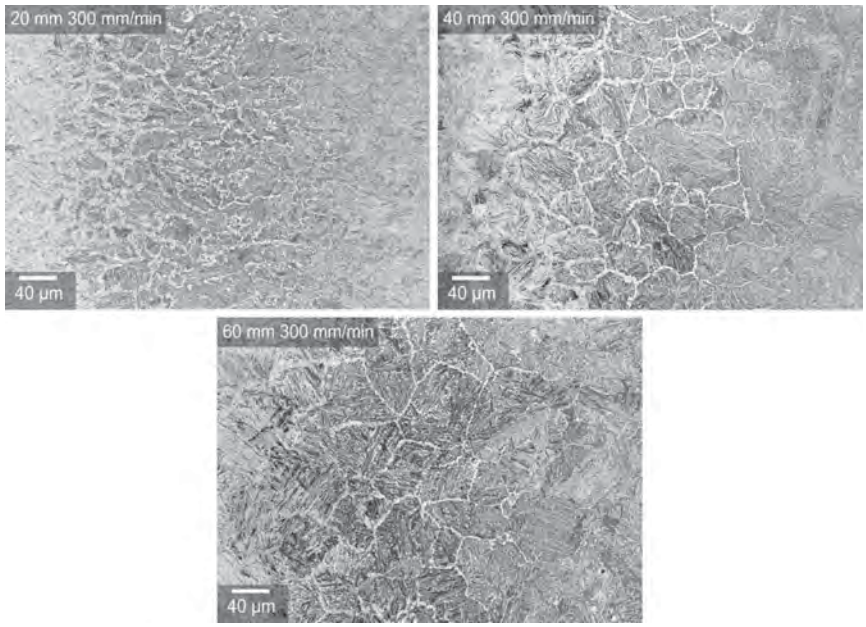

Fig. 10—Two-phase regions from the centerline of 20-, 40-, and 60-mm plates produced by a 300-mm/min flame cutting speed.

has also been shown[21] to refine the subsequent martensitic packets and blocks. In the present study, the martensite structure in the 20-mm plate results in lower impact toughness than the bainite-martensite structure of the 40-mm plates and the mainly bainitic structure of the 60-mm plates. In this case, the microstructure affects the impact toughness more than the prior austenite grain size (20-mm plates had smaller prior austenite grain size than the 40- or 60-mm plates). However, it seems that the bainite structure of the 60-mm plate has lower impact toughness in 0.5 thickness (in both the transverse and rolling directions) than does the

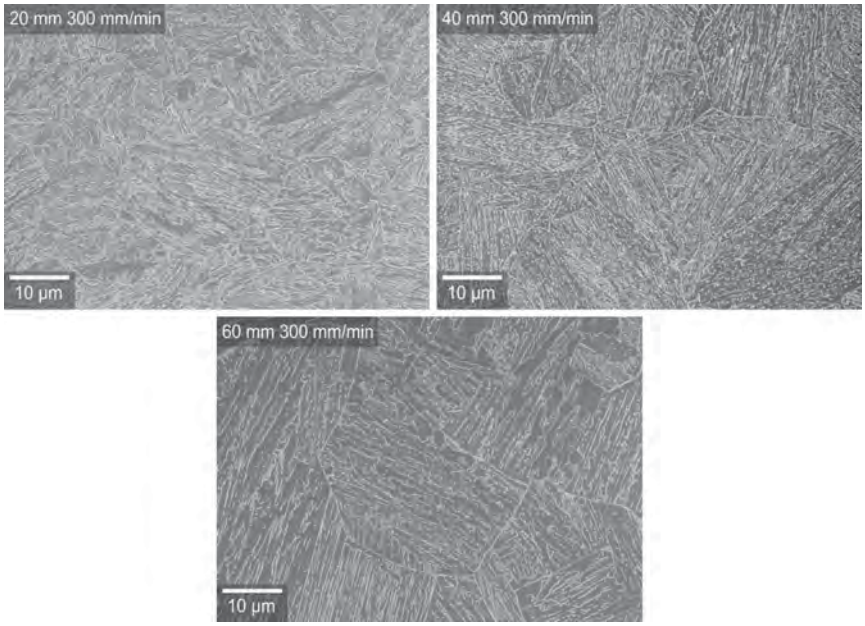

Fig. 11—Tempered regions (1.6 mm from the cut surface) of the 20-, 40-, and 60-mm plates formed at 300-mm/min cutting speed.

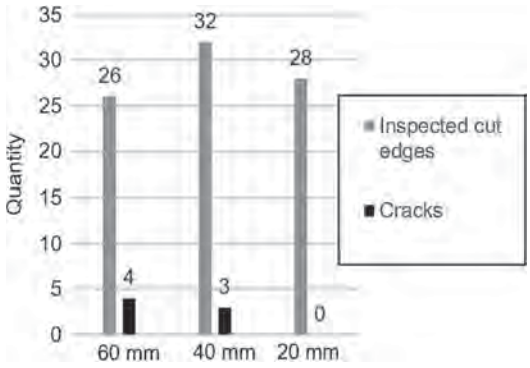

Fig. 12—Ultrasonic inspected flame cut samples of different plate thicknesses.

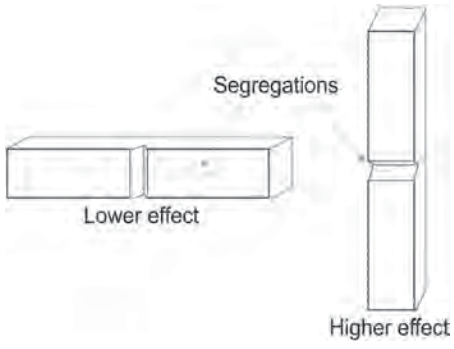

Fig. 13—Location of segregations relative to Charpy V-notch impact test specimens.

bainite-martensite structure of the 40-mm plates. In addition, the impact toughness of the 40- and 60-mm plates varies depending on the distance from the upper surface. The 40-mm plates have higher impact toughness (rolling and transverse directions) in 0.5 thickness compared to 0.25 thickness. This might be due to the different cooling conditions at different depths of the plate during quenching. The 0.5 thickness of the plate cools more slowly compared to the 0.25 thickness, and consequently, the microstructures are different depending on the depth. As a result of the faster cooling, the microstructure of 0.25 thickness can be almost fully martensite while the slower cooling in the centerline produces a mixture of bainite and martensite. In contrast, the 60-mm plates have better impact toughness in 0.25 thickness than in the centerline. Similarly to the 40-mm plates, the cooling conditions are different in 0.25 thickness and 0.5 thickness. However, with the 60-mm plate, the cooling in 0.25 thickness is slower than in 0.25 thickness of the 40-mm plates, and therefore, the resulting microstructure is a mixture of bainite and martensite. As the cooling of the 0.5 thickness is even slower, the produced microstructure in the centerline is mainly bainite. The large prior austenite grain size and segregations in the center region produce low impact toughness in the rolling and transverse directions at 0.5 thickness. Test results also show that impact toughness values are significantly lower in the thickness direction than in the transverse and rolling directions. A similar result was obtained by Wang *et al.*[3] This can explained by the location of segregations relative to the test specimens as it is shown schematically in Figure 13. Segregations have a smaller effect in the rolling direction and the transverse direction in the middle section as

their portion in the sample cross section is smaller. However, the effect increases in the through-thickness samples where the segregations cover more area in the test direction.

In addition, the impact toughness is lower in samples that had a notch in the segregation region than in samples that had a notch next to the segregation. Both impact toughness results and fracture surfaces indicate that the areas of segregation exhibit more brittle fracture behavior than do those next to the segregation. The reason for this might be the enrichment of the alloying elements, such as carbon, which locally increases the hardenability and makes the segregations more brittle compared to the regions next to them.

The residual stress measurements of flame cut surfaces show that the residual compressive stress decreases in the surface region (< 1 mm) as the plate thickness increases. As a previous study[13] has shown, a region of compressive stress is formed due to martensite transformation and the accompanying volume expansion occurring close to the cut edge. In addition, it has been shown[13] that rapid and significant changes of temperature should be avoided during flame cutting as they create high thermal stresses in the cut edge of the plate before martensite transformation. One reason why thinner plates produce more compressive stress close to the cut surface than thick plates might be that the heating flame heats the cutting edge of the thin plates more than that of thicker ones. This heating acts similarly to preheating and lowers the temperature differences between the surface and interior. In contrast, the heating flame warms only the upper edge in thicker plates and does not create a similar preheating effect in the cut edge. However, this preheating effect from the heating flame in 20-mm plates should not be confused with the actual preheating treatment carried out on the thicker plates (40 and 60 mm). In addition, the heat transfer by conduction is higher in the thicker plates, which also increases the temperature difference between the surface and interior. As a result, the temperature difference is lower between the surface and interior during heating and cooling with thin plates, which leads to a lower thermal stress state before martensite transformation and eventually a lower final stress state after martensite transformation. In addition, a thin plate produced the lowest residual tensile stress values compared to thicker plates at a cutting speed of 150 mm/minute. However, as the cutting speed increases to 300 and 500 mm/minute, the tensile stress peak values are almost identical, with only small variations between the studied thicknesses. Residual stress measurements of 300- and 500-mm/minute cutting speeds indicate that plate thickness does not influence the tensile stress region as much at high cutting speeds compared to a lower cutting speed. A possible explanation for this is that as the cutting speed increases, large local variations in material temperature appear regardless of the plate thickness; *i.e.*, even the thinnest plate is too thick for the temperature to equilibrate during high-speed cutting. However, in the case of higher cutting speeds, a very high speed of 700 mm/minute caused the lowest tensile stress region in the 20-mm plate. In addition, the tensile stress peak at 700 mm/minute is not as wide as at 300 and 500 mm/minute. This might be due to the fact that the tempering effect (and the negative volume change during tempering) in the HAZ decreases as the cutting speed increases. From the residual stress point of view, these results indicate that a fast cutting speed is not necessarily the worst option for thinner plates. The results also indicate that low cutting speed and preheating have positive effects on the residual stress formation, as they increase the compressive stress in the surface and lower the tensile stress values. In addition, it can be seen that a lower cutting speed shifts the tensile stress region deeper into the subsurface. Preheating decreases the effect of the thermal shock that creates the thermal stresses by reducing the temperature differences inside the sample.[13]

As the earlier study[9] by the current author showed, the HAZ consists of three regions: the newly formed martensite region, the two-phase region, and the tempered region. It was also shown that hardness profiles from the cut edge follow the microstructural regions of the cut edge. The extent of the microstructural regions depends more on the cutting parameters used than on the different plate thicknesses. A low cutting speed produces wider regions than a fast cutting speed, and different plate thicknesses cut with the same speed have almost similar width microstructural regions. All the studied plate thicknesses produced a high hardness martensite region close to the cut edge. In the two-phase region, the hardness is reduced as the newly formed martensite becomes mixed up with the tempered original structure. The two-phase regions of different plate thicknesses show that thinner plates contain more newly formed martensite and the amount of martensite decreases as the plate thickness increases. In addition, two-phase regions highlight the existing prior austenite grain boundaries as the austenization and martensitic transformations occur heterogeneously in prior austenite grain boundaries. The shape of the prior austenite grains is mostly equiaxed in all the studied plate thicknesses. However, the two-phase region also shows that the size of the prior austenite grains increases as the thickness of the plate increases. The lowest hardness occurs just after the two-phase region, and generally, the hardness values gradually increase toward the base material. However, in the 40-mm plate, the hardness levels do not increase in the tempered region as much as in the 20-mm plate, and the hardness values of the 60-mm plates are almost constant after the two-phase region. The tempering effect is different between the steel thicknesses studied due to the different original microstructures of the studied plates. In the previous study,[9] it was shown that tempering of martensite during flame cutting produced a fine structure of dispersed cementite (Fe_3C) particles and that the tempering effect gradually decreased with increasing distance from the cut edge. However, it has been shown[22] that there are significant differences in the tempering behavior of bainite and martensite. Unlike martensite, bainite contains only a small amount of carbon in solution as most of the carbon in the bainite structure is in cementite particles, which tend to be coarser than

cementite in a tempered martensite structure.[23] For this reason, a bainite structure exposed to elevated temperatures is less affected than martensite. Major changes in mechanical properties only occur when the bainite plate microstructure coarsens or recrystallizes into a structure of equiaxed grains of ferrite.[23] Within the small amount of time available at elevated temperatures during the cutting process, sufficient coarsening of the cementite does not occur and therefore the mechanical properties of bainite do not change as much as in martensite.[22] As the results show, the tempered region of the 20-mm plates consists of a fine structure of dispersed cementite because the original structure contained purely lath martensite. Also, the tempered regions of the 40-mm plates consist of finely dispersed cementite particles. However, the number of particles is somewhat less than in the 20-mm plates and a small amount of coarsening of the cementite might also occur during tempering. The reason for this is that the original structure of the 40-mm plate consists of a mixture of bainite and lath martensite. The fine cementite particles mostly originate from the martensite regions while the slight coarsening of the cementite occurs in the bainite regions. In the tempered regions of the 60-mm plates, there are no similar dispersed cementite particles in the microstructure as in the tempered regions of the 20- or 40-mm plates. This is because the centerline microstructure of the 60-mm plates consists mainly of bainite. The tempering may cause some slight coarsening of the existing cementite, which is difficult to distinguish. In addition, the hardness depth profiles of the 60-mm plates show that the elevated temperatures during flame cutting do not affect the bainite structure as much as the martensitic structure. The hardness values are almost constant after the newly formed martensite region and the two-phase region. This indicates that there is not in fact a lower hardness region after the two-phase region because the tempering time is too short for bainite to influence the hardness levels. If the original structure is a mixture of bainite and martensite, as in the 40-mm plates, tempering has an effect on the martensite regions but hardly any on the bainite regions. This can seen as decreased hardness values after the two-phase region and a slow increase in hardness values when going deeper into the subsurface.

Ultrasound inspection of the flame cut samples revealed no cracks in the 20-mm plates. However, the cracking tendency is higher in thicker plates (40-mm plate: 1 crack/1600 mm and 60-mm plate: 1/975 mm). The inspection results indicate that thin plates withstand the residual stress state that is formed in flame cutting. In addition, most of the 40- and 60-mm plates were found to be intact after flame cutting. However, since some cracks were detected in the 40- and 60-mm plates, it can be stated that on some occasions the residual stress levels are high enough for crack formation. In addition, the impact toughness results are significantly lower in the thickness direction compared to other directions. It was also observed that the 40- and 60-mm plates contained more segregations in the center region than did the 20-mm plates. Thus, it seems that the cracks are commonly located in the segregations, which tend to be harder and more brittle than the base material. These results indicate that the susceptibility to cracking increases as the strong manufacturing-induced segregation occurring in the center region of thick plates is combined with the high residual tensile stress produced by high-speed flame cutting. However, all the tested steel plates exhibited ductile behavior macroscopically and most of the plates were found to be intact even in the presence of relatively large local residual tensile stresses. This highlights the stochastical nature of the cracking in flame cut steel plates. To lower the susceptibility to cracking, the residual tensile stresses should be lowered by utilizing the most optimal flame cutting parameters: low cutting speed and preheating. In addition, the formation of segregations should be avoided by improving manufacturing practices of thick plates.

V. CONCLUSION

Wear-resistant steel plates in three different thicknesses were investigated to study the effect of plate thickness on residual stress formation and cracking in flame cutting. The main conclusions of this study are summarized as follows:

1. Hardness and tensile strength properties reduce as the plate thickness increases. The centerline microstructure of thin plates is fully martensite, and the fraction of bainite increases with increasing thickness. The reason for this is that the centerline of thicker plates undergoes slower cooling during manufacturing. In addition, the hardness profiles in the thickness direction have more fluctuations in the center regions due to segregation as the plate thickness increases.
2. Thin plates have low impact toughness due to their fully martensitic microstructure. The impact toughness of thicker plates varies depending on the distance from the upper surface. Microstructures consisting of a mixture of bainite and martensite have the best impact toughness properties. Impact toughness in the thickness direction is significantly lower compared to the rolling and transverse directions. In addition, impact toughness is lower in segregation regions than in areas next to the segregation.
3. Flame cutting produces a hard martensite region close to the cut edge at all cutting speeds and all thicknesses. Hardness values decrease in the two-phase region as the newly formed martensite mixes with the tempered original structure. The two-phase regions contain more newly formed martensite as the cutting speed and plate thickness reduce. The tempered regions of thin plates consisting of martensite produce a fine structure of dispersed cementite particles. However, the fine cementite particle structure diminishes in the tempered region

as the bainite fraction increases with increasing thickness of the plates. The bainite is practically unchanged as the material is exposed to high elevated temperatures for only a short amount of time during flame cutting. Consequently, the hardness levels of thicker plates after the two-phase region are almost constant or slightly increased.

4. Residual stress measurements near the flame cut surfaces show that the residual compressive stress decreases in the surface region (< 1 mm) as the plate thickness increases. A lower cutting speed causes a lower tensile stress region in the thin plates. However, the residual tensile stress values are almost the same at a higher cutting speed and for all thicknesses. In addition, a slow cutting speed and cutting with preheating have an advantageous effect on the residual stresses by increasing the compressive stress close to the surface and lowering the tensile stress deeper in the material.
5. Thicker plates tend to be more exposed to cracking. The susceptibility to cracking increases as the high residual stresses caused by flame cutting are combined with the manufacturing-induced, strong center segregation that occurs in thick plates. However, most plates were found to be intact even in the presence of relatively large local residual tensile stresses, and this highlights the stochastical nature of the cracking in flame cut steel plates.

ACKNOWLEDGMENTS

The work was mainly funded by the Tampere University of Technology graduate school. The authors would like thank Mr. Turo Salomaa for his considerable help with mechanical testing. Dr. Matti Isakov is gratefully acknowledged for his comments on the manuscript. This work made use of Tampere Microscopy Center facilities at Tampere University.

OPEN ACCESS

REFERENCES

1. N. Yang, C. Su, X. Wang, and F. Bai: *J. Construct. Steel Res.*, 2016, vol. 122, pp. 213–25.
2. Y. Wang, X. Liu, Z. Hu, and Y. Shi: *Fatigue Fract. Eng. Mater. Struct.*, 2013, vol. 36, pp. 1258–73.
3. Y. Wang, X. Liao, Y. Zhang, and Y. Shi: *J. Zhejiang Univ. Sci. A*, 2015, vol. 16, pp. 217–28.
4. L.R. Soisson: *Oxyfuel Gas Cutting, Welding, Brazing, and Soldering. ASM Handbook*, ASM International, Materials Park, 1993, vol. 6, pp. 1155–65.
5. R. Thiébaud, J. Drezet, and J. Lebet: *J. Mater. Process. Technol.*, 2014, vol. 214, pp. 304–10.
6. W. Wood: Report No. FHWA-RD-93-015, U.S. Department of Transportation, Federal Highway Administration, Virginia, 1994.
7. A. Martín-Meizoso, J. Aldazabal, J.L. Pedrejón, and S. Moreno: *Fratt. Integrita Strutt.*, 2014, vol. 30, pp. 14–22.
8. A.D. Wilson: *Eng. J.*, 1990, vol. 27, pp. 98–107.
9. T. Jokiaho, S. Santa-Aho, H. Järvinen, M. Honkanen, P. Peura, and M. Vippola: *Mater. Perform. Charact.*, 2018, vol. 7, pp. 655–74.
10. P. Withers and H. Bhadeshia: *Mater. Sci. Technol.*, 2001, vol. 17, pp. 355–65.
11. P. Withers and H. Bhadeshia: *Mater. Sci. Technol.*, 2001, vol. 17, pp. 366–75.
12. L. Lindgren, A. Carlestam, and M. Jonsson: *J. Eng. Mater. Technol.*, 1993, vol. 115, pp. 440–45.
13. T. Jokiaho, A. Laitinen, S. Santa-aho, M. Isakov, P. Peura, T. Saarinen, A. Lehtovaara, and M. Vippola: *Metall. Mater. Trans. B*, 2017, vol. 48B, pp. 2891–2901.
14. T. Jokiaho, T. Saarinen, S. Santa-Aho, P. Peura, and M. Vippola: *Key Eng. Mater.*, 2016, vol. 674, pp. 103–08.
15. H. Bhadeshia and R. Honeycombe: *Steels: Microstructure and Properties*, 4th ed., Butterworth-Heinemann, Oxford, UK, 2017, pp. 387–88.
16. EN 15305: *Non-destructive Testing Method for Residual Stress analysis by X-ray Diffraction*, 2008.
17. SFS-EN ISO 6892-1: *Mechanical Engineering and Metals Industry Standardization in Finland,* 2016, .
18. SFS-EN ISO 148-1: *Mechanical Engineering and Metals Industry Standardization in Finland*, 2016.
19. K. Abbaszadeh, H. Saghafian, and S. Kheirandish: *J. Mater. Sci. Technol.*, 2012, vol. 28, pp. 336–42.
20. C. Zhang, Q. Wang, J. Ren, R. Li, M. Wang, F. Zhang, and K. Sun: *Mater. Sci. Eng. A*, 2012, vol. 534, pp. 339–46.
21. T. Zhou, H. Yu, and S. Wang: *Mater. Sci. Eng. A*, 2016, vol. 658, pp. 150–58.
22. H. Bhadeshia: *Bainite in Steels*, 2nd ed., Institute of Materials, London, UK, 2001, pp. 91–116.
23. H. Bhadeshia and R. Honeycombe: *Steels: Microstructure and Properties*, 3rd ed., Butterworth-Heinemann, Oxford, UK, 2006, pp. 183–208.

PUBLICATION V

Cracking and Failure Characteristic of Flame Cut Thick Steel Plates

T. Jokiaho, S. Santa-aho, P. Peura, M. Vippola

-
-

Unpublished manuscript.